DEVELOPMENT OF DROPLET BASED MICROFLUIDIC SYSTEM FOR AGGLUTINATION ASSAYS

A THESIS SUBMITTED TO
THE GRADUATE SCHOOL OF ENGINEERING AND SCIENCE
OF BILKENT UNIVERSITY
IN PARTIAL FULFILLMENT OF THE REQUIREMENTS FOR
THE DEGREE OF
MASTER OF SCIENCE
IN
MATERIAL SCIENCE AND NANOTECHNOLOGY

By
Merve Marçalı
October, 2015

DEVELOPMENT OF DROPLET BASED MICROFLUIDIC SYSTEM FOR AGGLUTINATION ASSAYS
By Merve Marçalı
October, 2015

We certify that we have read this thesis and that in our opinion it is fully adequate, in scope and in quality, as a thesis for the degree of Master of Science.

Asst. Prof. Dr. Çağlar Elbüken (Advisor)

Asst. Prof. Dr. Ender Yıldırım

Asst. Prof. Dr. Aykutlu Dâna

Approved for the Graduate School of Engineering and Science:

Prof. Dr. Levent Onural
Director of the Graduate School

ABSTRACT

DEVELOPMENT OF DROPLET BASED MICROFLUIDIC SYSTEM FOR AGGLUTINATION ASSAYS

Merve Marçalı
M.S. in Material Science and Nanotechnology
Advisor: Asst. Prof. Dr. Çağlar Elbüken
October, 2015

Agglutination reactions have been carried out for several applications such as assessment of bacterial infection, blood typing or detecting non-infectious diseases. To observe agglutination reactions, several approaches have been developed. Although microfluidic methods are more costly compared to the common methods in clinical practice, microfluidic systems provide a reliable and more controlled environment. Due to the ability of droplet based systems to manipulate minute volumes of fluids, microfluidic systems allow screening of several agglutination reactions at a single run. In comparison to standard microfluidic devices, droplet based microfluidic systems provide efficient mixing which is a crucial parameter for agglutination reactions. This study reports detection of agglutination reactions of whole blood in microdroplets using impedimetric measurement method. As a proof of concept demonstration of agglutination reaction, blood typing method was implemented in microdroplets. Using label free impedimetric measurement approach, agglutination reaction in microdroplets was monitored. Impedance monitoring was achieved using microelectrodes in the microchannel to measure the impedance signal generated by droplets in the continuous phase. Besides monitoring the reaction, an empirical approach was applied to find the lumped element model of the system. This model can be used as a guidance to design a detection system and to test the sensitivity of the detection system that is used for other type of immuno-diagnostic assays in microdroplets.

Keywords: droplet based microfluidics, droplet merging, droplet detection, impedimetric measurement, agglutination assay, equivalent circuit modelling.

ÖZET

AGLÜTİNASYON TAHLİLİ İÇİN DAMLACIK TABANLI MİKROAKIŞKAN SİSTEMİ GELİŞTİRİLMESİ

Merve Marçalı
Malzeme Bilimi ve Nanoteknoloji, Yüksek Lisans
Tez Danışmanı: Asst. Prof. Dr. Çağlar Elbüken
Ekim, 2015

Aglütinasyon reaksiyonları enfeksiyonel hastalıkları tespit etmek ya da kan tipini belirlemek için uygulanmaktadır. Aglütinasyon reaksiyonlarını gözlemlemek için birkaç yöntem geliştirilmiştir. Klinik uyguluma açısından mikroakışkan metodlar daha maliyetli olsa da, mikroakışkan sistemler daha güvenilir ve kontrollü bir ortam sağlamaktadırlar. Damlacık tabanlı mikroakışkan sistemlerde ayrı hacimlerdeki sıvıların manipule edilebilirliği sayesinde tek bir seferde farklı aglütinasyon reaksiyonları gerçekleştirilebilir. Ayrıca aglütinasyon reaksiyonları için önemli bir parametre olan karıştırma işlemi damlacık tabanlı mikroakışkan sistemlerde daha etkin bir şekilde gerçekleştirilmektedir. Aglütinasyon reaksiyon kavramının ispatı açısından kan tipi belirleme metodu kullanılmıştır ve etiketlemesiz empedans ölçüm metodu ile reaksiyon görüntülenmiştir. Empedans ölçümleri mikrokanalın altına yerleştirilen mikroelektrotlar yardımı ile yapılmıştır. Reaksiyonun görüntülenmesinin yanında, deneysel verilerden yararlanılarak analitik model yöntemi uygulanmıştır. Bu model farklı mikrodamlacık tabanlı immüno-teşhis tahlileri için ölçüm sisteminin dizaynında ve hassasiyetinin test edilmesinde rehber olarak kullanılabilir.

Anahtar sözcükler: damlacık tabanlı mikroakışkan, damlacık birleştirme, damlacık tespiti, empedimetrik ölçüm, aglütinasyon tahlili, eşdeğer devre modellemesi.

Acknowledgement

First of all, I would like to express my sincere gratitude to Dr. Çağlar Elbüken for his guidance, knowledge throughout my studies. I would like to offer my deepest appreciation to him providing me high quality education for my future carrier and assist me to develop my research skills and to collaborate in various projects. In addition, I would like to thank Prof. Dr. Bora Garipcan, Asst. Prof. Dr. Ayşe Begüm Tekinay for sharing their valuable knowledge during our collaboration. Moreover, I would like to thank Dr. Ender Yıldırım and Dr. Aykutlu Dâna for improving quality of my work and my thesis with their helpful comments and suggestions.

Funding for this research was partially provided by (Scientific and Technological Council of Turkey) TÜBİTAK, with grant number 213S127.

Special thanks belong to my friends, Ercan Savcı, Ozan Çelik, Meltem Erdem, Alican Noyan, İnci Dönmez, Deniz Kocaay, Levent Erdal Aygün, Dr. Fatih Bilge Atar, Feyza Bozkurt Oruç, Adem Saraç Ayşe Özcan, Berk Berkan Turgut, Volkan Hünerli, Canan Kurşungöz, İsmail Kupa, Elif Şimşek, Bartu Şimşek, Ahmet Emin Topal, Ali Haider, Seda Kizir, Türkan Bayrak, Sami Bolat, Hamit Eren and Abdullatif Önen for amusing memories we spent together. For those whom I have not mentioned above, I sincerely thank all people I met during last two years in UNAM.

I thank Elbüken group family members, Pelin Kübra İşgör, Berkan Aydoğdu, Mustafa Koç, Ömer Özdemir, Ozan Yakar for being nice friends to me. I also thank to UNAM cleanroom team Semih Yaşar, Fikret Piri and Hakan Sürel for their cooperation.

I thank all my collaborators, Özgen Özdemir, Berna Şentürk, Nurcan Haştar, Dr. Mehmet Kanık, Muhammed Yunusa, Dr. Bihter Dağlar for their help and contribution to this work.

There are no words to express my deepest sense of gratitude to my parents Esin and Mehmet Marçalı and my dear brother Emre Berke Marçalı, who always give me faithful support and inspirational advice. I always feel debted to them.

I would like to specially thank my boyfriend, Burak Tekcan. Since the day we met, his deepest love, patience and sense of humour made me feel more positive than ever. Without his endless support I could not manage to overcome obstacles that I face with. *(Thanks to "mervesan adaptör ")*

Contents

List of Figures

List of Tables

Chapter 1

Introduction

1.1 Motivation of the Thesis

In last few decades, microfluidics is known as one of the key technologies of the miniaturization. It has been developed in many disciplines such as biology, chemistry, and engineering in terms of applications. With the need of the miniaturization, droplet based microfluidics which is one of the branches of the microfluidics have been developed. In the light of these developments of droplet based microfluidics in recent years, this project aimed designing a droplet based microfluidic device that detects the agglutination reaction to take an advantages of parameters which are explained below.

Droplet based microfluidics have been defined as a new path for biological and chemical processes. In those processes, mixing of the reagents is the one of the fundamental requirement. Droplet based mixing is more efficient than mixing in other microfluidic systems due to the high surface/volume ratio in droplets. Since agglutination reaction requires a mixing of antibody and antigen molecules in the samples, better mixing property became a significant parameter while choosing the system to be developed in this study. Another concern of macro scale process

is remaining residues of the solutions that are used for reaction. Cross contamination of the reagents can be prevented due to the compartmentalization of the droplets in the channel. Last but not the least parameters for the chemical and biological processes is evaporation and consumption of the reagents. Due to the nature of the small size of the droplet, less reagents are wasted for the same quality reaction in comparison to macroscale reactions and due to the ability of droplets to encapsulate the reagents, evaporation of the solvents becomes negligible.

In addition, the analysis of the reactions in microfluidics are in wide range. Based on the analysis requirements, it is crucial to determine a better detection system that is suitable for analysis. In general, for the optical based detection systems, a fluoregenic substrate is used which is used by attaching an extra reagents to label the desired material. This labelling process increases the contamination of the reactions and also effects the cell viability. Since this project included a reaction with the cells, impedimetric detection method which is one of the label free detection method was preferred.

Besides label free detection, electrical measurements provide analysing the data using an analytical approach like an electrical circuit model of the microfluidic devices. By using this model single cell in microchannel was investigated in order to understand the electrical properties of a single cell. However, there is gap in the modelling of the cells or any biological and chemical reactions inside droplets. In this study, an equivalent circuit model of cells of the whole blood sample in droplets was demonstrated. Moreover, agglutinated cells that occurred after reaction in droplets were also modelled. Using the empirical results, electrical components in the models were estimated. By considering the estimated values of the components in the simulation as a limit, sensitivity of the detection system can be tested. In addition, these estimated components can be a guide to understand whether the detection system is enough to measure such kind of reaction in droplet or not for future applications.

1.2 Overview of Thesis

This work is organized into the following chapters: Chapter 2 introduces literature review that composes of droplet based microfluidics, detection methods used in microfluidics and mechanism of the agglutination reaction. Chapter 3 represents the fabrication of the microfluidic device, design parameters of the microdevice and modification and characterization of the microdevice. Chapter 4 reports the impedimetric measurements that are executed to detect agglutination reaction in droplets. Chapter 5 discusses the results of the simulation for equivalent circuits of the microdevice. Chapter 6 gives a summary of this research and possible future work.

Chapter 2

Literature Review

2.1 Introduction to Microfluidics

In this chapter, a basic physics that microfluidics rely on are explained. Classification and biological applications of microfluidic devices are mentioned. Moreover, this review examines the development of the detection methods, especially the impedimetric detection method.

2.1.1 History of Microfluidics

Roots of the microfluidics lie in the microelectronics industry. In the mid-20th century, Golay et.al. [1] have showed that, reducing the size of the columns and particles that were used for gas chromatography (GC) could increase the performance of their technique. With the help of the microelectronics fabrication techniques, first silicon based gas chromatography was developed at Stanford University by Terry et.al. [2]. Afterwards, first capillary electrophoresis (CE) was developed in a microchannel by Mathies et al. [3]. As the researchers continued to work on miniaturizing the GC and CE, new microfluidic devices have begun to be investigated by the researchers for the other applications as well.

2.1.2 Advantages of Microfluidics

With the scope of the miniaturizing, the most obvious advantage of the microfluidic device is reduction of reagent consumption. This is important especially when reagents are expensive. In addition, with the small reagent requirements, the microdevices provide running an experiment even the reagents are limited. Depending on the application, heat transfer is another crucial parameter. Because of the micron scale nature of the microfluidic devices, dissipation of heat is more efficient than other macro scale devices. Moreover, it is more effective to mix reagents in microchannel. Because, only diffusion provides mixing different reagents in the channel by itself.

In terms of the integrating the steps that is used for the analytical investigation, microdevices provide an easier way to combine steps in one device. These devices generally are known as μTAS (Micro Total Analysis System) or LOC (Lab on a Chip) devices. By applying an integration, contamination that mainly comes from human involvement can be reduced automatically.

2.2 Basic Physics of Microfluidics

2.2.1 Continuum Approximation

In macro scale, generally, fluid mechanics, all liquids are taken as continuous. While considering the properties of the liquids such as velocity and density, these parameters are taking as an average value instead of considering each molecule velocity and density in the liquid. This approximation is called as continuum approximation. Even though, every individual molecule becomes dominant in microscale, in order to analyse fluid behaviour in microscale this approach is used. This approximation suffers when gas molecules are used or few micron scale channels are used.

2.2.2 Flow Profiles in Microchannel

There are three basic flow profiles that is governed in the microchannel. Electroosmatic flow, Couette flow and the Pouseuille flow profiles [4]. In microfluidics devices, these flow profiles almost always are laminar. In order to understand the flow profile, there is a dimensionless number which is called as Reynolds Number. This parameter is used to determine whether the fluid flow profile is turbulent or laminar in the channel. The Reynolds number is defined as explained in the Equation 2.1.

$$Re = \frac{vL}{\eta} \tag{2.1}$$

where η is the kinematic viscosity, v is the flow velocity and L is the characteristic dimension of the channel. When Re < 2300, flow in the most of the microfluidics system is laminar. Viscosity is a term that explains the fluid resistance to the flow and can be defined as in the Equation 2.2,

$$\nu = \frac{\mu}{\rho} \tag{2.2}$$

where μ is the dynamic viscosity and ρ is the material density.

In addition, in the microdevice that is used for this study to detect agglutination reaction, the flow is pressure-driven based flow type. Therefore, Navier-Stokes equation for the incompressible fluids in that flow profile can be derived as explained in the Equation 2.3,

$$\frac{d\vec{u}}{dt} + (\vec{v} \cdot \nabla)\vec{v} = -\frac{1}{\rho}\nabla P + \frac{\eta}{\rho}\nabla^2\vec{v} \tag{2.3}$$

where η is the dynamic viscosity, P is the applied pressure and $\vec{v}$ is the velocity of the fluid. Left side of the equation includes time dependent inertial component and non-linear inertial component. On the right side of the equation, the first

term is pressure gradient that is applied to the system, and the second term is related to viscous dissipation. Since, inertial terms become smaller than viscous terms where the velocity of the fluids is small and time dependent property of fluid velocity, both terms on the left side of the equation are cancelled. Hence, fluid flow becomes proportional to the applied pressure and equation changes as shown in the Equation 2.4,

$$\nabla P = \eta \nabla^2 \vec{v} \tag{2.4}$$

2.2.3 Dimensionless Numbers that Effects Droplet Formation

One of the important parameter to form droplets is the surface tension between the liquid-gas interfaces. These forces effect the parameter which is known as Bond number that is explained in Equation 2.5. Bond number is the parameter that compares the gravitational force and surface forces [5]. In microchannel Bo < 1 means, the effect of gravitation is negligible.

$$Bo = \frac{\Delta \rho g L^2}{\gamma} \tag{2.5}$$

where $\Delta\rho$ is the difference in mass density between the two fluids, g the gravity acceleration, L is the characteristic length scale, and γ is the interfacial tension. Besides Bond number, the other dimensionless number that relates to surface forces is the Weber number. This number compares the inertial force with the surface forces which is important in the moment of the breakup of droplets. In order to define the Weber number Equation 2.6 is derived.

$$We = \frac{\rho L v^2}{\gamma} \tag{2.6}$$

where v is the fluid velocity,ρ is density of fluid and γ is interfacial tension of

the liquid. We < 1 means, the inertia becomes unimportant when the dimensions of the channel is decreased [5, 6].

Shape of the droplet also depends on the other dimensionless number which is called as Capillary number. Capillary number can be defined in Equation 2.7. As explained in the equation, the capillary number compares the viscous forces with the interfacial tension. As the interfacial tension increases, the interfacial area of the liquid decreases which is crucial for the stability of the droplets [7].

$$Ca = \frac{\eta v}{\gamma} \tag{2.7}$$

where η is dynamic viscosity of the most viscous fluid in the two-phase system, v is the velocity of that phase, and γ is the interfacial tension. Ca >1 means viscous forces are dominant which results deformation in droplet shape and droplets started to break up at the downstream of the channel [7, 8].

2.3 Classification of Microfluidics

Microfluidics systems can be divided into four main groups such as paper based microfluidics, droplet based microfluidics, continuous microfluidics, passive microfluidics and digital microfluidics.

In paper based microfluidic system, basically the chromatography paper is patterned to form a channel using a printer. These types of systems are also known as PAD (microfluidic paper-based analytical devices). For example, Whitesides's group initiated a simpler and an inexpensive paper-based platform for 3D cell culture which was used to validate different cell proliferation profiles in oxygen and nutrient gradient environment [9]. The main advantages of this system is low cost fabrications of a microchannels, high compatibility with the biological materials, and the property of self-triggered flow due to the capillary force that occurs in the paper [10]. Passive microfluidic systems are govern by the capillary

force as well. In order to control fluid flow capillary force is utilized [11].

Flow in the digital microfluidics base on the electrolyte- electrodes interactions and generally is generated by the help of the external voltage. When a voltage is applied to electrodes, an electric field is generated between those electrodes. This field effects the surface properties of the material and results transfer of the desired material from one electrode surface to the other electrode surface. Therefore, it can be said as advantage that, there is no external pump to drive fluid flow in the device. In these kind of systems, instead of using a channel like microdevice, open structures are used to transport liquids. In addition, these type of microfluidic devices require only a few microliter drop of the reagents which reduce reaction time. These systems are also known as EWOD (electrowetting on dielectric). Shen et.al. [12] have shown a EWOD-based immunoassay. In this method, by manipulating the magnetic beads, modification of bead with the antibody was done. In this functionalization process of beads, washing protocols were done in one chip by transferring the droplet of the magnets from one reservoir to the other. Hence, all the steps in the process were accomplished in a single chip without any cross-contamination of the reagents.

In continuous microfluidics, basically fluids in the channel are moved using an external source like pressure pump and syringe pump. These systems are usually used for the chemical reactions. Because of the continuous property of the flow in the channel, these systems suffer from ineffective fluid manipulation. In droplet based microfluidics, compare to continuous microfluidics, liquid flow in the channel is in segmented form. Droplet based microfluidic systems are the systems where the liquids are encapsulated by droplets and are carried by liquid which is immiscible to droplet content. In addition, droplet based systems provides a reliable control to manipulate reagents in the channel. Chemical reactions in droplets are more rapid in comparison to in continuous microfluidic device. Furthermore, droplet based systems provide less contamination of the reagents in the channel due to the presence of droplet membrane [13].

2.3.1 Droplet Based Microfluidics

Droplet based microfluidic systems are evolved with the concept of the segmented flow in the microchannel. Because of the high surface to volume ratio, mixing is more effective in the segmented flow. However, segmented flow was not efficient enough to mix two different reagents and in the segmented flow; the channel walls were contaminated where the reaction took place. Therefore, a need to droplet based microfluidics has shown up. As the droplet based microfluidics developed, new applications to manipulate droplet flow were developed. In this section, all principles that are used in droplet based system are explained.

2.3.1.1 Droplet Generation

The basic principles of the droplet based microfluidics rely on the generation of the droplet in the channel. To form droplets in the channel, few parameters are needed to be considered such as viscosity of the fluids, channel dimensions, flow rates of the fluids, channel geometry and immiscibility of the liquids. Researchers have developed various droplet formation techniques. In this part, only four of them will be discussed.

Droplet formation in the T-junction geometry occurs basically by interfering of two immiscible liquids at the T-junction. From the dispersed phase of the channel fluid flows to the main channel. Within the pressure gradient and shear forces in the channel, dispersed phase elongate through the main channel. Then, with the shear forces, dispersed phase thinned gradually and breaks into droplets. The size, shape, velocity of the droplet depends on the flow rates viscosity of fluids and the channel dimensions [14, 15].

In flow focusing geometry, droplets are formed by forcing both dispersed and continuous phase through the narrow channel. In the narrow channel, continuous phase starts to squeeze the dispersed phase. At some point, dispersed phase breaks into droplets. The size of the droplet can be altered by changing the flow rate of the continuous phase [16, 17].

DEP-driven droplet formation is basically a method that pulls the droplet from the reservoir by polarizing the fluid with a non-uniform electric field. Forces that cause to move the droplet depend on the interfacial tension of droplet with the surface, surrounding medium and body force of the liquid [18, 19, 20]. Similar approach to DEP-driven droplet formation, in EWOD-driven droplet formation, droplets occur when an electric field is changed that is applied to microelectrodes in the channel. By changing the electric field, the contact angle of the droplet on the electrode changes. Hence, droplet can be formed and removed from its reservoir [21, 22, 23].

2.3.1.2 Droplet Fission

Droplet fission which is also known as droplet splitting can be classified into two methods. One of them is a passive splitting. In this method, there is no external power to split droplets. Fission of droplets can be done by altering the shear forces in the channel, changing the flow rates, and changing the resistance in the channel. Generally T-shape channel is used which is also called bifurcation junction. At this junction, because of the equal flow rate at both side of the junction, droplets stretched and break up into two equal size automatically [24, 25, 26]. In active methods, splitting can be applied with many other external sources. Thermally induced splitting is one of the active splitting method. In this method, by applying the higher temperature, the viscosity of the liquid is decreased. So that, an interfacial tension of the liquid decreases. Hence, some part of the liquid separates from the main droplet and moves to higher temperature field [27].

2.3.1.3 Droplet Fusion

Droplet fusion is a method which is also known as droplet merging. In this method, two individual droplets are generated in the channel. Then these two droplets are brought together. In the passive fusion, one droplet is located in one part of the channel and by altering the flow rate in the channel, the other

droplet is brought into contact with the steady one [28]. In addition, instead of altering the flow rate, merging can be applied by changing the surface property of specific part of the channel. For example, Wilhelm et.al. [29] have showed a selectively hydrophilic channel where droplets were merged. In one of the active fusion method, merging simply is executed by applying a voltage to the droplet with the electrodes by using same principle to form droplets in EWOD-driven droplet formation [30].

2.3.1.4 Droplet Sorting

Sorting of the droplets provides a way to separate specific droplets from the other droplet population. Various approaches have been proposed. One of them is sorting by looking size of the droplets. Tan et.al. [24] designed a channel that small droplets are transferred by continuous phase to the side channel whereas, larger droplets tended to flow to the main channel because of the higher velocity flow rate on the larger droplet. Applying an electric field is also provides to sort droplet into branching channels [31]. Ahn et.al. [32] have developed a DEP-based sorting device, where an electrodes is located under the channel. By applying an electric field to these electrodes, droplets are moved to the desired branch channel.

2.3.1.5 Mixing within Microfluidic Device

Mixing of reagents in microfluidic devices is more effective than mixing in conventional methods in terms of few advantages. One of them is the requirement of the less reagents due the small scale of the microchannels. In addition small dimension also provides a better mixing because of the high surface volume ratio.

In macro scale, mixing generally achieved with a turbulent flow. However, in the micro scale, as mention in section (2.1.3.2), turbulent flow cannot be achieved in small Re number. In order to avoid this limitation, mixing in microchannel can be executed by taking advantage of channel design, especially in passive mixing. The passive mixing does not require any external energy source. Passive

micromixers generally rely on the diffusion length and the contact surface area. Passive micromixers can be classified into few different methods. T-Y shape micromixers based on the diffusion of two liquid in coflow at the downstream of the channel. Kamholz.et.al. [39] have developed a method that splits and recombine the fluids in the channel in order to mix them. By using 3D structure in the channel, two different fluids are sorted so that the surface area of the liquids increased. When the liquids combine with each other, due to the increased surface area liquids get mixed better and mixing time decreases. By generating a whirl flow or recirculation in the channel can also cause a mixing. In order to generate such flow profile, Bhagat et.al. [40] have designed a channel that has a postures in cubic and rectangular inside.

In active mixing, applying an external source is needed such as magnet, voltage, temperature, or ultrasounds. Deshmukh et.al. [33] have developed a method to generate segmented flow in the channel by altering the pressure in the channel. Using T-junction geometry, two different liquids were flown into channel, by driving and stopping the flow with the altered pressure, two liquids aligned sequentially and mixed [33, 34]. The other active mixing method is generating a magneto-hydrodynamic disturbance in the channel. To do that, electrodes that are deposited in the side walls of the channel generate an electric field. By coupling this electric field with a magnetic field, deformation in the fluid stream is occurred, so that liquids get mixed [35, 36, 37]. As another example to active mixing, Krishnaa et.al. [38] have designed a channel which traps the air bubble inside. This bubble acted as a mixer when a sound wave was applied. Hence, when two fluid in coflow met the air bubble trapped region of the channel, liquids mixed in the channel.

In droplet based mixing, the mechanism is based on the turns and bends of the liquids that are encapsulated in droplet. When a droplet flows through the serpentine channel, body and the edges of the droplet contact with the channel at different angle [41]. For example, a trailing edge of the droplet exposes to larger arc whereas the receding edge of the droplet makes contact at small angle. So that, smaller circulation of liquids in droplet happen at receding edge compare

to trailing edge. In addition, turning in the serpentine channel causes the liquids become upside down and reoriented in droplet. So that, an extra stirring is generated. Since the droplets are isolated from the carrier in the microchannel, different types of mixing reactions can be run in a single channel. In the agglutination reaction, which is the main focus in this study, large numbers of reactions are need to be performed based on the type of the blood and antibody that is used. Therefore, droplet based microfluidics was the most applicable approach due to ability to generate parallel reactions in channel.

2.3.1.6 Biological Applications of Droplet-Based Microfluidics

Droplet based microfluidics have been used for the biological applications such as cell growth, single cell detection, separation and counting, and drug discovery as explained in below.

With the development of the protein analysis using MALDI (matrix assisted laser desorption/ionization) in droplet based microfluidics [42], protein based drugs started to be investigated by researchers. In order to characterize protein drugs, generally crystallization of the protein is done. During crystallization process, various chemical experiments are needed to be run at the same time. Due to the ability of droplet based microfluidics to run different types of experiments in parallel, protein crystallization can be applied easily. Lau et.al. [43] have developed a device that crystallize glucose isomerase, ferritin and thaumatin
.

In order to achieve cell growth in the microchannel, the environment conditions such as oxygen, carbon dioxide concentration, the medium to feed the cells, temperature and humidity of the chamber that cells requires are needed to be provided. Hung et.al. [44] have shown a microfluidic design that has high aspect ratio to provide stable microenvironment for mammalian cell growth. This high aspect ratio in channel dimension provides a better gas diffusion. In addition, due to high surface area/volume ratio, microchannel became more prone to lose less volume of liquid which is important to avoid cell suffering from lack of medium.

Separation of the desired cell from its population has been developed using various methods. One of the separation device was designed using an optical method by Joensson et.al. [45]. This device is used for the enzyme amplification to observe abundance of the biomarkers to specific cells. Cells were labelled with fluorogenic substrate and also with a biomarker. Based on the fluorescence intensity that reaches the detector, cells were sorted.

2.4 Detection Methods for Microfluidic System

Several methods have been developed for the detection of the bioanalytical and biochemical reactions. In this chapter, two main detection methods are explained: optical detection method and electrochemical-electronic detection method.

2.4.1 Optical Detection

Optical detection methods are generally based on the detection of absorbed UV (Ultra Violet), fluorescence and luminescence. To detect such quantities, many filters, lenses, light sources are required. In addition in microscale, these required components may be needed to be miniaturized. In order to avoid these obstacles, optoelectronic devices were used such as light-emitting diodes (LED), laser diodes, and complementary metal oxide semiconductors (CMOS). As an example for laser based detection, Xu et.al. [46] have developed a compact disc microfluidics device to analyse alcohol level in blood. In this system, a calorimetric assay of alcohol was used. A laser was exposed to the detection chamber; by looking change in the optical path length of the laser due to the change in the colour of the blood, detection was done.

Fluorescence detection can be used for any kind of reaction that is available to be labelled with desired material with a fluorogenic substrate in microchannel [46, 47]. Dittrich et.al. [48] have demonstrated a method that analysed a phenotype of the gene. They designed a flow focusing device to generate droplets. Every single

droplet that included enzyme-amino acid, fluorogenic material, and RNA's mixed with the random gene library. As a result of mixing chromophore was formed and based on the intensity of the fluorescence that chromophore phenotype analysis of the gene was accomplished.

2.4.2 Electrochemical and Electronic Detection

Electrochemcial reactions can be classified in three main group: amperometry, impedimetry and potentiometry. Basic principle of the potentiometry for the measurement of the biological quantities is measuring the cell potential difference by applying zero current. In the amperometic measurement method, generally two different electrodes were used. A voltage difference is applied between these electrodes. Measurement is done by looking the current change due to the reduction and oxidation reactions on the surface of the electrodes. Similar to amperometric detection method, two different electrodes are used in impedimetric detection method as well. By applying an AC electric field to the electrodes, an impedance analyser measures the changes in the impedance of the solution. In electronic based systems, generally FET (Field Effect Transistor) is used. Working principle of these devices is sensing the change in the ion concentration of the material that is to be tested [49, 50, 51, 52]. In addition, there are electronic based other methods which is developed using custom-electronic devices. For example, Elbuken et al.[53] have developed a capacitive sensor that measures the capacitive change in the solution that flows in the microchannel. Using this approach, Isgor et al.[54] have developed a droplet content detection method to sense ethanol concentration in droplet capacitively. In this project, the basic approach was to detect the agglutination reaction in droplets impedimetrically. Theory of the impedimetric measurement is explained in section (2.2.2.1). A variety of the biological and biochemical reactions have been developed using impedimetric detection methods. Especially, single cell impedimetric analysis has been developed for many years [55, 56, 57, 58]. In this kind of analysis, underlying parameters such as electrical conductivity of the medium and the cell, dielectric character of the cells are needed to be understood very well. Jang et.al. [59] have developed

a method that trapped a HeLa cell in the detection region and the measured the impedance of a single HeLA Cell using Precision Impedance Analyzer. By changing the applied frequency and the voltage, impedance response of the cell was observed. Besides analysing the electrical characteristic of a single cell, by using this impedimetric approach, cells can be differentiated from its population and can be counted. Gou et.al. [60] have developed a device that measured the resistance and capacitance of the cells under flow. They were able differentiate apoptotic and necrotic SMMC-7721 cells by measuring the impedance of the cells. Moreover, Holmes et. al.[61] have shown a detection method that is able to separate cells in the whole blood. In this method two parallel electrodes were excited with an AC signal. One pair was for the detection and the other pair was used as reference. As the cells pass through the detection region, impedance change was measured by subtracting the signals that electrodes measured. As a result of this measurement, lymphocytes, monocytes, and granulacytes were differentiated. In comparison to these methods, an impedimetric detection system which measure the electrical properties of cells inside the droplets. In the one of the scope of this study, it is aimed to model the agglutination reaction in a droplet using an electrical circuit approach. In the literature, an equivalent circuit model was developed for a single cell in a microchannel [62, 63, 64, 65]. Holmes et.al. [63] have developed a circuit model for the leukocytes. Using this model they fit the simulation results with the experimental data. Even though the simulation data were fit with the experimental results, the components of the circuit model was not explained. In further development of this model was done by Kemna et.al. [66] which is explained a single cell modelling inside the droplet. Although, the construction of the model was done properly, in order to indicate the exact values of the components a simulation was not executed. In comparison to these methods, a model with an approximated number of the components in the circuit was developed in this study as explained in detail in chapter 5.

2.5 Agglutination Reaction Mechanism and Detection Methods

Agglutination comes from Latin aglutinare which means coming particle together and stick to each other. Agglutination is a serological reaction. Serology is the branch of the immunology which is related with the diseases that caused by the infection of viruses and bacteria. In some diseases these bacteria and virus can cause an agglutination of body fluids. In agglutination reaction, the basic mechanism composes binding of a specific antibody to specific antigen of the cell and clumping of cells together. Binding antigen to antibody resembles a key-lock interaction as shown in Figure 2.2. After the key-lock shape is formed, by binding of antibody to the free sites of the antigen, lattice of the cells is formed which is also called as clumps of the cells.

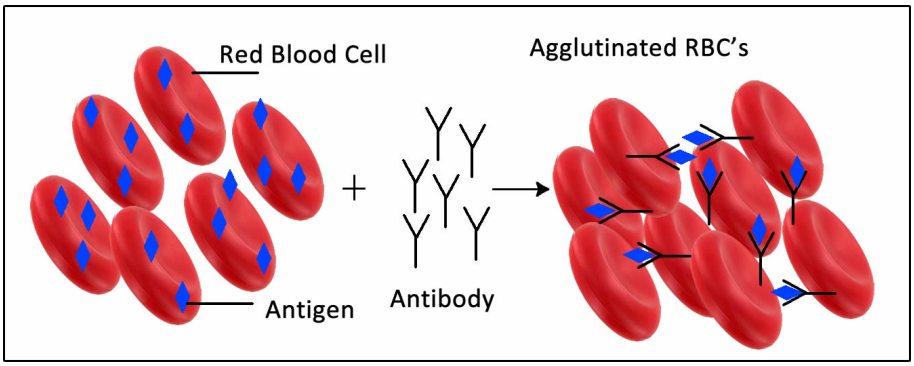

Figure 2.1: Illustration of agglutination reaction of RBC's

Agglutination testing helps you to find antigens or antibodies in a sample. The sample can be any body fluids such as urine, blood, saliva, and cerebrospinal fluid (CSF). Therefore, agglutination reaction is important in the diagnostic laboratory to identify the cause of the diseases such salmonella, brucellosis, protozoa or parasites. Agglutination reaction can be classified into three main groups based on the reaction mechanisms. Direct agglutination occurs when a particle has a self-antigen naturally. However, in the passive agglutination reaction, artificial particles are used which are coated with an antigen. Hemagglutination involves the agglutination of the red blood cells (RBC's).

In the immunology laboratories, the agglutination test is performed using two simple different techniques. These techniques are grouped as rapid agglutination tests and slow agglutination tests in tubes. In the rapid agglutination test, mixture of undiluted patient serum and the specific antigen in plate and this mixture is done by rotating the plate. In comparison to rapid agglutination test, the patient serum is diluted and mixed in tube in the slow agglutination tube test. Blood typing is one of the hemagglutination reaction. A-B-O blood groups are classified as A, B, AB, O and Rh depending on the presence or absence of the A or B, Rh antigens on the red blood cells. For example, a blood type which has A-type antigen on RBC's, the agglutination only occurs if the anti-A type antibody is mixed with the blood sample.

The aim of the study was to detect any kind of agglutination reaction in droplets. In order to realize the reaction inside the droplet, blood typing method is used due to the simplicity to run in a microchannel. In the literature there are several techniques were developed to determine the type of the blood [67, 68, 69, 70, 71, 72, 73]. Kline et.al. [72] have developed a droplet based microfluidics to determine the type of the blood and the type of the bacteria optically. Using a serpentine channel shape, mixing of blood sample with the specific antibody was done. However, in this method a tedious silanizaton method was used to prevent cell stiction to the channel walls. In this study, compare to silanization process, simple modification method was developed. In addition, in the silanized channel, each antibody serum droplet were separated with trapped air. However, trapped air could not prevent the cross contamination of the serums in droplets. In this project it is prevented by separating the reagents with the silicone oil segments in PTFE tubing as explained in section 4.2.

In another approach, Al et.al. [67] have developed a paper based microfluidics to validate blood typing. A paper was introduced with a few microlitre of antibody serum . Then blood sample were spotted on this paper. After reaction occurred, agglutinated RBC's were fixed on the paper and could not be washed away which provides determination of blood type. However, since the reaction depended on the capillary force which provided to wick the blood sample through

the antibody serum spot, efficacy of the reaction is limited. Since mixing in serpentine channel also depends on the flow rate of the droplet, by adjusting the flow rate mixing efficacy is more controllable. Therefore, droplet based microdevice is determined to use.

Chapter 3

Fabrication, Design and Characterization of Microfluidic Device

In order to measure electrical properties of biological samples in suspension, notably particles and cells, several techniques have been developed over the last century. More recently, screening the properties of single cell in suspension becomes possible to investigate using lab on a chip systems. These systems require microfabrication techniques to fabricate microfluidic systems.

This chapter outlines fabrication procedure of PDMS microfluidic device and microelectrodes using photolihtography and PDMS molding methods which are one of the fundamentals of the microfabrication techniques. In addition, design parameters and the characterization techniques of the microchannels are explained. Problems that were encountered during designing and fabricating the channels are presented as guidance to future researchers as well.

3.1 Fabrication of Microfluidic Device

3.1.1 Fabrication process of Microchannel

Most of the microfabrication processes for microfluidic device include two important procedures. First one is photolithography and the second one is PDMS molding by using softlithography.

3.1.1.1 Photolithography

In photolithography process, photoresist is patterned on master with the UV-light transfer from a photomask. Depending on the design of the photomask, UV-light can be blocked in some parts of the mask or can pass through the mask. Exposure dose of the UV-light can be altered using Mask Aligner. Photoresist solubility can be changed by altering exposure dose of UV-light. There are two major type photoresist in terms of solubility response to the light. For the positive photoresist, the parts that expose to light become soluble and are removed during etching process. On the other hand, for the negative photoresist, parts that are exposed to the light remain on master while other parts are etched away. In addition, depending on the type, photoresist may has various viscosities. In general, more viscous photoresists are used to achieve thicker layer on the master. Therefore, the higher dose of UV-light should be applied.

In this project for the photolithography process, silicon wafer was used as a master and as a photoresist SU-8 (Micro-Chem 2050-2005) was used. Process steps are shown in Figure 3.1. On silicon wafer, first SU-8 2005 was spinned at first 500 rpm for 25 s (Figure 3.1.a). Right after, the photoresist was spinned at 2500 rpm for 40 s. The reason for using SU-8 2005 in advance was to prevent adhesion of cured PDMS on wafer. Final thickness of this photoresist was 2 μm. In order to cross-link the photoresist, a ramped heating process was applied (Figure 3.1.b). Then silicon wafer was put on hot plate at 65°C for 2 min, then 95° for 4 min and finally 65° for 1 min. In final cooling step was done to prevent

stress of photoresist surface because of the temperature difference between hot plate and room temperature. During this heating process, it is important not to use convention ovens because of incomplete drying of photoresist issue. After the photoresist dried, wafer was exposed to the UV-Light at 120 mJ with blind exposure mode (Figure 3.1.c). Afterwards, wafer was put on hot plate for further cross-linking of photoresist at 65° for 1 min, 95° for 3 min, 65°for 1 min in order. (Figure 3.2.d) Then, SU-8 2050 was applied with a designated speed to achieve desired thickness of the microchannel Figure 3.2.e. Because of the high viscosity of the SU-8 2050, first the photoresist was directly poured at the center of the wafer from its bottle. Then, spinned the sample at 500 rpm for 45 s, then 2000 rpm for 35 s (Figure 3.1.e). During this process, build-up of the SU-8 2050 photoresist occurred at the edge of the wafer. By using a glass slide these residues were trimmed away from the edges. So that, a better contact with photomask was provided. This step is important to achieve better resolution in side walls of the feature. After that, the photoresist was baked at 65° for 4 min, 95° for 8 min, and 65° for 2 min to evaporate the solvent (Figure 3.1.f). Then, photoresist was exposed to UV-light at 230 mJ using transparent mask which had the desire channel design (Figure 3.1.g). After exposure step, wafer was put on hot plate to evaporate solvent of photoresist effectively. During this process, visible latent image of the design of the channel should be observed on the wafer. If this latent is not observed, it means that, heating and cooling are done insufficiently. In order to reveal final structure, SU-8 must be etched in a MicroChems SU-8 developer for 7 min (Figure 3.1.i) Duration of etching depends on the freshness of the developer. Finally, the wafer was taken out from developer and was dried with nitrogen. Due to the spinner parameters determines the height of the channel, after this process with a given spinning parameters above, the height of the channel was 80 μm.

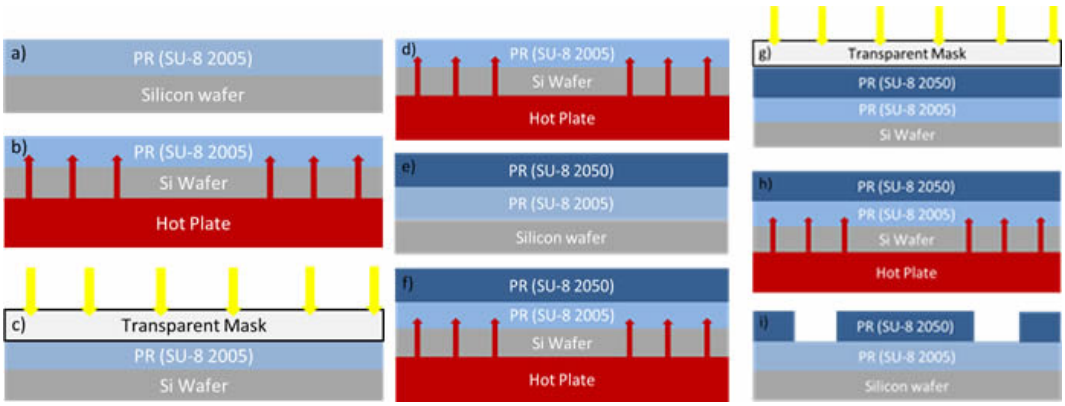

Figure 3.1: Schematic of photolithography process for SU-8 2050.

3.1.1.2 Softlithography-PDMS Molding

Softlithography is a process for replicating structures using elastomeric materials, most notably PDMS. This method is originally developed by Whitesides's group [74, 75]. The detailed steps of softlithography process are schematically represented in Figure 3.2.

In this project, PDMS microfluidics device was fabricated using this method. In order to create PDMS replica, first, an epoxy was needed to apply to the edges of the wafer to avoid delamination of SU-8 layers during peeling off cured PDMS on master. After applying epoxy, the wafer was placed on hot plate at 100°for overnight. On dried epoxy, powder was applied to prevent stiction of PDMS. Afterwards, PDMS prepolymer was prepared in a mixture of 10:1 (base polymer: curing agent- w/w) by using a mass balance. Based on the curing agent ratio in the mixture, the stiffness of the PDMS prepolymers can change. Bubbles that occurred during mixing were degassed by putting the mixture in vacuum chamber applying for 80 kPa 30 min. After that, the mixture was poured over the master that was placed in aluminium dish and was baked at 100° for 4 h. At the end of the baking process, PDMS mixture was solidified on master and was peeled off from the master. After peeling off PDMS replica, in order to prevent contamination of channels, the cured PDMS was covered from both side. Then cured PDMS were cut using scalpel depending on the design on master. Then,

using biopsy punch inlets and outlet of the microchannel were punched. Finally, PDMS microchannel was bonded on a desired substrate in order to enclose the microchannel. To sealing the channel, most notably oxygen plasma treatment is used. By the help of oxygen plasma treatment, silanol groups on the PDMS surface generated oxidations of methyl groups. These groups tend to bond to similar surfaces such glass, silicon dioxide and silicon nitride covalently. The optimized procedure to bond PDMS channel on glass surface was achieved by applying 50 W RF power in vacuum chamber during 30 s either surfaces of PDMS and glass.

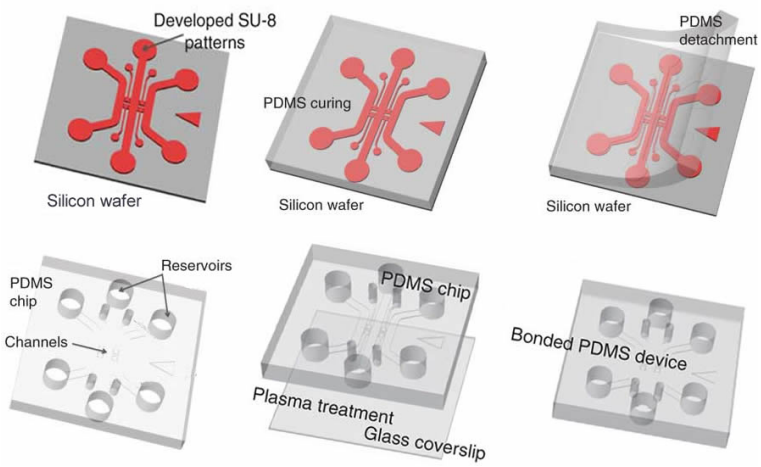

Figure 3.2: Schematic of softlithography process for PDMS microchannel. [76]

3.1.2 Fabrication Process of Microelectrodes

Electrodes were patterned on a glass slide (25 mm x 75 mm) using photolithography as explained in section 3.1.1.1. Firstly, in order to prevent organic contamination on glass slide, glasses were rinsed with acetone, then glasses were dipped in IPA (isopropyl alcohol) and finally, were rinsed with DI-water. After that, glass slide were dried with nitrogen and were put on hot plate at 120° to evaporate the residuals of solvents on the glass surface. In order to increase the adhesion of second photoresist layer, Hexamethyldisiloxane (HMDS) was spinned on the glass first at 5000 rpm for 40 s. Then, AZ5214E positive photoresist was coated

on glass slide at 4000 rpm for 40 s. A commercial transparency mask that was designed using AutoCAD was used to transfer the desired geometry to the glass slide. At 40 mJ dose UV-light (365nm-EVG620) was adjusted to expose photoresist on glass slide and the photoresist was patterned with the final developing step in AZ400K: DI-water (1:4 v/v) solution.

3.1.2.1 Deposition of Metal Layer

In order to achieve metal contacts on the glass slides, two different metal deposition techniques were used: Sputtering and Thermal Evaporating techniques.

- ***Sputtering:*** In sputtering method, highly ionized argon or nitrogen gases bombard the target of the desired material to be deposited on the substrate as shown in Figure 3.3. This bombardment generates an atomic flux of target material in the reaction chamber and atom of the target material eject from the surface. The ejection occurs when bombarded ion energy is higher than the binding energy of the target atom on the material surface. The flux can be altered by changing the power of DC source which ionized the inert gases. Thickness of the deposited material can be adjusted by changing the amount of the gases in the chamber that involve in the reaction. Based on this parameters, glass slide that AZ5214E photoresist was spinned on top, was coated with 15 nm Cr (Chromium) and 35 nm (Copper) respectively by using magnetron sputtering (Vaksis, NanoD-4S) Performed recipes are given in Table 3.3.

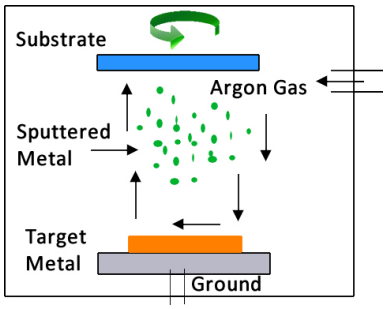

Figure 3.3: Schematic of deposition in sputtering system.

Material	DC Power	Chamber Pressure	Ar Flow	Deposition duration
Chronium (Cr)	150 W	8 mTorr	70 sccm	2 min
Copper (Cu)	150 W	20 mTorr	50 sccm	8 min

Table 3.1: Recipe of metal layers for microelectrodes.

- ***Thermal Evaporating:*** In this technique, based on the joule heating, as high current is passed through the filament, filaments gets warmer. The target material which is evaporated placed on these filaments. As the filament gets warmer, the material to be deposited is heated to the vapor pressure point. Under vacuum condition, the evaporated target material condenses on the substrate and forms a thin film as shown in Figure 3.4. Based on the current that is applied to the filaments and material density, thickness of the deposited film can be adjusted. Using this technique, 15 nm Cr (Chromium), 35 nm Au (Gold) were deposited on photoresist spinned glass slide respectively using thermal evaporator (Vaksis, PVD, Vapor 3S). Deposition parameters for Au, Cr metals are shown in the Table 3.2 below:

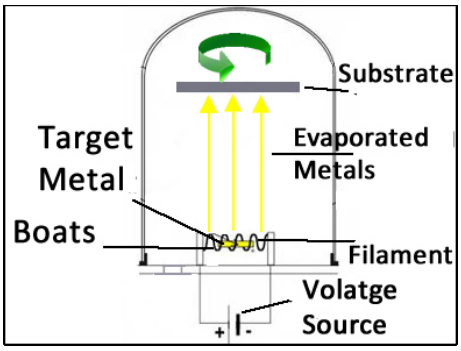

Figure 3.4: Schematic of deposition in thermal evaporator system.

Metal	Density	Acoustic Impedance	Tooling Factor
Gold	19.3	23.18	70
Chromium	7.15	28.95	60

Table 3.2: Recipe of metal layers for microelectrodes.

- ***Lift Off:*** After deposition of metal contacts, in order to achieve final pattern, the lift off process was done for both type of deposition techniques. During lift off process, acetone was used as etchant of photoresist. This etchant removed entire photoresist on the glass slide as shown in Figure 3.5

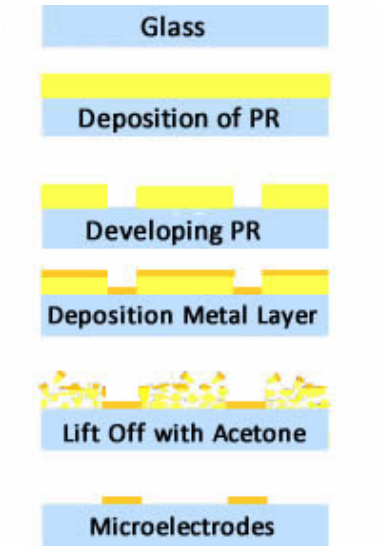

Figure 3.5: Schematic of lift off process.

3.1.2.2 Deposition of Passivation Layer

During experimental studies, pining of the solutions on bare coplanar electrodes is a familiar issue when the passivation layer was not used [77, 54]. In order to prevent cross contamination between microelectrodes and the material that is tested, a passivation layer of was deposited. To deposit the layer, optically transparent SiO_2 was chosen as a passivation layer. Using PECVD deposition technique, microelectrodes were coated with SiO_2. In this technique, the chemical reaction of the ionized target gases with the substrate was utilized. The capacitive coupling electrodes in the reaction chamber energized the target gases and create plasma. This plasma induces a chemical reaction with the heated substrate in the chamber. Then, energized gases turns from the gas phase to solid phase on the substrate as shown in Figure 3.6. In order to deposit SiO_2, silane gas was combined with the oxygen. The thickness of the deposited layer depends on the

plasma power, chamber pressure and amount of the gas reactants in the chamber. By using this method, 220 nm SiO_2 thickness was achieved for 30 min reaction time.

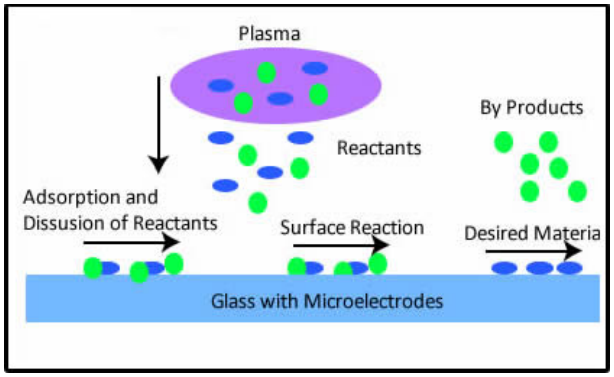

Figure 3.6: Schematic of reaction mechanism in PECVD.

3.2 Surface Modification of Microfluidic Chip

Since this project based on generating the agglutination of red blood cells in droplet, surface property of the PDMS microchannel was significant parameter. Although, PDMS is a biocompatible material, modification of PDMS surfaces can be vital based on the application of the chip and the material is used. In this project, main parameter was generating a droplet and mixing whole blood droplet with the antibody serum to observe agglutination reaction. As explained in section 2.3.1.1, droplet formation based on several parameters such as surface tension and channel geometry. Since red blood cells have more tendency to adhere to the PDMS wall, surface tension becomes so dynamic that prevents droplet formation. In order to avoid adhesion of RBCs to surface the of the PDMS wall, several surface modifications were tried on PDMS surface which is applied to achieve super hydrophobic PDMS and glass surfaces. After modification was accomplished characterization and droplet formation was executed as explained in section 3.4.

- ***Modification A:*** Aytug et.al. [78] have explained that modification of both PDMS and glass surfaces using a mixture of *1H, 1H, 2H, 2H* Perfluoro-1 Octanol (PFOTS) and n-hexadecane caused the facials to turn to super hydrophobic surfaces. Based on this method, PDMS channel was modified with a mixture of 1H, 1H, 2H, 2H Perfluoro-1 Octanol (PFOTS) and n-hexadecane. The mixture was flowed through the channel using a syringe pump and the channel was exposed to the flow for 10 min. After sample was loaded with the solution, PDMS channel was baked at 100°for 1 h. Then, droplets were tried to be generated in FC-40 (Fluorinated oil-which is also flour based solution) as a carrier of droplets. However, droplets tended to stick to the walls as explained in section 3.4.1.

- ***Modification B:*** Instead of physical absorption of the mixture of *1H, 1H, 2H, 2H* Perfluoro-1 Octanol (PFOTS) and n-hexadecane to the channel walls, PDMS channel was exposed to oxygen plasma before modification in order to achieve chemical absorption. After oxygen plasma treatment, oxygen molecules breaks to -OH bonds on the surface of the PDMS and open free sites for bonding of *1H, 1H, 2H, 2H* Perfluoro-1 Octanol covalently. By loading channel with the mixture of *1H,1H,2H,2H* Perfluoro-1 Octanol and n-hexadecane using syringe pump right after plasma treatment, cause to covalent bonding to be formed. However, similar adhesion profile was observed with the process in modification A.

- ***Modification C:*** In this modification process, contrary to loading the microchannel with the mixture, a piece of PDMS was tested by dropping a fluorinated mixture on top. PDMS sample was washed with Piranha solution for 30 min (Piranha is a mixture of sulfuric acid (H_2SO_4) and hydrogen peroxide (H_2O_2) to clean organic residues on substrates [79]. Then sample was rinsed with DI-water and dried with nitrogen. The sample was inserted into a solution which included %1 v/v PFOTS and toluene for 1 min. After that, sample was dried in an oven at 80° for 5 h. As a result of exposing PDMS to Piranha solution, the surface roughness of the PDMS increased. Therefore, this modification process was not preferred to be used for droplet generation.

- ***Modification D:*** As it is explained in the previous process, a piece of PDMS sample was prepared. First, sample was rinsed with sulphuric acid for 2 min and then rinsed with hydrofluoric acid (HF) for 10 min [80]. For the following, sample was baked at 80° overnight. In order to generate covalent bonding, sample first treated with oxygen plasma and right after plasma treatment, sample was immersed in the solution of 5 mL of ethanol containing 5 L PFOTS for 1 h. Then, sample was placed on hotplate at 80°. On the contrary of the process in modification C, the sample surface was smooth. However, the adhesion of RBC's to the walls of the channel was noticed.

- ***Modification E:*** Due to the failure of the modification process with PFOTS, silicone oil (Viscosity 100 mPa s, Ultrakim) was used to increase the hydrophobicity of the channel. Beginning of the process, glass slide was rinsed with acetone, IPA and DI-water in order. Then, glass slide was placed on hot plate for 2 h at 100°, during this process glass slide was covered to prevent contamination from environment. After heating, the glass slide and a PDMS microchannel was inserted in plasma asher to be exposed to oxygen plasma for 3 sec at 900 W. Then, the microchannel was bonded on glass slide. Throughout plasma treatment, the surface of the PDMS becomes hydrophilic, in order to increase the hydrophobicity of the surface, the microchip placed on hot plate for 2 h at 100°. After two hours, the channel was loaded manually with silicone oil (Viscosity 100 mPa s) using a standard 5 mL syringe and was baked at 100° overnight. Finally, droplet generation was tried and no adhesion issue was observed during an experiment as explained in section 3.4.1.

3.3 Characterization and Optimization of Microfluidic Chip

3.3.1 Ellipsometer

Ellipsometry can be used to measure the output polarization of light that is reflected or transmitted from the sample surface. Output polarization of light includes the information of the changed amplitude and phase.To collect data, ellipsometry setup includes the following: light source, polarisator, sample polarization analyser, and detector as shown in Figure 3.7.a. In order to get the desired information from the sample surface, model-based analysis should be done. As a result of this analysis, film thickness, refractive index, surface roughness, and uniformity of the material can be extracted. Generally, ellipsometry is used to measure the thickness of the films on sample. As shown in Figure 3.7.b, the light wave is reflected and absorbed from the surface of the sample. If the refractive index of the film, material of the sample and the model that is used to fit are known, thickness of the film can be calculated. Due to the non-destructive measurement method of ellipsometer, it is preferred to measure the thickness of the SiO_2that is deposited with PECVD on our coplanar electrodes as a passivation layer. Variable Angle Spectroscopic Ellipsometer (J.A. Woollam, V-VASE, UK) were used for thickness measurements at an incidence angle of 65 degree from 400 nm to 2058 nm. Cauchy dispersion function was used in order to determine passivation layer thickness. In order to fit experimental data, refractive index of PDMS and SiO_2 were taken as 1.42 and 1.55, respectively and the thickness of the film was measured as 220 nm.

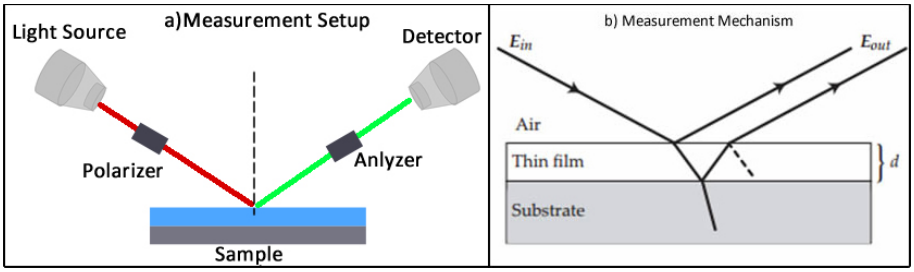

Figure 3.7: Schematic of ellipsometer measurement setup (a) and measurement method (b).

3.3.2 Profilometer

A profilometer is basically contact measurement method of sample which is also known as Stylus profilometer. It is used to measure the variations on the sample surface. Stylus profilometer has the following components: Scan head, electronics, and PC interface as shown in Figure 3.8. As the scan head is moved across the sample surface, vertical displacement of the scan head generates an analog signal. Then this signal is converted into digital signal that includes the information a height value of the sample studied. We measured the width and height of the channel that is patterned on silicon wafer using stylus profilometer as 80 m for the recipe which is given in section 3.1.1.1. (KLA Tencor, P6 Surface Profiler, and USA).

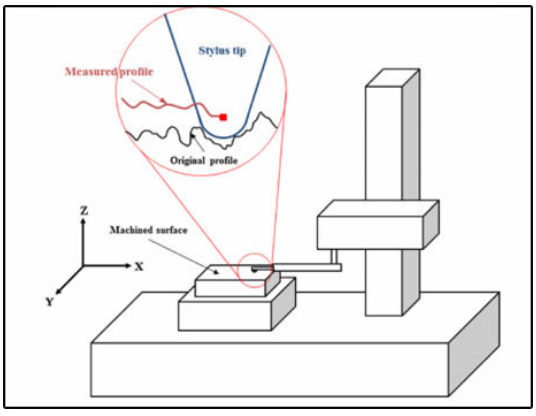

Figure 3.8: Schematic of a profilometer and measurement method. [81]

3.3.3 Surface Characterization with XPS (X-Ray Diffraction Spectroscopy

XPS is one of the techniques that is used to analyse chemical composition of surface, chemical states of components and charging behaviour of surfaces in nanoscale. The analysis in XPS is based on the photoelectric effect. As demonstrated in Figure 3.9, sample is exposed to X-Ray radiation. Then, photoelectrons which binding energies are enough to be removed by radiation from inner core are extracted. These photoelectrons are emitted from sample are measured in an electron energy analyser. This analyser provides to discriminate photoelectrons depending on their kinetic energies and give us an information about the binding energy of distinct chemicals, elemental composition of top layer of sample. From Equation of Einsteins relation, the binding energy of emitted photoelectrons can be measured as defined in Equation 3.1 below. Beside chemical composition of the sample, it is possible to find atomic ratio of these components with this relation. X-ray photoemission is governed by Einstein relation,

$$BE = h\upsilon - KE - \Phi \tag{3.1}$$

KE shows kinetic energy of the emitted photoelectrons, Φ is the work function of electron energy analyser, BE indicates the binding energy and $h\upsilon$ is the energy of the x-ray photons.

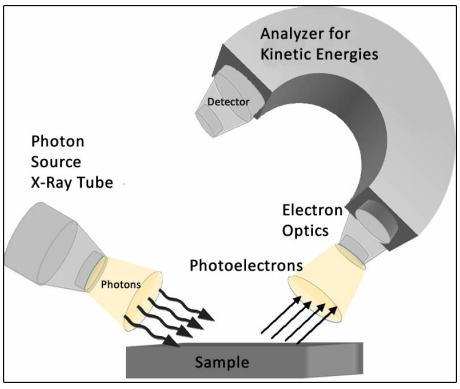

Figure 3.9: Schematic of XPS working mechanism.

To characterize the composition of atoms in the surface chemistry of the modified PDMS surfaces in detail, XPS analysis was done for each modification. XPS measurements were performed under vacuum at 83.9 eV for Al K Alfa energy source. In the elemental analysis of PDMS surface for the modification A, analysis indicates increase in the carbon, silicon, oxygen, and Flor elements. Percentage of the flour concentration in the PDMS surfaces confirms that the modification was done uneventfully. As shown in Figure 3.10, the percentage of the Flor was low and was in the noise signal level. This indicates that, Flor molecules in this modification method could not bind to the PDMS surface.

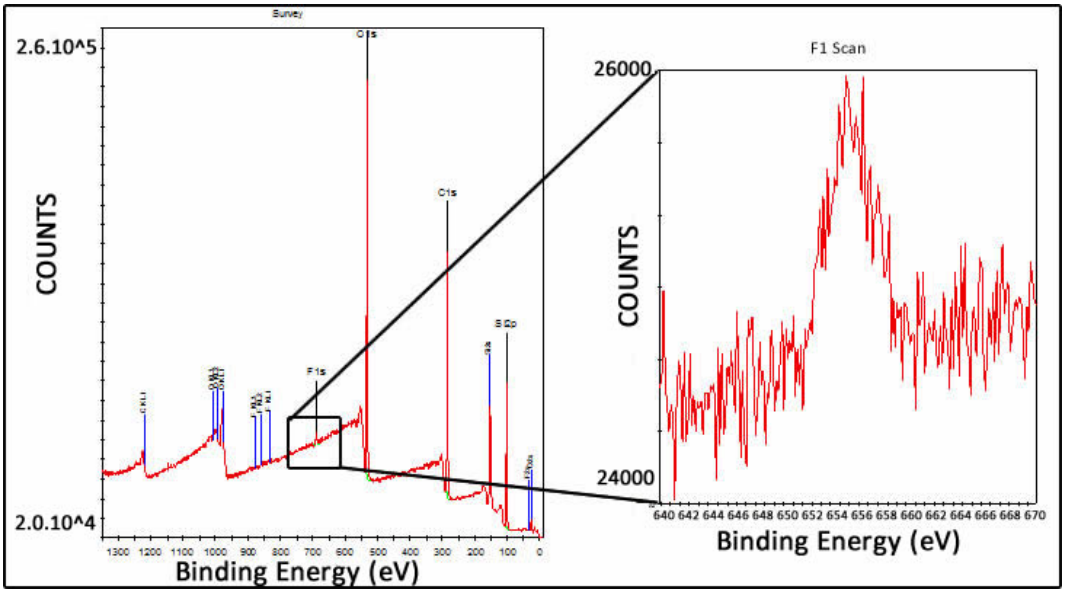

Figure 3.10: XPS measurement result of the PDMS surface that was used in Modification-A, percentage of the Flor molecule concentration was % 1.62.

However, in the modification B, after applying oxygen plasma provided to bind flour molecule to the PDMS surface covalently which caused increased in the concentration of the flour in the signal up to % 72 percentage of the composition as shown in Figure 3.11.

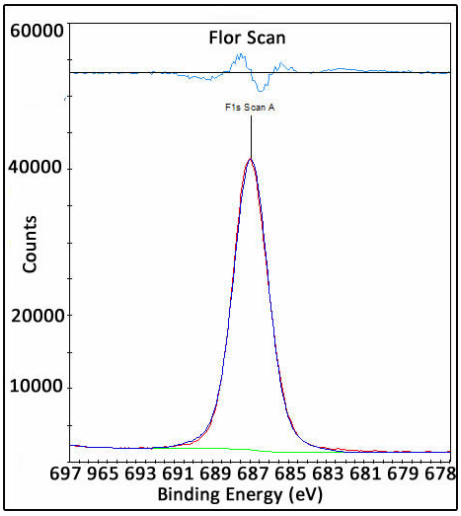

Figure 3.11: XPS measurement result of the PDMS surface that was used in Modification-B, percentage of the Flor molecule concentration was % 72.

3.3.4 Contact Angle

Contact angle measurement is used to measure the angle of the drop on a solid surface to determine property of the surface. As shown in Figure 3.12, measurement is done by dropping designated litre of water to the solid surface. This angle gives us an information about the interfacial tension between the solid surface and liquid drop, wettability of solid surface and roughness of the surfaces. The static shape of the droplet on the surface and the angle between liquid/solid/gas interfaces are determined by Youngs equation (Equation 3.2),

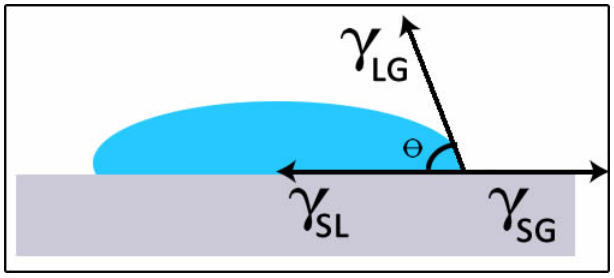

Figure 3.12: Illustration of contact angle and surface tension between surfaces.

$$0 = \gamma_{SG} - \gamma_{SL} - \gamma_{LG}\cos\theta_c \tag{3.2}$$

solid/gas γ_{SG}, solid/liquid, γ_{SL} , and liquid/gas , γ_{LG} are surface tensions between the interfaces and θ_c is the contact angle. In general, if the contact angle of water drop on surface is larger than 90 degree, the material is called as hydrophobic otherwise the material is known as hydrophilic. By doing surface modification on PDMS surface as explained in section.3.4, the contact angle of water and blood drop on each PDMS surfaces were measured by using sessile drop with contact angle measurement system.

Because of the Flor percentage in the modification A, was quite low, contact angle measurement was not done for that sample. However, for the PDMS surface which bounded flour element covalently in modification B, measurement was done for the verification of the hydrophobicity. As shown in Figure 3.13, the contact angle of water drop was lower than 90 degree which indicated that we could not achieve super hydrophobic PDMS surface with this modification method.

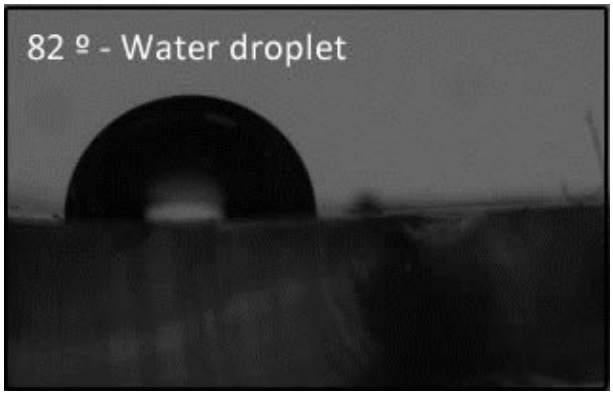

Figure 3.13: Measured contact angle of PDMS that was treated using modification B.

Then, the measurement was done for the PDMS surfaces that was exposed to Piranha solution as explained in modification C. As a result of the measurement the contact angle of water drop was 102° as shown in Figure 3.14. Thus, it cannot be said that, super hydrophobic surface was obtained compare to angle which was given in the literature.

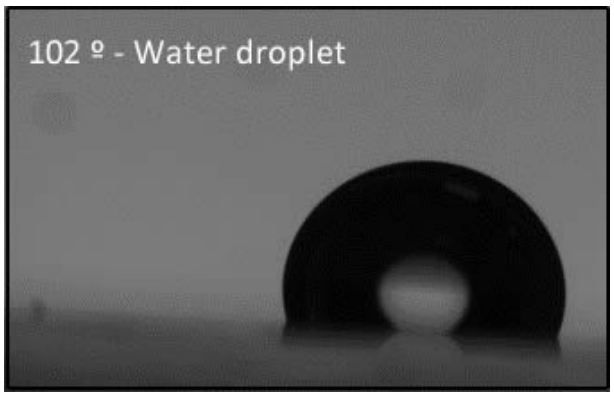

Figure 3.14: Measured contact angle of PDMS that was treated using modification C.

PDMS sample that was exposed to method in modification D was measured and the angle of blood and water droplets indicated that the super hydrophobicity was not achieved as shown in Figure 3.15.

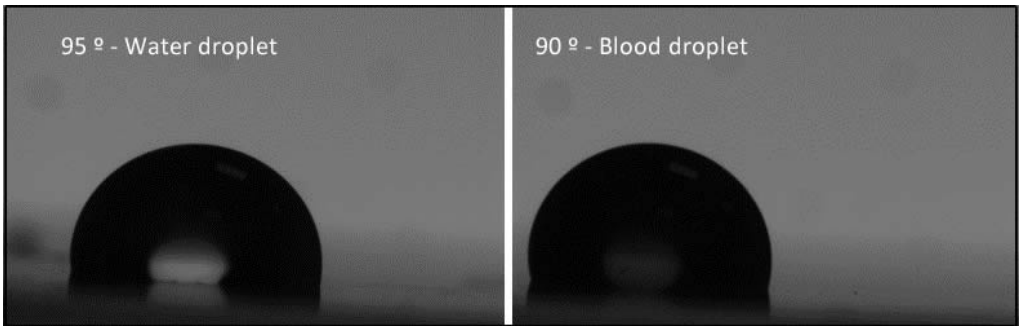

Figure 3.15: Measured contact angle of PDMS that was treated using modification D.

3.4 Design of Microchip

3.4.1 Design of Microchannel

In order to execute droplet formation and mixing in droplets for the agglutination reaction in microchannel, following parameters are required to be designed: width and height of the channel, shape of the junctions to generate droplet, number of inlets and outlets and aspects of detection region in channel. Concerning

these parameters, several approaches have been demonstrated. As explained in section for microchannel fabrication, the channel shape depends on the design of the transparent mask that was drawn using CAD program. First design of the microchannel is shown in Figure 3.16. Because of intended purpose of the microchip was forming a droplet, T-junction geometry was used in design. The microchip was also consisted of three inlets and an outlet. As shown in Figure 3.16, Y- Shape channel was designed to create coflow of RBC's and antibody solutions. At the junction, droplet of both liquid that was flowing parallel to each other was formed. Then, at the downstream of the T-junction, where serpentine channel were placed, these two reagents in droplet were mixed. The channel height was 100 μm. In the section of Y-Shape of channel, width was 75 μm and at the intersection, the channel width was enlarged to 150 μm in order to eject droplets effectively as shown in Figure 3.16. The channel in the detection region which was located at the downstream of serpentine channel, was expanded to 300 μm in width based on the hydraulic resistances and flow rates calculations of the solutions and droplets inside the channel.

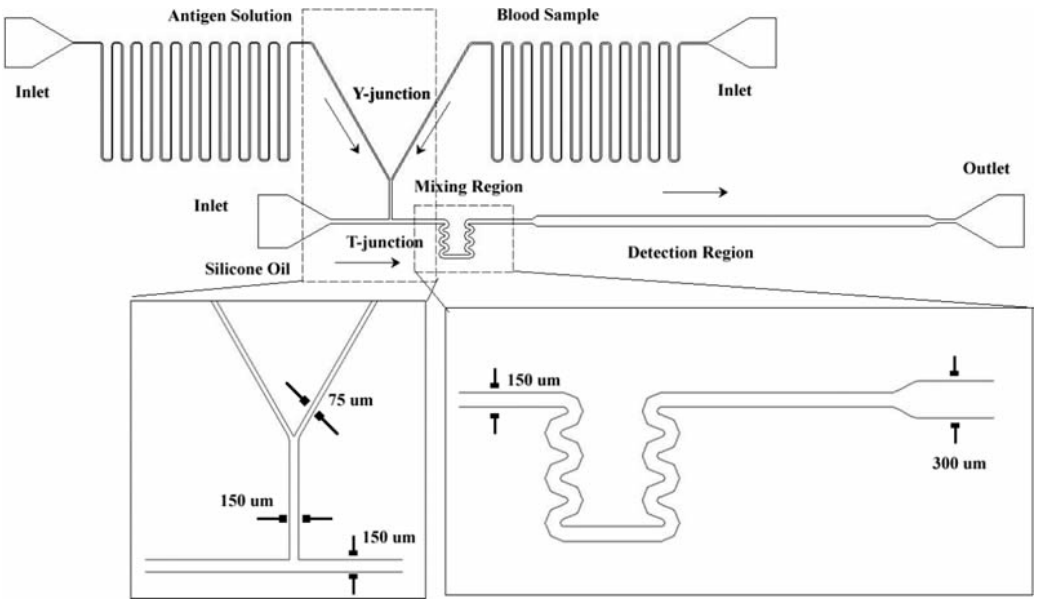

Figure 3.16: Schematic of microfluidic channel design.

For the experimental part, blood sample was diluted in 3:1 ratio with PBS (Phosphate buffer saline) and flowed through the channel using pressure pump from one inlet. The other inlet was plugged to prevent leakage. As a continuous phase, silicone oil (Ultrakim) with various viscosities was used. During an experiment, a surface wetting issue was observed while droplets were tried to form at the T-junction as shown in Figure 3.17. However, for both type of silicone oil could not prevent the wetting of the surface. It was assumed that the reason of the wetting of channel walls might be originated from the wetting properties of the PBS solution that was used in dilution of blood sample. Then, generation droplet of PBS solution in channel using both type of silicone oil was tried. Droplets of the PBS solution were formed properly in the presence of all type of silicone oil as shown in Figure 3.18.

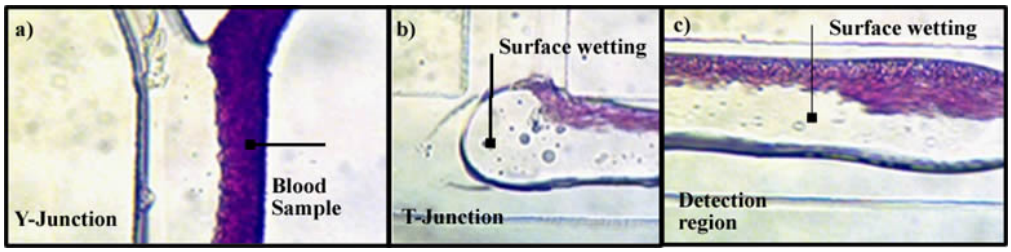

Figure 3.17: Microscope image of PDMS surface wetting.

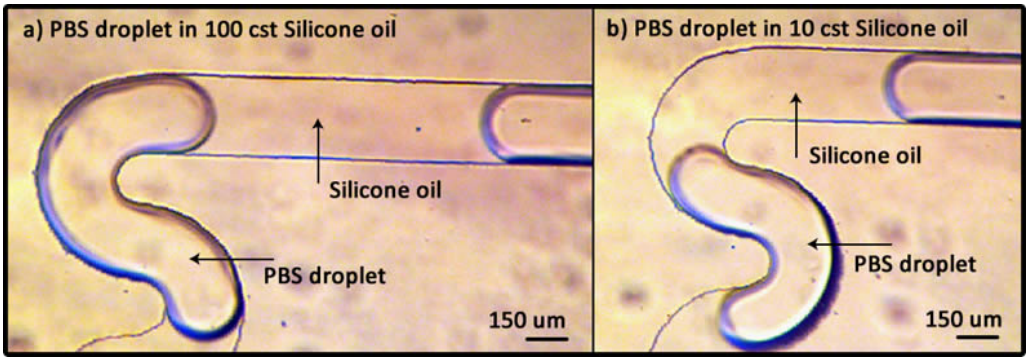

Figure 3.18: Microscope image of PBS droplet formation in T-junction.

Then it was suggested that the wetting of surface occurred because of blood sample itself. In the direction of RBC's adhesion concern, a specific type of oil which is coherent to apply biological sample was decided to use. Then, fluorinated carrier fluid FC-40 (Sigma, Aldrich) was purchased to be used as a continuous

phase in the channel. The fluorinated based oil has been used in microchannel during the investigation of biological sample, for example; red blood cells, yeast cells and E.coli. [72]. By using same design as mentioned above, droplets of blood sample was tried to form at the T-junction. Firstly, the PDMS channel was bonded on glass slide with oxygen plasma treatment. Then, fluorinated oil was flown through the channel by using syringe manually. Blood sample was loaded from both side of the inlets of dispersed phase. It was observed that fluorinated oil prevented wetting of the surface of the channel. However, adhesion of cells to the channel walls was observed as shown in Figure 3.19. Droplet formation depends also on the ratio of viscosity of the liquids of both phases, flow rates of the liquid and interfacial dynamics of the liquids in the channel as mentioned in section 2.3.1.1. Therefore it was assumed that viscous forces of FC-40 was not enough to form droplets. In addition to viscosity of FC-40 oil, the adhesion of cells prevented blood sample to be formed as a droplet as well.

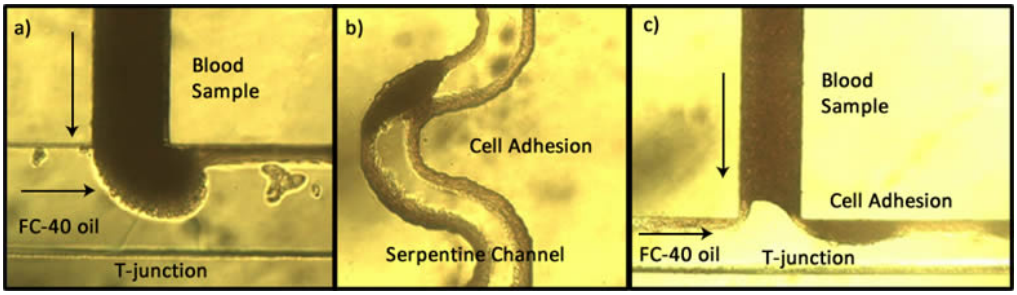

Figure 3.19: Microscope image of cell adhesion in channel.

Shape of the channel is one of the parameter that affects the formation of droplet. In flow focusing geometry, droplets were formed by squeezing the dispersed phase with the continuous phase as explained in section 2.3.1.1. By utilizing the squeezing phenomenon of dispersed phase, it was assumed that blood sample could break into droplets without any adhesion of cells to the side walls. Therefore, a microdevice in flow focusing geometry was designed as shown in Figure 3.20. In this design, the channel height was 100 μm. Width at the intersection and parts for the dispersed phases of the channel were 75 μm. Width of the continuous phase was designed as 300 μm as shown in figure. Because at the junction of this geometry, the continuous phase surrounds the dispersed phase,

so that dispersed phase does not make contact to the side walls. Therefore, it was suggested that possibility of the adhesion of cell to the side walls could be reduced with this geometry.

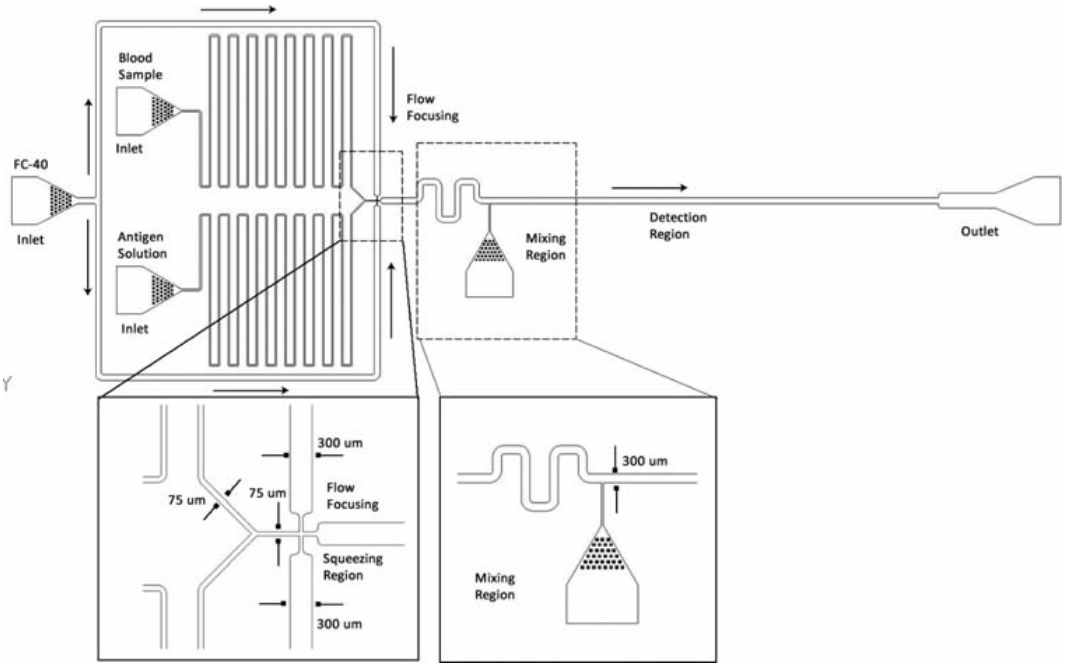

Figure 3.20: Schematic of microfluidic channel design.

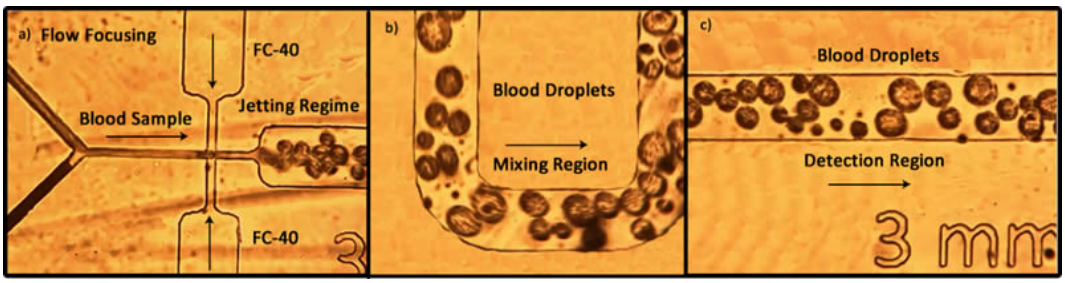

Figure 3.21: Microscope image of droplet formation in jetting regime.

During an experiment, FC-40 was used as continuous phase and blood sample was loaded into the channel from both inlets of dispersed phases. Droplets were able to eject from the junction without any adhesion of cells. But, inertial forces between liquid/liquid (FC-40/Blood sample) caused to generate droplet in jetting regime as shown in Figure 3.21. So that, droplet size and loaded volume of antibody serum could not controlled. Albeit the size of droplet was not important during measurement, the volume of blood and antigen that were loaded into droplet had effect on agglutination reaction. Moreover, as the blood sample was kept running in our device, wetting of surface increased as shown in Figure 3.22.

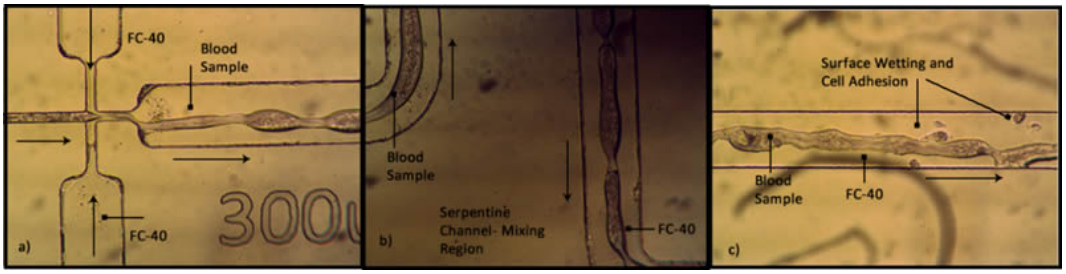

Figure 3.22: Microscope image of surface wetting (a) flow focusing region, (b) serpentine part of the channel, (c) detection region of the channel.

After failing to generate droplet using FC-40 carrier oil, PDMS and glass slide surface were modified with fluorinated based solutions to develop the hydrophobicity of surfaces as explained in section 3.2. Although the modified surfaces became close to super hydrophobic to water drops, when droplets of blood sample were tried to be formed, adhesion of cells was observed for all the fluoro based modifications that were used. For example, the microchip that was treated with the steps in modification A, was not capable to from droplets continuously. For the first few droplets that surrounded with FC-40, fluorinated oil was generated properly in the channels which have flow focusing geometries. Then, wettability of the PDMS surface increased gradually. Hence, the RBC's sticked to the walls; the droplets of RBC's could not formed as shown in Figure 3.23.c,d.

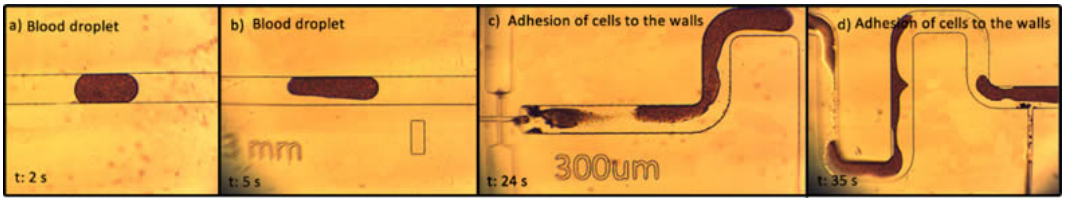

Figure 3.23: Microscope image of droplet formation in fluorinated channel (a) single droplet in flow focusing region, (b) droplet that was flowing through the outlet, (c,d) sticking of the blood sample to the surface.

Then, it was approximated that using more viscous oil than fluorinated oil like silicone oil, dispersed phase could be squeezed more effectively due to the outcome of higher viscous force of silicone oil than FC-40 in channel. As shown in Figure 3.24, droplets were generated precisely in flow focusing device. In order to do that, device was treated with silicone oil after bonding process of the channel on glass slide. Before using the chip for the experiment, the chip was waited in room temperature for two weeks. As shown in figure 3.26, droplets were formed precisely.

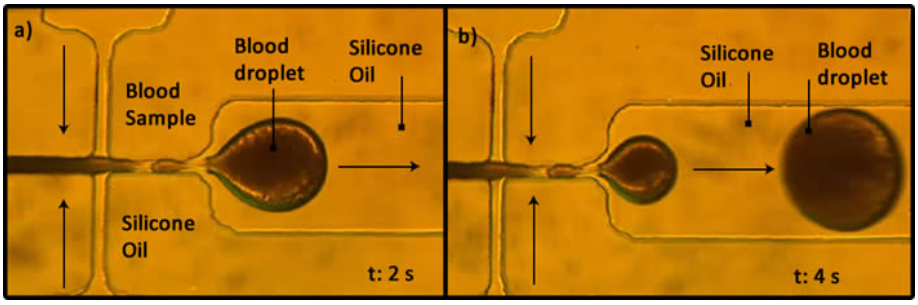

Figure 3.24: Microscope image of droplet formation using silicone oil in flow focusing channel design.

After proper droplet generation, the antibody serum was tried to be loaded from one of the inlets. At the intersection of continuous phase and dispersed phase, the antibody serum and blood sample were flown together and squeezed by silicone oil from two opposing side channels. After squeezing, droplets were formed and antibody-antigen reaction was started in droplets. However, droplet generation was not automated, so that applied pressure was needed to be adjusted from droplet to droplet. Moreover, during droplet formation volume of

two dispersed phases liquids were not equal which affects the agglutination reaction inside droplet. In addition the formation of droplets were different from one chip to another. In order to prevent these issues, only droplets of blood sample was decided to form and antibody serum was injected into those droplets from side channel as shown in Figure 3.25.

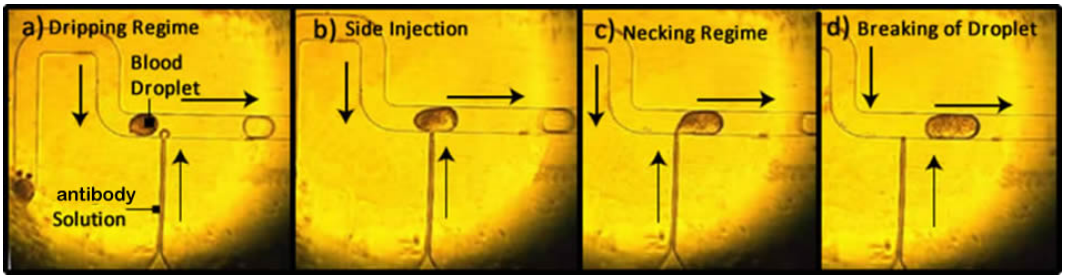

Figure 3.25: Microscope image of droplet formation using silicone oil in flow focusing channel design and injection of antibody serum from the side channel.

Although the formation was accomplished smoothly in flow focusing device, a new method is developed to increase hydrophobicity of the PDMS surfaces which is similar to previous oil treatment method that took long time before running an experiment. In order to reduce the waiting time of chip before operation, new treatment method was developed using silicone oil as explained in section step E. After smooth formation of droplets using this modification in the design as shown in Figure 3.26, the design of the chip was switched to another flow focusing device. In this design, it was able to insert three different types of antibody serum from side channel as shown in Figure 3.26. As a result of the design, the microdevice worked well for the only one antibody serum injection and droplets of all antibody serums could not be injected into whole blood droplets synchronously due to the dynamic pressure change at the T-junctions of side channel of antibody serums.

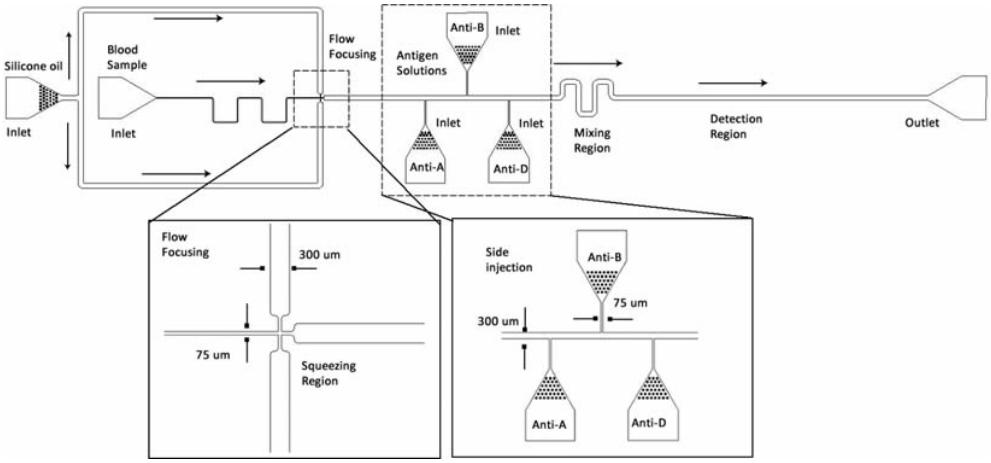

Figure 3.26: Schematic of microfluidic channel design.

By using final treatment method, droplets were tried also to form using T-junction geometry in channel as well. Using the modification E, droplets also were formed without any adhesion of cells in the one of the T-junction geometry. However, instead of forming droplets of whole blood sample, antibody serum droplet was tried to form for T-junction and blood sample was decided to inject these droplets. Therefore, a channel which includes four T-junctions and four side injection channels were designed. Three of the side injection at the up side of the channel was designed for the antibody serums and bottom side channel was designed for blood sample loading as shown in Figure 3.27. It was assumed that, by adjusting the channel lengths of the side channels longer than other side channel, could cause formation of antibody serum droplets synchronously. However, due to the dynamically increasing resistance of the channel because of the generated antibody serum droplets in the channel, droplet generation was not occurred one by one. Therefore, for the generation of multiple antibody serum solutions in a single run, the antibody serums were separated by silicone oil segments and were loaded into a PTFE (Polytetrafluoroethylene) tubing using a syringe manually. Using a silicone oil for separation of reagents, prevented a cross contamination of antibody serum with each other as well. Then, this tubing was connected to the pressure pump and one of the inlets to form antibody droplets at the T-junction. The other two inlets were plugged to prevent leakage. After formation of the droplets, blood sample was injected from the side channel into these droplets as shown in Figure 3.28.

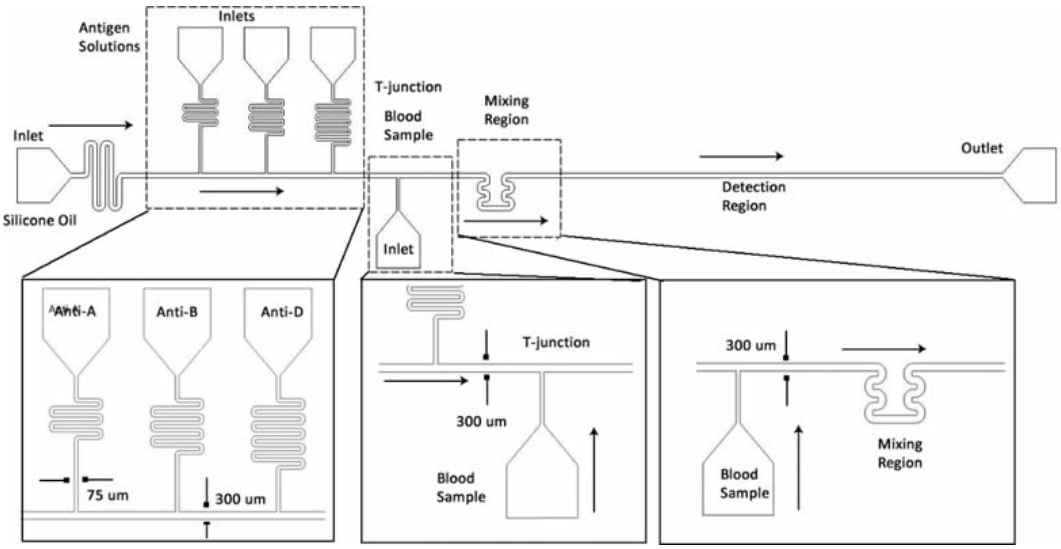

Figure 3.27: Schematic of microfluidic channel design.

Figure 3.28: Microscope image of droplet formation and blood sample injection in the channel.

3.4.2 Design of Microelectrodes

Detection of agglutination reaction was measured by using coplanar electrodes underneath the channel. While designing electrodes, there are several parameters are needed to be concern such as width of electrode pairs, spacing between electrodes pairs, channel width and height. By considering such parameters, coplanar electrodes were designed as shown in Figure 3.29. Space between pairs of electrodes was determined as 20 μm and width of the electrodes were determined as 20 μm.

As the electrode width is decreased, sensitivity of the system increases. Because, compare to wide space distance electrodes, in electrodes with narrow spacing, it is more possible to measure each point of content in droplet. Otherwise, since the large volume of droplet enters the detection region, an average value of the content will be measured. So that, sensitivity will be decreased. Therefore, 20 μm to 20 μm width and spacing was fabricated. In addition, two different type of electrodes are used in terms of coating with passivation layer.

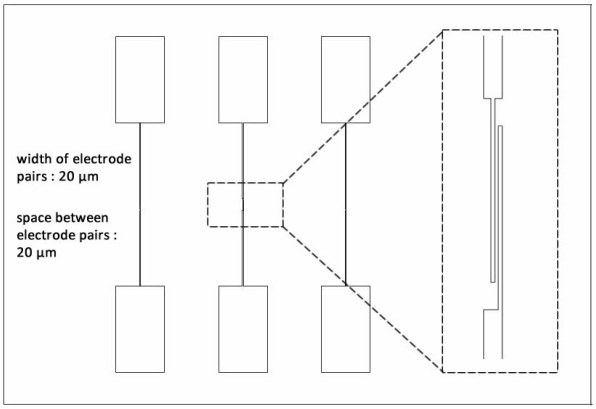

Figure 3.29: Schematic of microelectrode design.

Sensing mechanism of the coplanar electrodes and effect of passivation layer on electrodes are explained in Figure 3.30 in more details. When electrodes are coated with passivation layer due the extra capacitance that comes that layer, sensitivity of the system decreases. As shown in Figure 3.30, for the passivated electrodes, impedance of droplets were measured from 3 MΩ to 2MΩ. However,

for electrodes without passivation layer, impedance measurement on the order of kΩ level can be measured. In addition, as the larger droplets are formed, volume change can be detected by looking the change in signal in x axis.

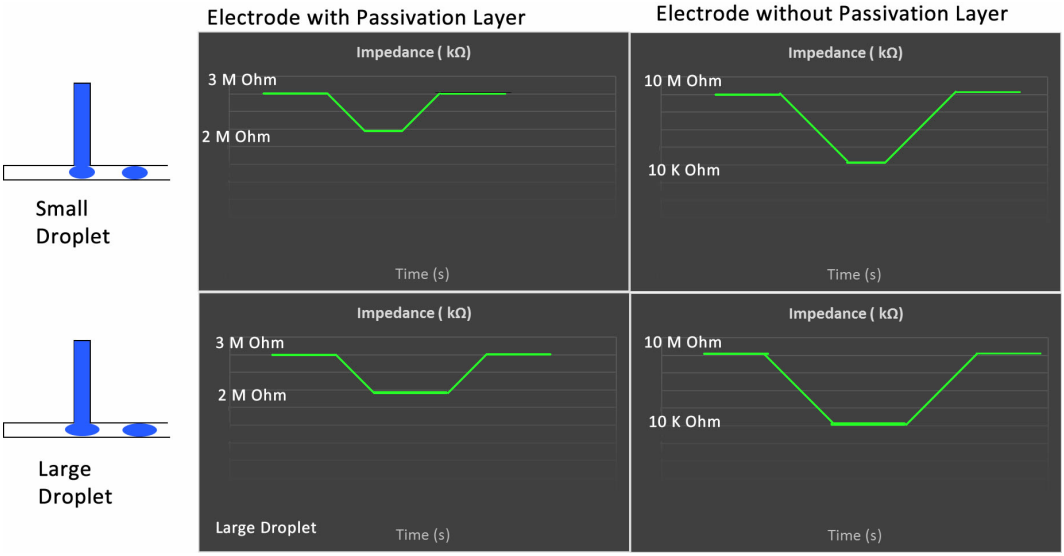

Figure 3.30: Illustration of data acquisition with passivated and bare electrodes.

Chapter 4

Impedimetric Measurement of Agglutination Reaction in Droplets

4.1 Introduction

In this chapter, impedimetric measurement of droplet was accomplished. In order to determine the agglutination, during experimental studies basically, four different types of droplets were generated and measured impedimetrically. Before explaining experimental results, it is important to mention theory of impedance.

4.1.1 Impedance Theory

Impedance (Z) is a response to the applied voltage by a current flow through the sample. This response composed of the charged electrons in the bulk sample and in the interface between the sample and electrodes. Impedance can be represented as a complex quantity. As defined in the Equation 4.1, impedance consists of a real part (resistance) and an imaginary part (reactance). In coordinate system,

the impedance is expressed as shown in Figure 4.1. Reciprocal of the impedance is called as admittance as defined in Equation 4.1,

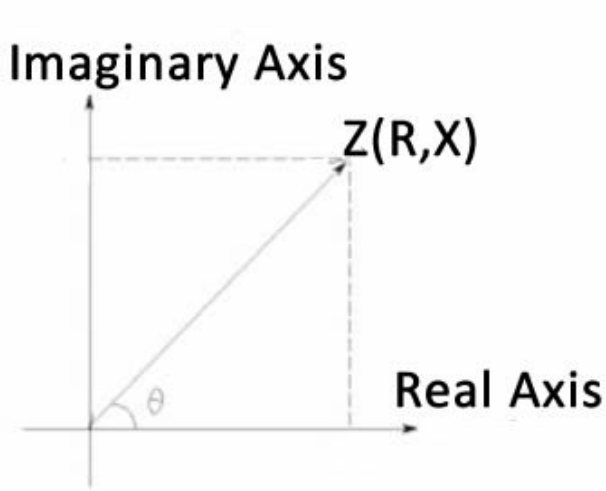

Figure 4.1: Illustration of impedance in coordinate system.

$$\frac{1}{Z} = \frac{1}{R + jX} = Y = G + jB \tag{4.1}$$

where Y represents admittance, G conductance, and B susceptance. Recatance has two components, an inductance X_L and the X_C is capacitance as shown in Equations 4.2 and 4.3,.

$$X_L = 2\pi f L \tag{4.2}$$

$$X_C = \frac{1}{2\pi f C} \tag{4.3}$$

where f is the frequency of interest, L is inductance, and C is capacitance.As seen in the equations, all the measurement of the droplets were related with resistance, capacitance and inductance. Based on this measurement approach, agglutination reaction was run and impedance of droplets were measured as explained in detail in experimental section.

4.2 Experimental Studies

4.2.1 Materials and Blood Sample Preparation

4.2.1.1 Materials

Blood samples were obtained from adult donors with a written consent in health centre of Bilkent University. Blood samples were drawn into 4 ml EDTA (ethylenediaminetetraacetic acid) tube in order to prevent coagulation of the blood sample before running an experiment. For the agglutination reaction, antibody serum which binds to antibodies of the red blood cells was obtained from a local store (Anti-A, Anti-B, Anti-D, Agape Diagnostics). As a continuous phase, silicone oil (μ=100 mPa.s, Ultrakim) was used to carry droplets in channel.

4.2.1.2 Blood sample preparation

Blood samples were diluted before running an experiment. Due to the isotonic property of the PBS solution, it is used for the dilution of blood sample. Isotonic property of the PBS provides cells not to haemolysed. First, blood sample is drawn from the EDTA tube for 1 mL using pipette and is released into 10 mL glass vial. Then, PBS solution is drawn for 2 ml and mixed with blood sample in glass vial.

4.2.2 Microdevice Design and Droplet Generation Mechanism

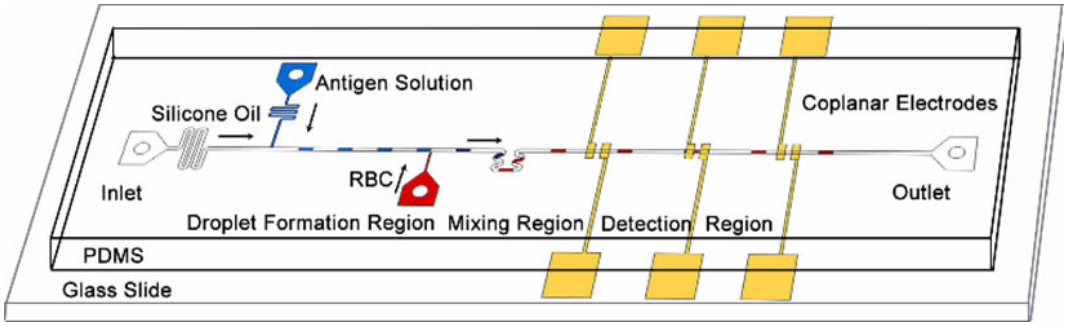

Figure 4.2: Schematic of final microchannel design.

As shown in Figure 4.2. a microfluidic chip was designed which allows the screening of agglutination reaction in droplet. Firstly, all antibody solutions were loaded into a PTFE tubing respectively using a syringe pump withdrawn mode. In order to prevent cross contamination of the antibody solutions, silicone oil is drawn after each reagent to separate them from each other. The loaded PTFE tubing inserted into the pressure pump connection of glass vial. After that, vials that include blood sample and antibody solution are connected to the input of the pressure pump. In order to control flow rates of the reagents, the pressure pump is used. The inlet pressures of dispersed and continuous phase were set as 45 mbar and 50 mbar respectively. Droplets of the antibody serum in the microchannel were generated using a pressure pump from the T-junction geometry of the channel. Then these droplets were carried with silicone oil to mix with blood sample to the second T-junction at the downstream of the channel. From this side inlet, 6 nl of blood sample is injected into the serum droplets. In order to inject blood sample into droplets, inlet pressure of whole blood was increased up to 42 mbar. Using a serpentine channel, droplets were mixed in order to increase antigen-antibody binding affinity. At the end of the serpentine channel, droplets that contain agglutination reaction started to separate blood sample to its plasma. Then, separated cells started to bind to each other like a chain and formed clusters. This clusters accumulated at trailing edge of the droplet as shown in Figure 4.3. The accumulation phenomenon occurs depending on the droplet velocity, viscosity ratio of the fluids, surface tension and sedimentation

rate. As explained in Seeman et.al. [82] , the non-agglutinated red blood cells could also accumulate at the trailing edge based on the sedimentation rate of the droplet. However, in our experiment we did not observe any accumulation of the RBC's because of the high capillary number and cells were suspended homogeneously in droplets. Finally, droplets were send to the detection region where coplanar electrodes were located underneath the channel. The droplet formation is run without any pressure adjustment of the inlet pressures synchronously during an experiment. Synchronization of droplets from two different T-junction was explained in Phan et.al. [83] They showed that droplets that were formed from the first T-junction in the channel caused to increase resistance in the channel and trigger inlet pressure of the second T-junction. So that, droplet of reagent in second T-junction was formed automatically. Based on this approach, whole blood inlet pressure was not altered during an experiment.

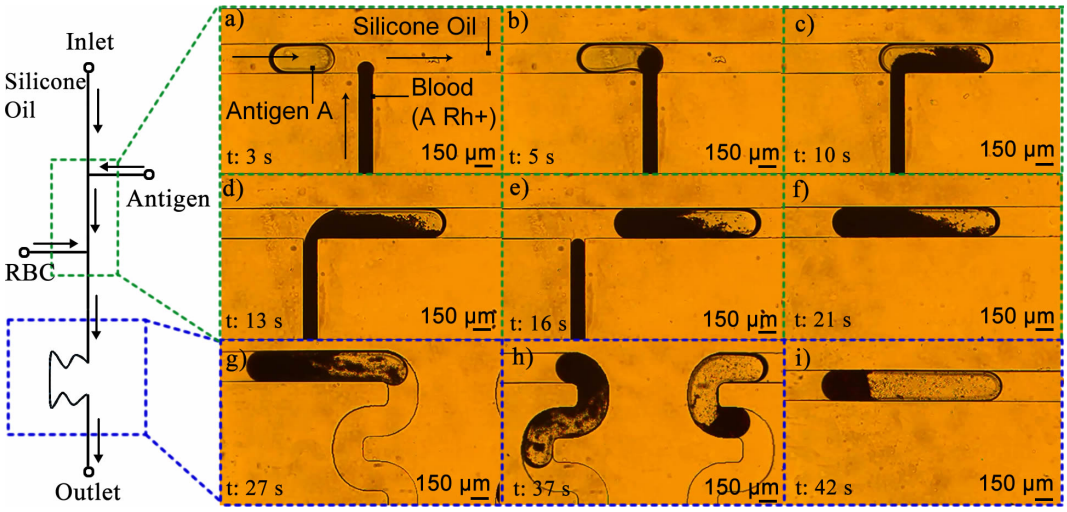

Figure 4.3: Microscope image of droplet formation.

4.2.3 Measurement Setup

The experimental setup consists of the following components: the microfluidic chip, an LCR meter (Agilent E4980A), an inverted fluorescence microscope with 5 MP camera (Omano OMFL600), a compressor; a pressure pump (Elveflow, OB1), three glass vials, a PC for LabView interface, PTFE and tygon tubings for the fluid connection to the chip, magnetic stirrer, coaxial cables and BNC connectors as shown in Figure 4.4.

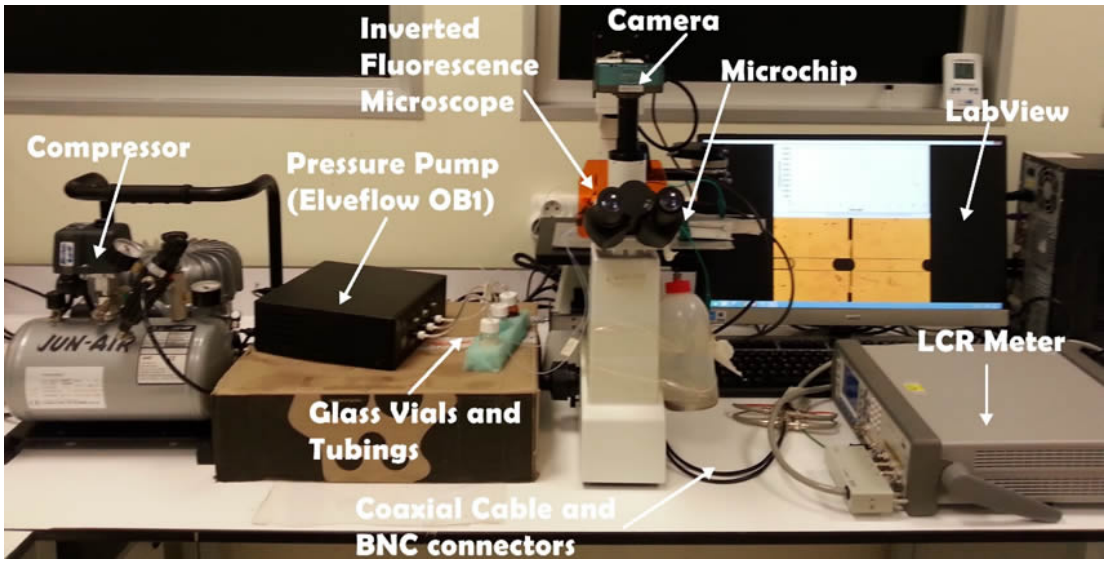

Figure 4.4: Image of measurement setup.

- ***LCR Meter:*** In this study, an LCR meter was used to measure impedance of the microdroplets. The LCR meter has different operation modes based on the working frequency. For the measurements that are needed the frequencies up to 110 MHz, generally auto-balancing bridge method is used. In this method, basically impedance can be determined by measuring the current that passes through the device and the applied voltage to the device as shown in Figure 4.5.

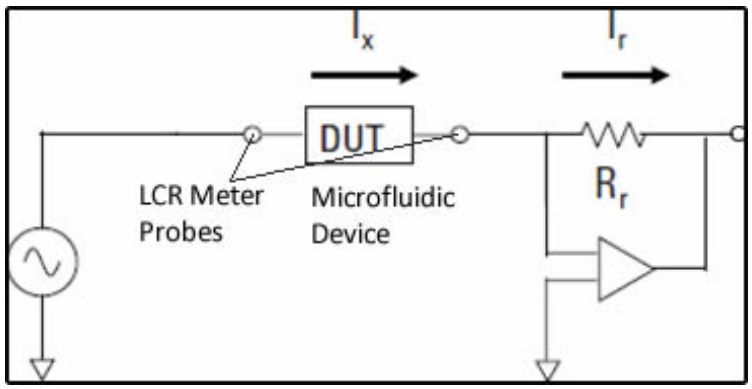

Figure 4.5: Illustration of circuit of LCR Meter connection to DUT.

The test current (Ix) is flowed through the device and the operational amplifier. From the negative feedback loop of the operational amplifier, Ix flow through the Rr (range resistor that is determine impedance measurement range), so that output voltage is measured as shown in Equation 4.4.

$$Vr = RrIx, \tag{4.4}$$

Ix is the test voltage that is determined based on the impedance of the device under test as explained in Equation 4.5.

$$Ix = \frac{Vx}{Zx} \tag{4.5}$$

So that, impedance of the device can be determined from Equation 4.6.

$$Zx = \frac{VxRr}{Zx} \tag{4.6}$$

Based on this measurement principle of the LCR meter, the microfluidic chip was a device under test. Device contact for the measurement was done from the coplanar electrodes by using coaxial cable probes as shown in Figure 4.6. The microelectrodes on the chip were supplied a sinusoidal signal at 1 V p-p amplitude by the LCR meter. The frequency of the excitation signal was in 50 kHz and 2 MHz frequency domain. Impedance measurements were performed in Z-θ mode. The sampling rate of the LCR meter was 184 Hz during measurement. The measurement time from trigger point

to the end of measurement is 5.7 ms. In order to achieve this limit, measurement time was set as short. Since measured silicone oil was on the order of M Ω in the channel, to prevent saturation of the measured signal impedance range (Rr -in Figure 4.5) was set as Auto. Auto mode helps to alter the range depending on the signal. For the control of these functions from computer LabView interface was developed. In addition, by using this interface, experimental data were transferred to the computer in real-time.

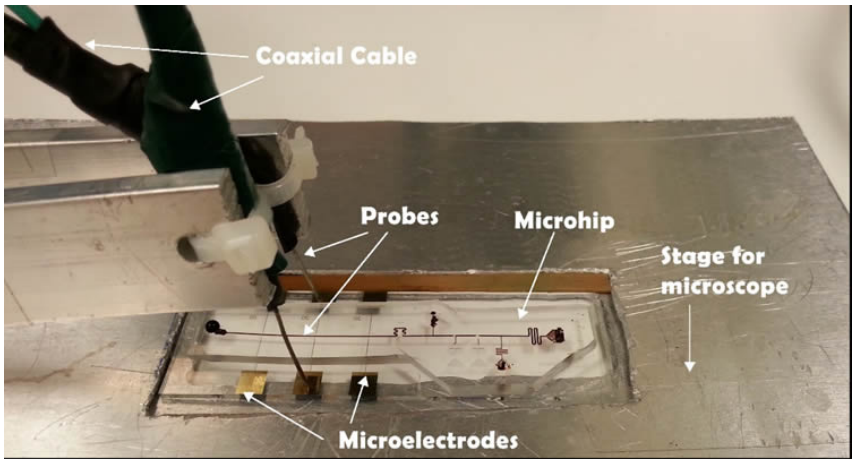

Figure 4.6: Probes of the LCR Meter.

- ***Pressure Pump:*** In order to control flow in microchannel, pressure pump was used. Pressure pump sucks the air using its compressor. Then using pressure regulators, air is pumped through the vial with help of tygon tubing at the desire pressure. Then air that is trapped in the vial is pressurized. The pressurized air in the vial pushes the fluid though the PTFE tubing as shown in Figure 4.7. By controlling the gas pressure in the vial, flow rate of the liquid can be adjusted.

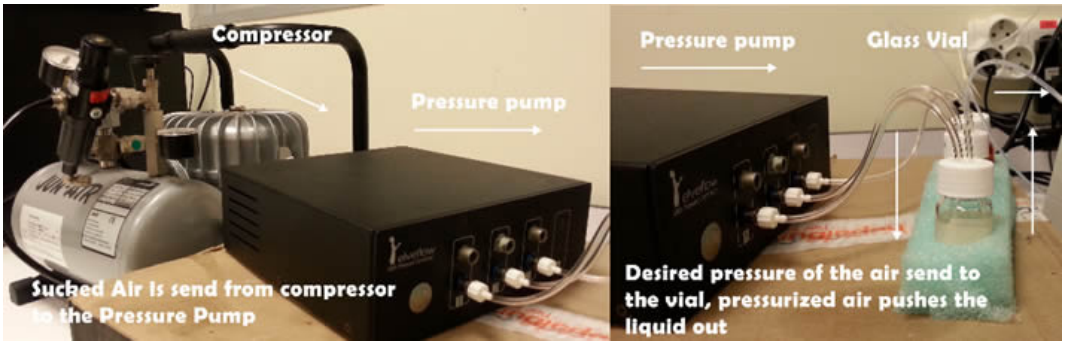

Figure 4.7: Pressure pump and vial connection.

- ***Glass Vials:***As it mentioned in MSDS form of the reagents that was used in the experiment, reagents were stored at 4°. In order to reduce the volume that is expose to room temperature, smaller volume glass vials were used as shown in Figure 4.8.

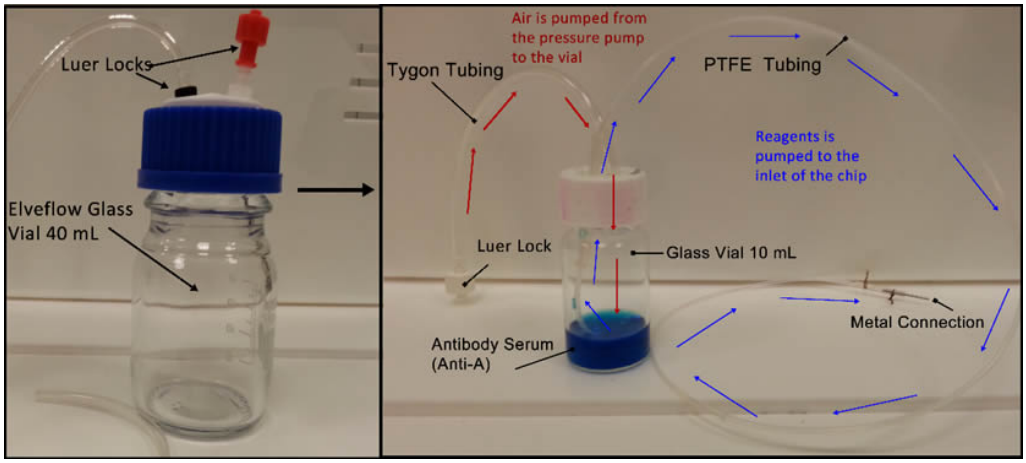

Figure 4.8: Glass vials and fluid flow direction.

- ***Microscope:***Inverted fluorescence microscope equipped with 5 MP camera was used to monitor droplets inside the channel while the impedance measurement was running. Using camera, images of the channel were transferred to the computer in real-time. From the software of the camera, the colour adjustment, intensity of the day light and frame that is needed to be taken per second was done.

- ***Magnetic Stirrer:*** Magnetic stirrer was used to prevent cells of blood sample aggregation at the bottom of the vial, PTFE magnetic stirrer bar

was placed into glass vial. As shown in Figure 4.9, DC motor was placed under the glass vial to spin the magnetic bar. Based on the applied voltage, the spin rate of the dc motor changes. Maximum spin rate was 2000 rpm when 12 V was applied using a battery. By using 6 V battery, it was possible to spin the motor at 1000 rpm. In order to spin the stirrer bar slowly, a voltage divider circuit was connected to the output of the dc motor as shown in Figure 4.9. So that, voltage was decreased to the half (3 V) and spin rate was decelerated to 500 rpm.

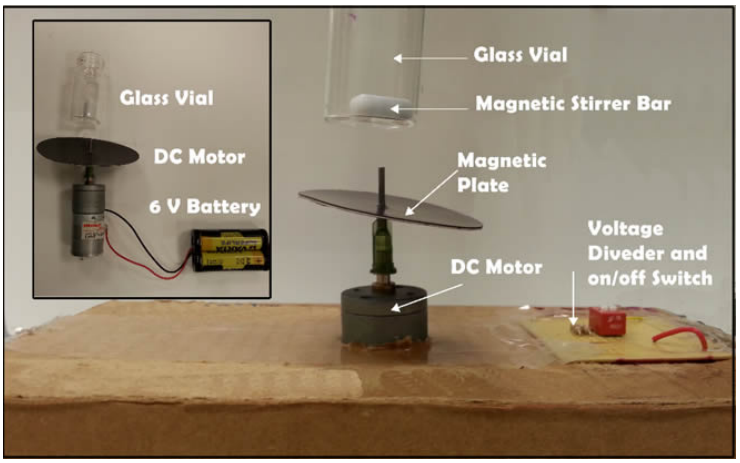

Figure 4.9: Magnetic stirrer and source connections.

4.3 Experimental Results

Resistivity is a measure of the materials ability to oppose the electric current. Resistivity and conductivity are reciprocals as explained in Equation 4.7. Therefore, when the material is more resistive to the electrical current, it means that the material is less conductive material. So that, the electric current cannot pass easily from the material.

$$R = \frac{V}{I}, G = \frac{1}{R}, \tag{4.7}$$

Hence the impedance includes resistance, as the resistance changes, magnitude and the phase of the AC current changes. Therefore, the impedance of the system changes as explained in Equation 4.8.

$$Z(j\omega) = \frac{V(j\omega)}{I(j\omega)}, \tag{4.8}$$

Since the conductivity of the antibody solutions and silicone oil are different from each other, it was approximated that, impedance signals of both solutions should be different from each other. To test the difference between impedance signals of the solutions, first channel silicone was loaded with silicone oil and the impedance was measured at 100 kHz, 1V applied voltage. As a result, silicone oil impedance was on the order of M Ω. However, when the channel was loaded with antibody solution (Anti -A), on the order of kΩ impedance was achieved. Since an impedance difference between solutions was measured, it was assumed that, the measurement system could be able to measure droplets and the reaction inside the droplets.

Based on this approach, droplets that contained different combination of the antibody solutions were formed and were send to the detection region as explained in the section 4.2.2. In the detection region, in order to measure impedance of these droplets inside the microchannel, a single frequency at 100 kHz, 1 V was applied to the microelectrodes. By applying AC signal through the microelectrodes, magnitude and phase of the AC current of the medium in the channel can be measured. So that, impedance of the medium was calculated using this approach. As the droplets travelled over coplanar electrodes, the impedance was recorded. Based on the conductivity and permittivity of the medium, magnitude and the phase of the AC current changes. As a result, impedance signals changed.

In addition, it was assumed that, impedance of the droplets would be different based on the solution conductivity inside. Therefore, droplets were formed that included four different types solution. In the first combination, whole blood droplet was formed and was not mixed with antibody droplet. In the second combination, droplet of antibody solution (Anti-A) was formed and was not mixed

with blood sample. Then, impedance of these droplets was measured sequentially. As shown in Figure 4.10, when the whole blood droplet passed through the electric filed line between coplanar electrodes, impedance decreased to 13 kΩ (Black line). When blood droplet left the detection region, silicone oil was placed on the electrodes. Then, impedance increased to 4 MΩ due to the high conductance of silicone oil. Afterwards, antibody solution droplet passed over electrodes and impedance decreased to 9 kΩ (Blue line). Although, whole blood is conductive material due to the cell cytoplasm, it was observed that, cell cytoplasm is less conductive than cell antibody solution. So that, impedance of whole blood droplet was higher than anti-A droplet as shown in Figure 4.10. Hence, differentiation of droplets that contain cells from the droplets that contain antibody solution was achieved. Right after these measurements, Anti-A droplet was formed and whole blood sample (A Rh+) was injected into the Anti-A droplet. Because of the antibody-antigen match between blood sample and antibody solution, agglutination reaction was occurred in droplet, while the droplet was passing through the serpentine channel. As explained in the section 4.2.2, clusters of the cells were trapped at the trailing edge of the droplet in PBS-antibody solution mixture . When the droplet was passed over electrode, electrodes first measured the impedance of PBS-antibody solution mixture which remains after agglutination reaction of cells. Due to the impedance of this mixture was measured around 10 kΩ level (Red line), it was approximated that conductivity of the the mixture is close to antibody solution conductivity. As the droplet flown to the outlet of the channel, the coplanar electrodes were faced with the trailing edge of the droplet. When impedance of the trapped clusters in droplet was measured, a dramatic increase in impedance up to 30-34 kΩ was observed as shown in Figure 4.10 (Red line). In addition, before the droplet left the detection region, sudden decrease in impedance signal was observed as shown in Figure 4.50 (Red line).

After the agglutinated droplet measurement was accomplished, finally, droplet that contained mismatch antibody solution (Anti-B) with blood sample (A Rh+) was measured. Due to the lack of the agglutination in the droplet, cluster of RBC's could not formed. So that, all cells were homogeneous in droplet with PBS-antibody solution mixture. Unlike the agglutinated impedance signal, when

the impedance of this droplet was measured, the peak in the signal was not observed as shown in Figure 4.10 (Green line). IN addition, th impedance was close to whole blood droplet (13 kΩ) as expected. Hence, presence of the peak in the signal was the reliable indication of the agglutination reaction in droplet.

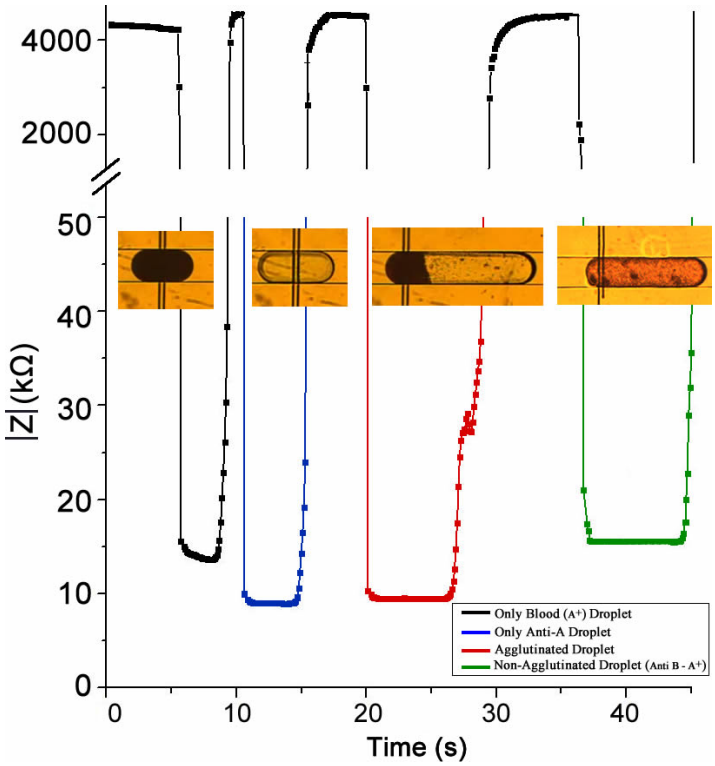

Figure 4.10: Impedance of four different droplets in the combination a) impedance of whole blood droplet - 13 kΩ b) droplet of antibody solution - 9 kΩ c) agglutinated droplet clusters - (30-34 kΩ), mixture antibody-PBS - (10 kΩ) d) non-agglutinated droplet - 15 kΩ.

In order to investigate the peak in the signal, agglutinated droplet was observed with a high magnification. As shown in Figure 4.11.a, first the impedance of PBS-antibody solution mixture was measured (red rectangle, t: 8s - t: 10s). As the droplet moved to the outlet, impedance of clusters was measured by electrodes. Due to the resistive effect of the clusters in droplet, impedance increased as shown in Figure 4.11.b (Green rectangle, t: 10s - t: 12s). Before the droplet left the electric field line between electrodes, impedance was giving a rise to a negative peak in Figure 4.11.c (blue rectangle, t: 12s - t: 13s). It was assumed that,

the reason of the peak in the signal might be the presence of more conductive solution in the region. As seen from the rectangles in the Figure 4.11 PBS-antibody solution mixture was that solution cause to decrease in impedance.

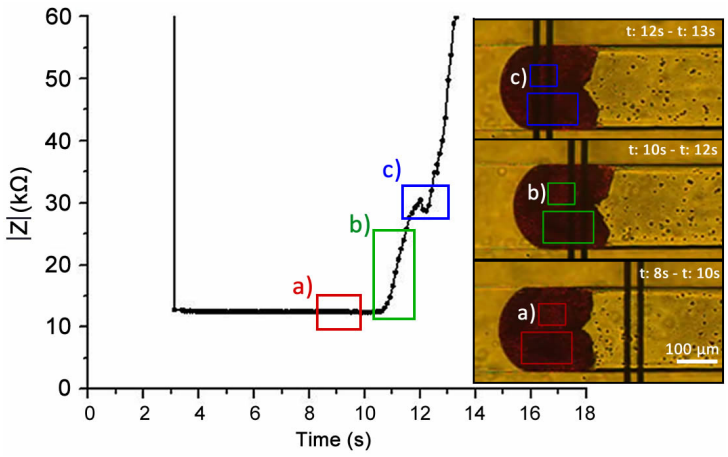

Figure 4.11: Microscope image of single agglutinated droplet at high magnification.

4.3.1 Effect of Bias Voltage on Impedance Signal

To test the voltage dependence of measurement system, the voltage that is applied to the coplanar electrodes was changed. Because the aim of detection system was giving an information about the agglutination reaction, voltage dependency test was accomplished on only agglutinated droplets. Firstly, the applied voltage was altered using LCR meter to 1 V 100 kHz. Then, an agglutinated droplet impedance was measured as shown in Figure 4.52 (Green line). Afterwards, the applied voltage increased to 10 V with the same excitation frequency and another agglutinated droplet impedance was measured. Increasing applied voltage from 1 V to 10 V ends up increase in the magnification of electric field. With this increased electric field, cells which could not bind to cluster chain due to the lack of free binding sites of antibody solution, started to move to the strong electric field line. Basic principle of this movement is the dielectric force. With that force, cells move and accumulated on electrodes at 10 V applied voltage. As a result of this

accumulation, impedance increased gradually as shown in Figure 4.12 (Blue line).

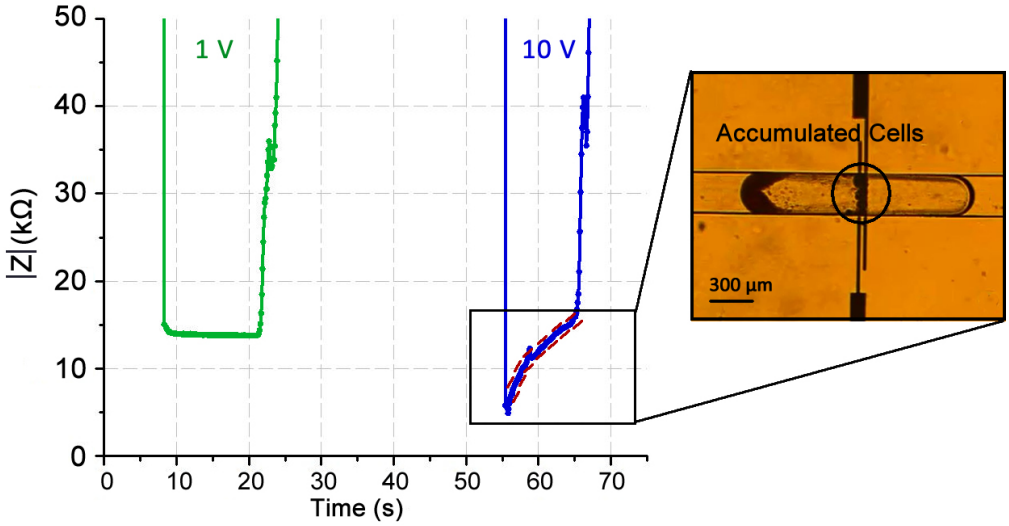

Figure 4.12: Voltage dependence of impedimetric measurement.

Moreover, when impedance of PBS-antibody solution mixture part in the droplet was measured, decrease in plasma impedance was observed as the applied voltage increased as shown in Figure 5.42.

When a voltage is applied to the electrodes which is used to measure impedance of the solutions, electrochemical reactions can occur between the surface of the electrodes and the solutions. At any interface between a charged electrode surface and the solution, ions accumulate to form a thin layer in order to maintain electroneutrality. This layer is known as electrical double layer. Electrical double layer effects the electrokinetic properties of particles and motion of solutions [84]. In this layer there are two different regions which are called as diffuse layer and stern layer as shown in Figure 4.13. Stern layer can be divided into two layer which are known as inner and outer Helmholtz planes. Surface potential falls linearly from the charged surface to the stern layer. Then the potential falls exponentially across the diffuse layer.

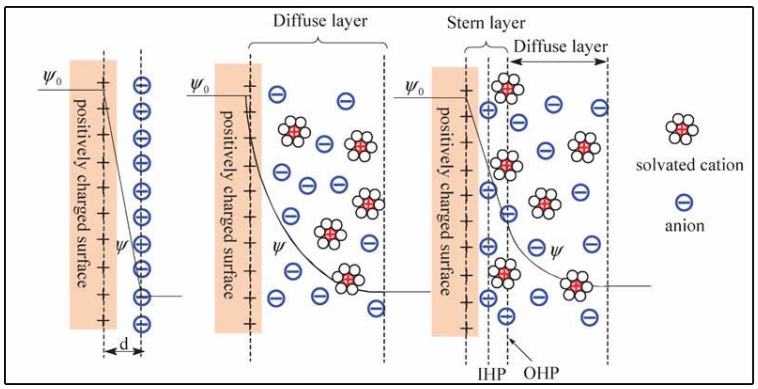

Figure 4.13: Schematic of EDL- electrical double layer on metal surface. [85]

These layers behave like a resistor and a capacitor in the system. Potential of these layers change when applied voltage changes because of the changes in charge distribution which is similar to charging of a capacitor.

The diffuse layer capacitor which is due to the ion depletion can be explained as shown in Equation 4.9.

$$C_d = \epsilon\kappa \tag{4.9}$$

with κ Debye length and ϵ dielectric of permittivity

Because of the linear potential drop in stern layer, capacitance of stern layer which is due to the free electrons at the electrode surface can be written as in Equation 4.10.

$$C_s = \frac{\epsilon}{d} \tag{4.10}$$

where d is the width of the layer and ϵ the relative permittivity of the layer.

Finally, the total electrical double layer capacitance is given in Equation 4.11 in the series of stern and diffuse layer.

$$\frac{1}{C_{total}} = \frac{1}{C_s} + \frac{1}{C_d} \tag{4.11}$$

From these equation, when the applied voltage increased, diffuse layer thickness increases. So that, the diffuse layer capacitance decreases. Because of diffuse layer and stern capacitance in series, stern layer capacitance becomes more prominent than diffuse layer. Since the admittance is proportional to stern layer capacitance, admittance increases. The impedance and admittance are reciprocals, impedance decreases as the admittance increases. Therefore, the impedance of PBS-antibody solution mixture decreased when applied voltage were increased to 10 V.

4.3.2 Effect of Blood Sample Concentration on Impedance Signal

During the experiments, blood samples were diluted with PBS solution. In order to investigate the effect of concentration of blood sample on impedance measurement, various concentration of blood sample were tested. In this experiment, only agglutinated RBCs with different dilution ratio in droplet were investigated. First blood sample was injected (A Rh+) which was diluted 1:3 v/v ratio with PBS into antibody droplet (Anti-A) and impedance measurement was done. Then, concentration of blood was increased gradually from 1:3 v/v to 3:1 v/v ratio and impedance data were recorded. As the volume of blood sample is increased in the mixture, number of the cells that was injected into droplets increased. As a result of dilution ratio, larger clusters were observed in droplets that contain more concentrated cells inside. Because of the clusters are the source of impedance increase, the maximum point of the peak in the signal was investigated. Average of the maximum point of the peaks in the signals from five different droplets was calculated. This calculation was executed for each dilution ratio. As a consequence of the measurements, the averages of the maximum points of the peak in the signals were close to each other (Table 1-Agglutinated Cell). In addition, it was assumed that conductance might change due to the concentrated PBS in blood sample. Since the PBS-antibody solution mixture remains after clusters

form in droplet, to investigate conductance difference, only impedance of PBS-antibody solution mixture was measured. As shown in Table.1 (PBS-antibody solution mixture), PBS concentration had no effect on the conductance of the PBS-antibody solution mixture part in droplet. Such that, average impedance of five droplets with the same concentration was similar with the other average results at different concentrations.

Concet. of Blood Sample Ratio	Ave. Imp. Value (Clusters)	Ave. Imp.Value (PBS- Anti Mixture)
1:3 v/v	34 kΩ	13.9 kΩ
1:1 v/v	35 kΩ	13. 7 kΩ
3:1 v/v	34 kΩ	13.8 kΩ

Table 4.1: Effect of concentration of blood sample on impedance signal.

Chapter 5

Numerical Modelling and Simulation of Agglutination Reaction of RBCs in Droplet

5.1 Equivalent Circuit Modelling

For a mathematical expression of a physical system such as cantilever in MEMS devices, mechanical springs and fluid channels, generally an electrical circuit is used which is also known as lumped-parameter modelling. For the microfluidic based systems, in this lumped model-parameter approach, an applied pressure, a flow rate, channel dimensions can be modelled as a voltage, a current, a hydraulic resistance respectively. In addition, especially for electrical measurements, it is an extensive approach to model electrolyte-electrode interaction in the microchannel using this model. For the modelling of electrolyte-electrode interaction in the microchannel, the equivalent circuit includes components that are analogous of a medium, electrodes and an electrical double layer that forms due to the interaction between electrolyte and electrode surface in the channel as explained in the section 4.3.1. The electrical double layer is generally represented by a capacitor and the medium as a resistor. When a single particle or a cell is included in the

channel, extra components are added to the circuit in the model. In the case of the single cell presence in the channel, because of dielectric properties of the cell membrane, the membrane is modelled as a capacitor in the model. The cell cytoplasm is modelled as a resistor that is in parallel to the capacitor in as shown in Figure 5.1.

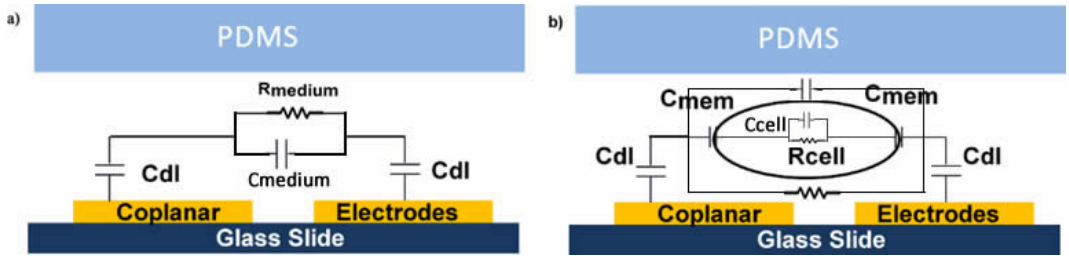

Figure 5.1: Equivalent circuit model of microchannel a) channel without cell, C_{dl} is electrical double layer, C_{medium} is the capacitance of of the medium, R_{medium} is the resistance of the medium b) channel with cell, C_{dl} electrical double layer, C_{cell} and R_{cell} are the capacitance and the resistance of the cells and C_{mem} is the membrane capacitance of the cell.

In this chapter, an equivalent circuit model for impedimetric detection of RBC's agglutination in microchannel was developed. In this model, five different droplets were modelled. In the first circuit design, only antibody serum droplet was modelled. Using the similar method to design circuit, whole blood droplet, agglutinated blood droplet and non-agglutinated blood droplet were modelled. Besides modelling droplets, continuous phase (silicone) was also modelled. Since the droplets surrounded by a carrier liquid (silicone oil) is immiscible with the dispersed phase, nanometric scale membranes between the carrier liquid and the solution inside the droplets were formed. Therefore, by using the similar analogy of a single cell, the droplets were modelled with membrane capacitors as shown in Figure 5.2.

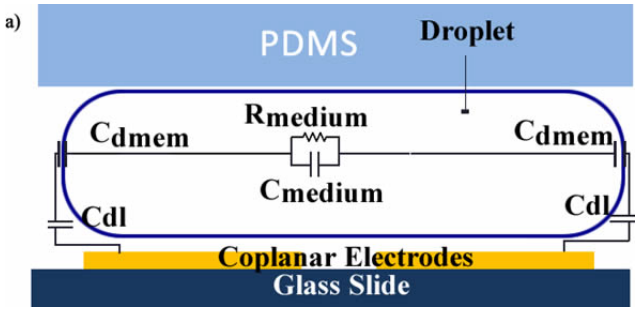

Figure 5.2: Equivalent circuit of microchannel with droplet (C_{dmem} is droplet membrane, R_{medium} and C_{medium} are the resistance and capacitance of the reagent in the droplet, and C_{dl} is electrical double layer capacitance).

In addition, in the measurement system, due to the droplets encapsulated more than one cell, every single cell should be modelled as RC circuit and connected to each other as serial. Due to the complexity of such circuit design, RBC's were modelled as a homogeneous analyte in the droplet that consisted of a single RC circuit as shown in Figure 5.3.

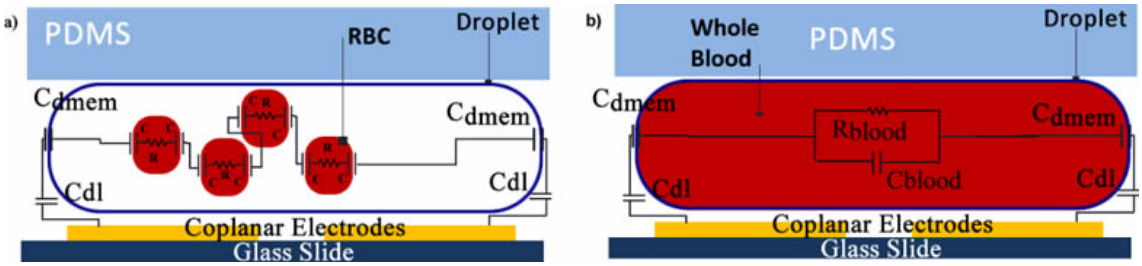

Figure 5.3: Equivalent circuit of microchannel with cells in droplet a) illustration of individual cells in droplet b) illustration of approximation of cells as a homogeneous analyte.

In this study, the equivalent circuit model of the microfluidic device was developed to fit the raw impedance data that is recorded during experimental studies. So that, approximated values of the components in the circuit could be proposed. This was accomplished with LTspice software by applying the circuit in the model and fitting the simulation results with experimental data. For a single cell applications, validation of the experimental data with the lumped-parameter analysis results is well described [62, 63, 64, 65]. In this study, the model was developed for the droplet that contained more than one cell inside. Using this simulation,

the values of R_{con}, C_{con}, R_{blood}, C_{blood}, R_{anti}, C_{anti}, $R_{non-agg}$, $C_{non-agg}$, R_{agg}, C_{agg}, C_{dl}, C_{mem}, $R_{anti-PBS}$ and $C_{anti-PBS}$ that were demonstrated in Figure 5.4 were found. Furthermore, besides modelling the components related to the droplet and the reagents in, circuit components that belong to LCR meter probes were also modelled.

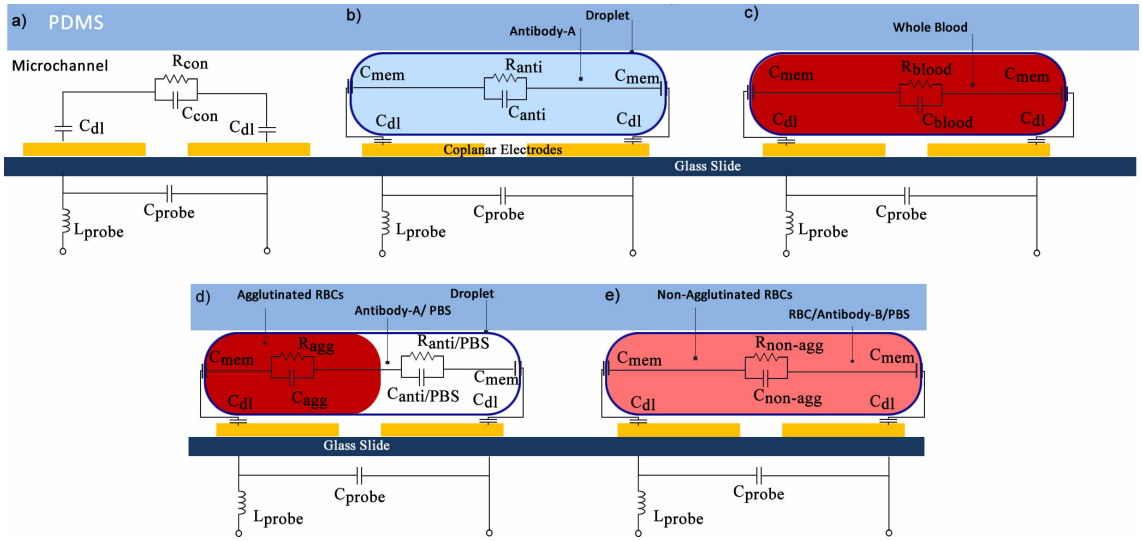

Figure 5.4: Whole equivalent circuit design for the simulation a) model of continuous phase in the channel b) model of antibody serum droplet c) whole blood droplet model d) agglutinated droplet model e) non-agglutinated droplet model (C_{dl} is the electrical double layer capacitance, C_{mem} is the membrane capacitance of the droplets, R_{anti} and C_{anti} are resistance and capacitance of antibody solution, R_{blood} and C_{blood} are the resistance and capacitance of blood sample, R_{agg}, C_{agg} are the resistance and capacitance relate to clusters of agglutinated cells, R and C antibody-PBS represents resistance and capacitance of antibody-PBS mixture that remain after agglutination reaction, $R_{non-agg}$, $C_{non-agg}$ components of non agglutinated droplets).

Before modelling the equivalent circuit of the microfluidic system, the parasitic (stray) capacitance, and inductance that effect the microdevice during measurement should be understood clearly.

5.2 Investigation of Stray Capacitance and Inductance of Probes

In order to achieve high accuracy measurement using LCR meter, it is important to compensate effect of stray capacitance and inductance that come from probes of a measurement setup. To compensate these parasitic effects, the stray capacitance and inductance were determined using LTSpice simulation.

5.2.1 Stray Capacitance Measurement

To test the stray capacitance that originates from probes of the LCR meter, first an impedance measurement of a single resistor was done. The stray capacitance is generally accepted as parallel in the circuit to the device under test. Therefore, the probes of the measurement setup were connected in parallel to the desired resistor as shown in Figure 5.5. Impedance measurement was done at 1 V, in Z-θ mode of the LCR meter. In addition, due to the frequency dependence of the capacitors, the applied frequency was swept from 20 Hz to 2 MHz during impedance measurement of the resistor. Moreover, this measurement was done for three different resistors (433 k Ω, 43 k Ω and 430 Ω), to investigate the effect of the capacitance on the resistors.

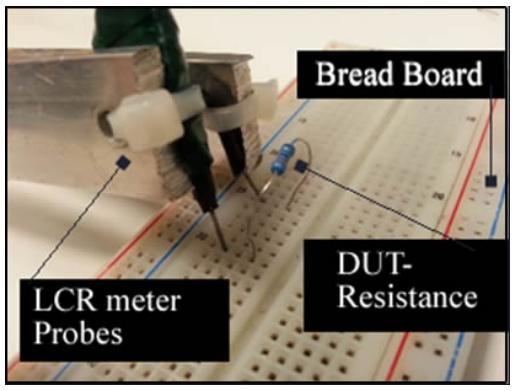

Figure 5.5: Image of resistor connection to probes.

As a result of the impedance measurement for a 433 k Ω resistor, above 80 kHz applied frequency, the impedance of the resistor started to decrease from 433 k Ω to 137 k Ω as shown in Figure 5.6.

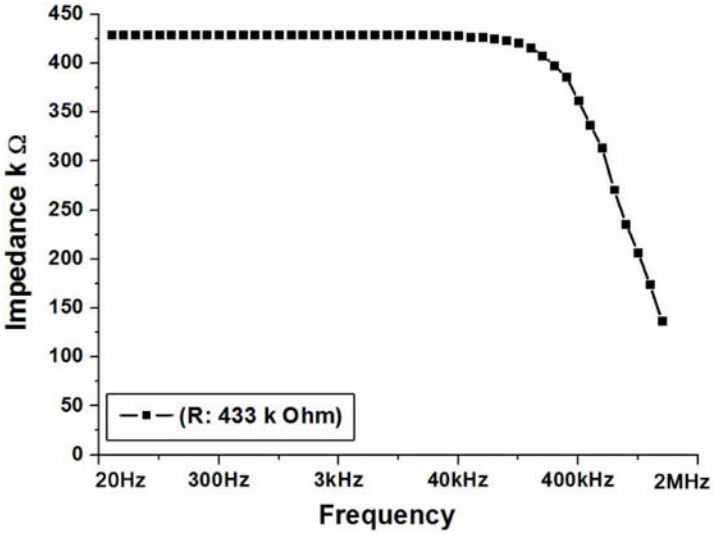

Figure 5.6: Frequency response of impedance for 433 kΩ.

The fall in the impedance was due the frequency response of the stray capacitance which was connected to the resistor in parallel. As the applied frequency increases, the resistance component of the capacitor decreases, which results decrease in the total impedance of the circuit. However, when stray capacitance was connected to the resistor in serial, change in total impedance was not observed. In order to verify this phenomenon, an analytical approach was used. Even though the equivalent impedance is more complicated due to the imaginary part; the impedance change can be imagined using more simplified form of the total impedance as explained in Equation 5.1 below.

Considering stray capacitance connected in parallel to the device under test, total impedance of the circuit can be derived as in the Equation 5.1.

$$Z = \frac{R \cdot Xc}{R + Xc} \tag{5.1}$$

$$Xc = \frac{1}{j\omega c} \tag{5.2}$$

$$\omega = 2\pi f \tag{5.3}$$

where Z total impedance of the circuit, Xc resistance component of the capacitor, excitation frequency of the LCR meter, and ω angular frequency. Let's assume that stray capacitance is 220 μF and resistance is 400 kΩ and applied frequency was 100 Hz. The resistance component of the capacitor became,

$$Xc = \frac{1}{2\pi fC} = \frac{1}{2{\cdot}3{\cdot}100{\cdot}220{\cdot}10^{-6}} = 7.5\Omega \tag{5.4}$$

So that the total impedance becomes 7.49 Ω as calculated in Equation 5.5,

$$Z = \frac{R{\cdot}Xc}{R + Xc} = \frac{400{\cdot}10^3{\cdot}7.5}{400{\cdot}10^3 + 7.5} = 7.49\Omega \tag{5.5}$$

When the applied frequency is increased to 2 MHz, the total impedance decreases as shown in Equation 5.7,

$$Xc = \frac{1}{2\pi fC} = \frac{1}{2{\cdot}3{\cdot}2{\cdot}10^6 220{\cdot}10^{-6}} = 3.7.10^{-4}\Omega \tag{5.6}$$

$$Z = \frac{R{\cdot}Xc}{R + Xc} = \frac{400{\cdot}10^3{\cdot}7.10^{-4}}{400{\cdot}10^3 + 7.10^{-4}} = 3.6.10^{-4}\Omega \tag{5.7}$$

Considering the stray capacitance was connected in serial to the device under test, total impedance of the circuit can be derived as in the Equation 5.8.

$$Z = R + Xc \tag{5.8}$$

At 100 Hz applied frequency, Xc was 7.5 Ω and for 2 MHz, Xc was $3.6.10^{-4}\Omega$. By inserting them into Equation 5.8, the total impedance became around $400{\cdot}10^{3}\Omega$ for both frequencies.

As seen from the results of the analytical calculation of total impedance, connecting the stray capacitor in serial to the resistor has no effect on the total impedance. Hence, the verification of the stray capacitance parallel connection was done. In addition, impedance of the other resistors were measured. However, the dramatic decrease of impedance signals at high frequencies were not observed for both resistors as shown in Figure 5.7 a,b. Due to the complex calculation of the total impedance of the circuit, it is assumed that, the stray capacitance had negligible effect on low resistor than high resistors.

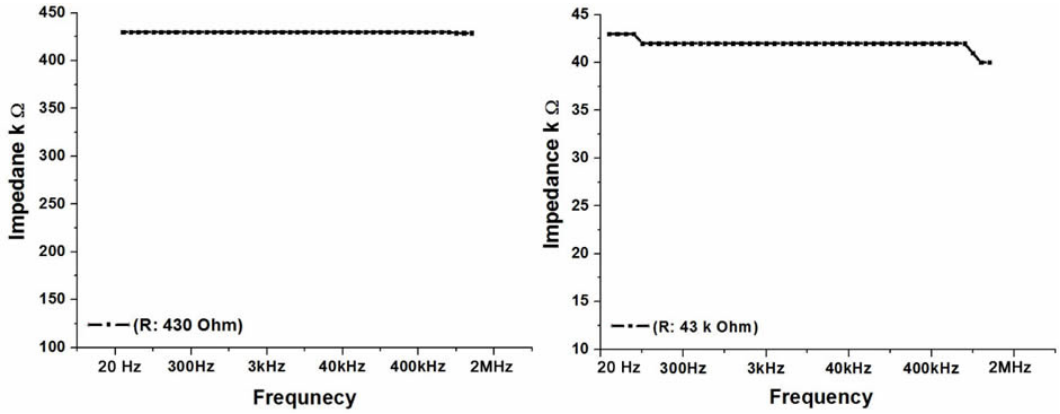

Figure 5.7: Frequency response of impedance for 43 kΩ (a) and 433 Ω (b).

Using the experimental results of the resistor measurements, the stray capacitor was determined using LTspice simulation. In order to do that, the circuit that 433 k resistor and an unknown capacitance in parallel was designed as shown in Figure 5.8. Working frequency range was in between 20 Hz to 2 MHz. The unknown stray capacitance was swept from 200 fF to 900 fF and the simulation was run.

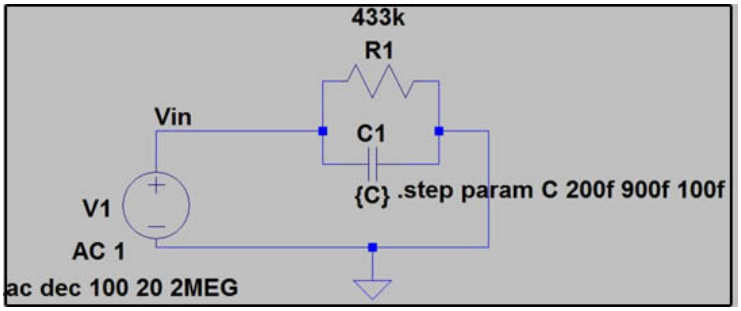

Figure 5.8: Circuit design in the simulation to determine stray capacitance.

Because of the stray capacitance showed up its effect at high frequencies and decreased the total impedance, the capacitance value which gave an identical slope with the experimental results at these frequencies was chosen. Decrease in total impedance of the 433 kΩ resistor connected circuit started at 100 kHz applied frequency as shown in Figure 5.6. Therefore, the capacitance was chosen which started to reduce total impedance at that same frequency. As shown in Figure 5.6, for all stray capacitances, impedance started to decay at 100 kHz. In order to determine which capacitance fits better to experimental results, the capacitance which gave 423 kΩ total impedance at 100 kHz was chosen. As shown in Figure 5.9, 150 fF was the capacitance which approximated to 423 k Ω impedance in the experiment.

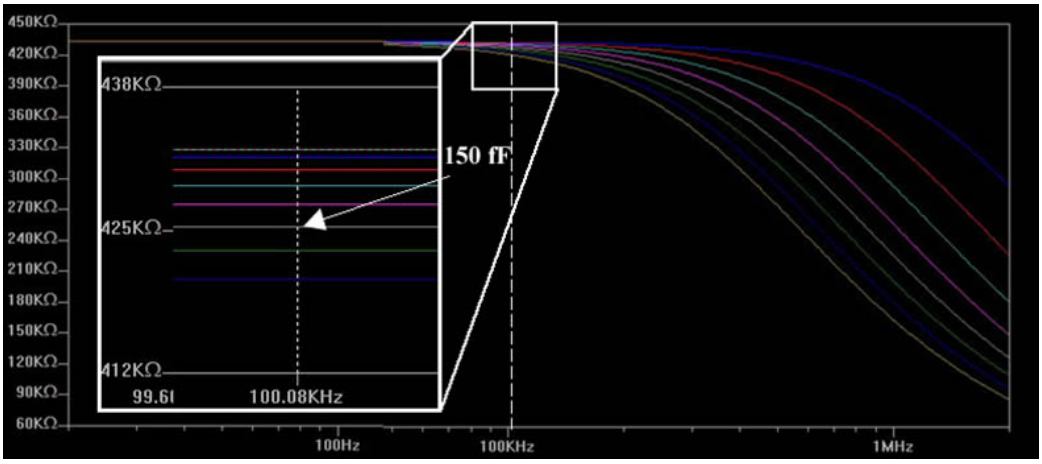

Figure 5.9: Simulation result for stray capacitance.

Then, impedance at the frequencies above 100 kHz were investigated to verify the fitting of the slope of the impedance plot. As shown in Figure 5.10, maximum impedance match with the experimental results was achieved at 150 fF stray capacitance.

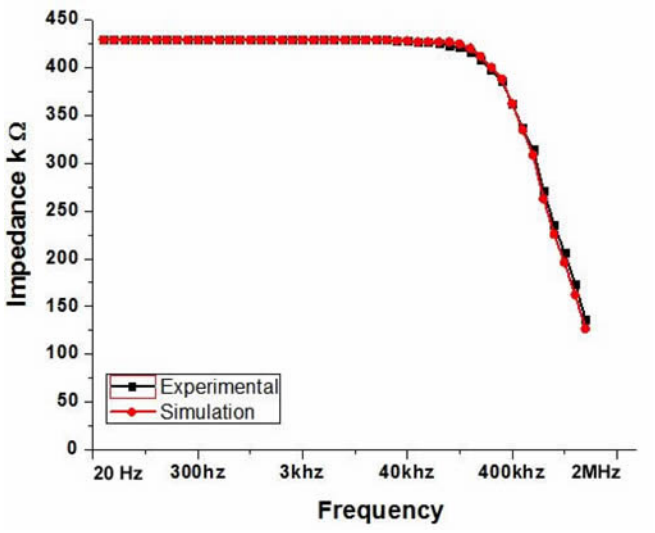

Figure 5.10: Fitting of experimental data with the simulation results for 433 kΩ resistor.

5.2.2 Stray Inductance Measurement

In order to determine a stray inductance that comes from probes of the measurement setup, a 220 μF capacitor was taken as device under test and probes were connected to the resistor in parallel as shown in Figure 5.11. In general, it is known that stray inductance is serial to the device under test. By using same approach that was executed for the stray capacitance measurement, impedance measurement of this circuit was done with the 1 Vp-p applied voltage at 20 Hz to 2 MHz frequency domain.

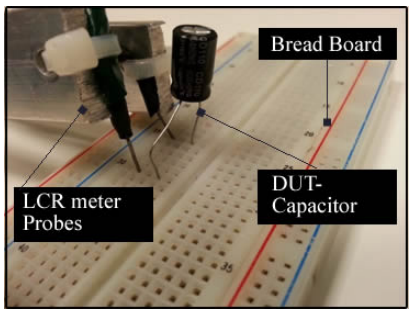

Figure 5.11: Image of capacitor connection to probes.

The experimental results were measured as shown in Figure 5.12. The total impedance of a whole circuit decreased as the applied frequency increased. However, above at a certain frequency, a slight increment of the impedance was observed.

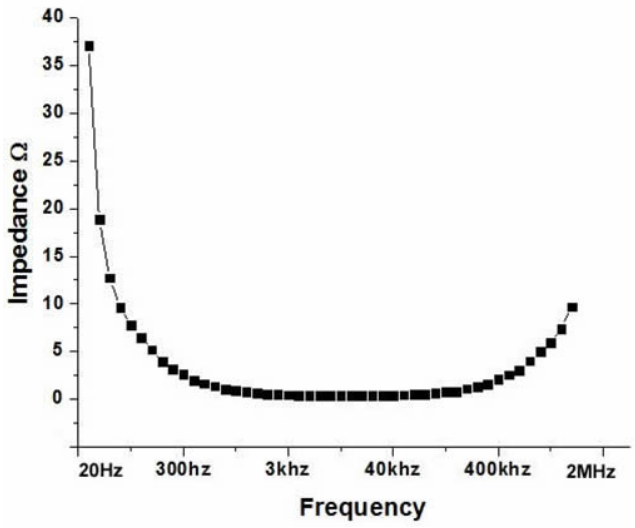

Figure 5.12: Frequency response of impedance for 220 μF.

As result of this increment in the signal, it was assumed that, the inductance connection in the circuit might be in serial to device under test. For the verification of this serial connection, a simple analytical approach was used similar to previous calculation that was run for the stray capacitance. Although the total impedance of such circuit is also complex due to the imaginary part of the impedance, a simple equation was derived for better understanding as explained in below.

Considering the stray inductance was connected in parallel to the device under test, total impedance of the circuit can be derived as in the Equation 5.9.

$$Z = \frac{Xl \cdot Xc}{Xl + Xc} \tag{5.9}$$

$$Xl = J\omega L \tag{5.10}$$

where, Z total impedance of the circuit, Xc resistance component of the stray capacitor, Xl resistance component of the stray inductance, f excitation frequency of the LCR meter, and ω angular frequency. Let's assume that the stray inductance is 100 H, the capacitance was 220 μF. In order to calculate total impedance, resistance component of the inductor and the capacitor (DUT-device under test) are needed to be calculated. Using Equation 5.10 resistance of the inductor for 100 Hz applied frequency,

$$Xl = J\omega L = 2 \cdot \pi \cdot f \cdot L = 2 \cdot 3 \cdot 100 \cdot 100 = 6.10^4 \Omega \tag{5.11}$$

$$Xc = \frac{1}{2\pi fC} = \frac{1}{2 \cdot 3 \cdot 100 \cdot 220 \cdot 10^{-6}} = 7.5\Omega \tag{5.12}$$

So that the total impedance becomes 7.49 Ω as calculated in Equation 5.13,

$$Z = \frac{Xl \cdot Xc}{Xl + Xc} = 7.49\Omega \tag{5.13}$$

When the frequency is increased to 2 MHz, the total impedance becomes,

$$Xl = J\omega L = 2 \cdot \pi \cdot f \cdot L = 2 \cdot 3 \cdot 2.10^6 100 = 12.10^8 \Omega \tag{5.14}$$

$$Xc = \frac{1}{2\pi fC} = \frac{1}{2{\cdot}3{\cdot}2.10^6 220{\cdot}10^{-6}} = 3.7.10^{-4}\Omega \tag{5.15}$$

$$Z = \frac{Xl{\cdot}Xc}{Xl + Xc} = 3.7.10^{-4}\Omega \tag{5.16}$$

Considering the stray inductance was connected in serial to the device under test, total impedance of the circuit can be derived as in the Equation 5.17.

$$Z = Xl + Xc \tag{5.17}$$

At 100 Hz applied frequency Xc was 7.5Ω, Xl was $6.10^8\Omega$ and for 2 MHz, Xl was $12.10^8\Omega$ and Xc was $3.7.10^{-4}\Omega$. By inserting them into Equation (5.17), the total impedance became $6.10^8\Omega$ for 100 Hz and $12.10^8\Omega$ for 2 MHz.

As shown in these equations, when the excitation frequency increased, the impedance increased only if the stray inductance was considered as serial in to circuit. Therefore, in order to obtain the exact value of the stray capacitance, the stray inductance was connected as serial component to the circuit in the LTspice simulation as shown in Figure 5.13. Simulation was run from 20 Hz to 2 MHz and an unknown inductance was swept from 300 nH and 900 nH.

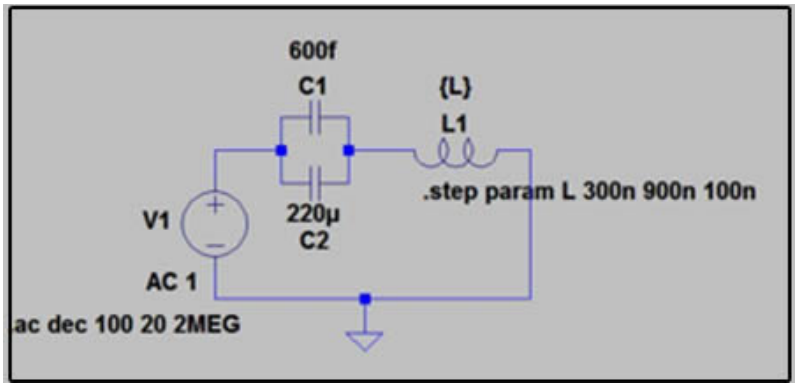

Figure 5.13: Circuit design in the simulation to determine stray inductance.

Since the impedance increases at higher frequencies than 80 kHz as shown in Figure 5.12, to fit the slope of the curve with the experimental curve, impedance at 1 MHz applied frequency was cincestigated for all inductance from 300 nH to 900 nH. Then, at this frequency, the inductance was chosen which gave identical slope with the experimental.

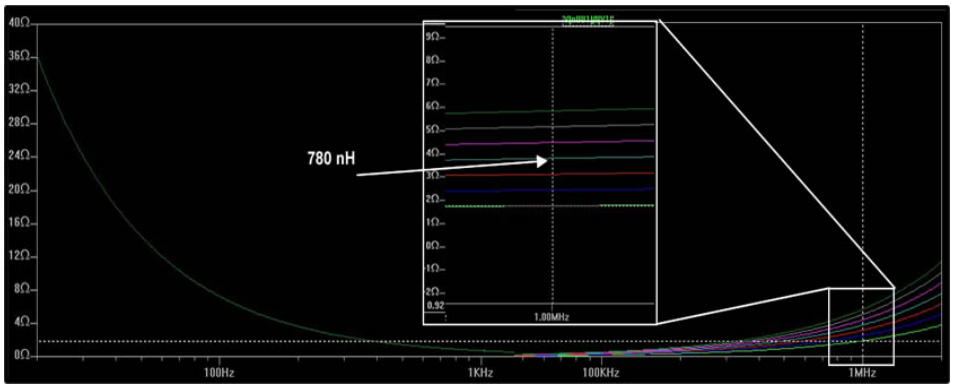

Figure 5.14: Simulation result for stray capacitance.

As shown in Figure 5.14, best results were achieved at 780 nH stray inductance and there was a small deviation between the experimental and simulation results.

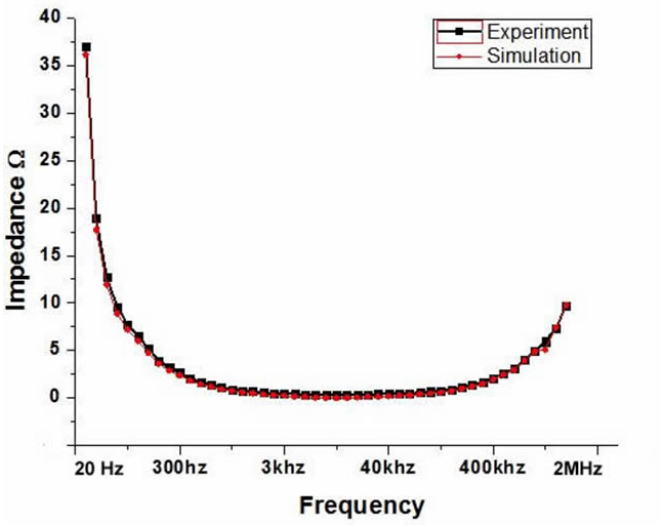

Figure 5.15: Fitting of experimental data with the simulation results for 220 μF capacitor.

As a result of these measurements, probes of the measurement setup had a 150 fF stray capacitance in parallel and a 780 nH stray inductance in serial to the device under test as shown in Figure 5.16.

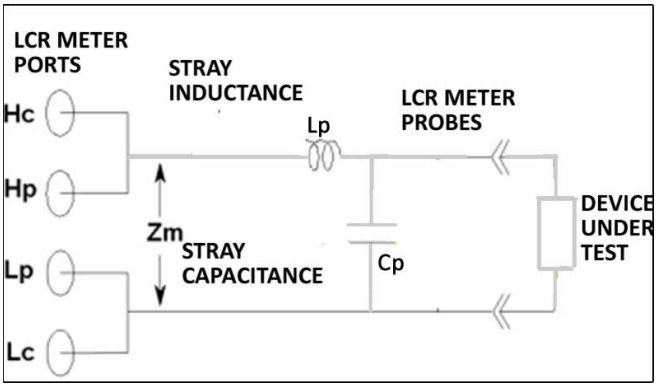

Figure 5.16: Schematic of final circuit design of LCR Meter.

5.3 Determining Electrical Properties of Solutions

In order to investigate agglutination reaction in droplets, silicone oil, various antibody sera, and whole blood sample were used as reagents in the channel. In order to model these reagents as an electrical circuit components, Lumped parameter model for electrolyte-electrode interaction was used. Based on this approach, firstly, impedance measurements of these reagents under flow in different channels were executed. Using the results of the measurements, components of the model were derived.

5.3.1 Modelling Silicone Oil in Channel

As it is mentioned at the beginning of this chapter, in order to model an aqueous solution impedance in the microchannel, the solution is generally modelled as

RC circuit. To model silicone oil as an electrical component, an RC circuit was designed in the model. Estimation of the circuit components, was done by first measuring impedance of the silicone oil in the channel. During impedance measurement, the microchannel was exposed to continuous flow of silicone oil. 1 Vp-p was applied to microelectrodes, and the measurement frequency was in between 150 Hz to 2 MHz. Since the model included a capacitance component, the impedance of the silicone oil was dependent on the applied frequency. By looking the response of the capacitor to these frequencies, estimation of the components in the model could be derived. As shown in Figure 5.17, at the high frequencies, a decrement from 6 G Ω to 519 k Ω in the impedance was observed.

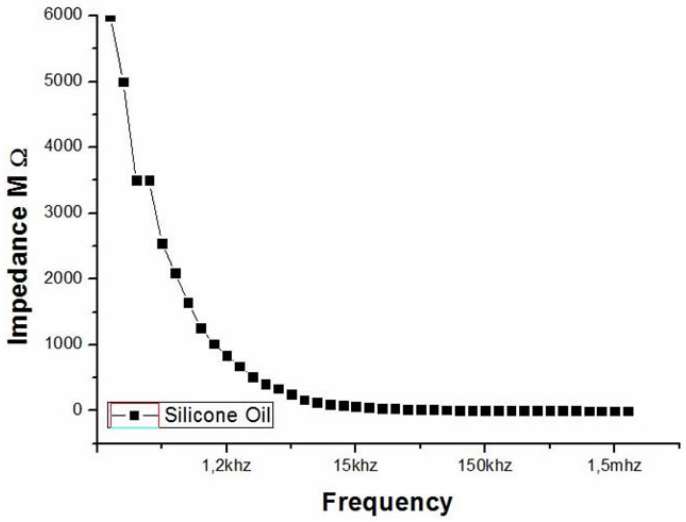

Figure 5.17: Frequency response of silicone oil impedance in microchannel.

Before determining the R, C component of silicone oil, an electrical double layer that is formed on the electrodes due to the ion polarization in the presence of the electric field was investigated. The capacitance of this layer was approximated close to the value that is given in the literature [84]. As shown in the model in Figure 5.18.a, the capacitance of this layer was determined as 100 pF. In addition the capacitance of the bulk solution was also approximated as 10 fF. By sweeping the resistance component in the circuit from 5 G Ω to 40 G Ω at frequencies between 150 Hz to 2 MHz, the total impedance of the circuit was tried to fit to experimental data for each applied frequency. As shown in Figure 5.18.b, the best results were achieved with 25 G Ω resistor.

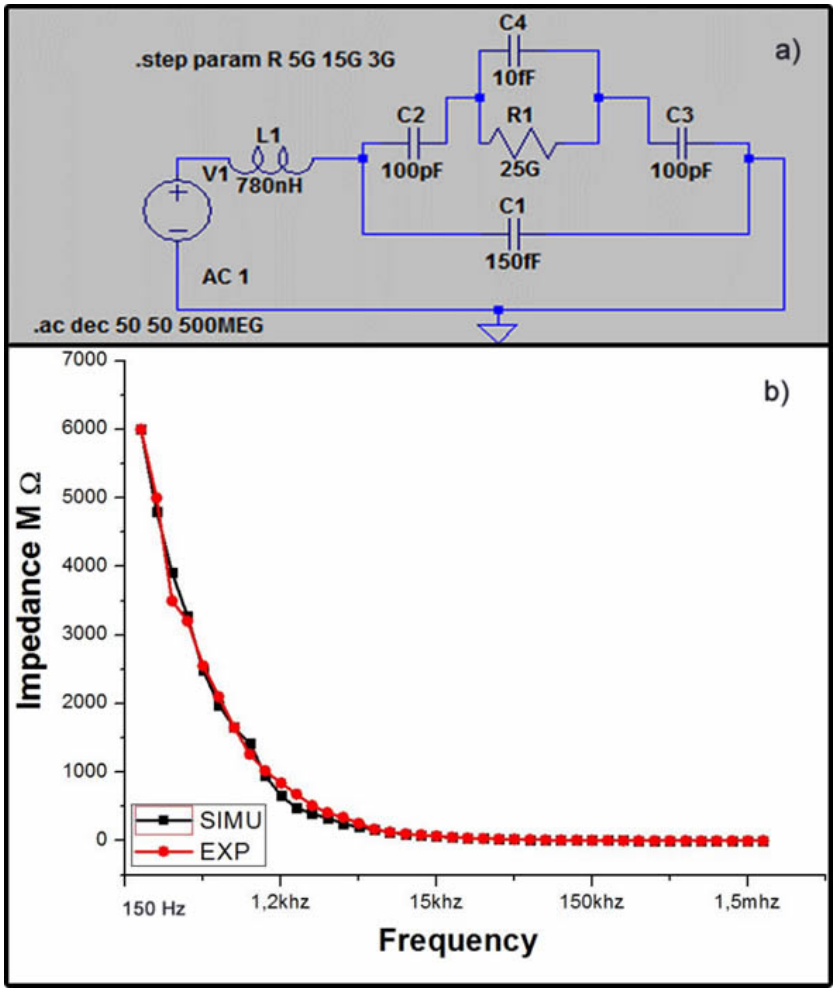

Figure 5.18: Circuit design for silicone oil in the simulation (a) and fitting results (b).

5.3.2 Modelling Antibody Serum in Channel

By applying same measurement method that was used for silicone oil, the measurement of antibody serum in microchannel was done. For this measurement, only one of the antibody serum type (Anti-B) was loaded in to channel. The measurement was done by applying 1 Vp-p AC signal at different frequencies. As shown in Figure 5.19, impedance of the whole circuit decayed at high frequencies as a result of RC circuit.

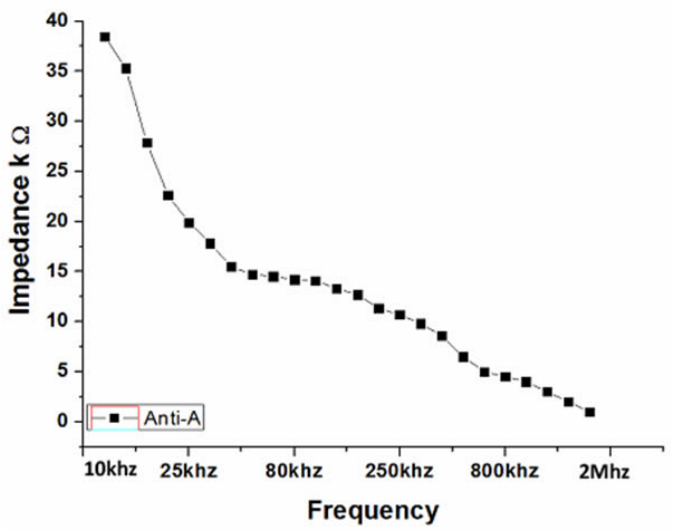

Figure 5.19: Frequency response of antibody sera impedance in microchannel.

Before extracting the R and C component that belong to antibody serum, an electrical double layer on the electrode surface was needed to be determined. Because of the electrical double layer material dependent property, when the solution is changed, the thickness of the diffuse and stern layer changes automatically. As a result of these changes, the electrical double layer capacitance changes. So that, the electrical double layer that was used for the silicone oil was not used in this model. Based on the conductivity and the permittivity of the antigen solution, the electrical double layer of an antibody serum was determined as 800 pF as shown in Figure 5.20. Afterwards, R and C components were swept from 5 k Ω to 30 k Ω and from 100 pF to 900 pF respectively. However, output impedance of the circuit in the simulation was far from the experimental results at high frequencies. Then, the simulation was run at capacitance from 1 fF and 100 fF. Best result that fits with the experimental data was achieved at 10 k Ω resistance and 25 pF capacitance as shown in Figure 5.20.

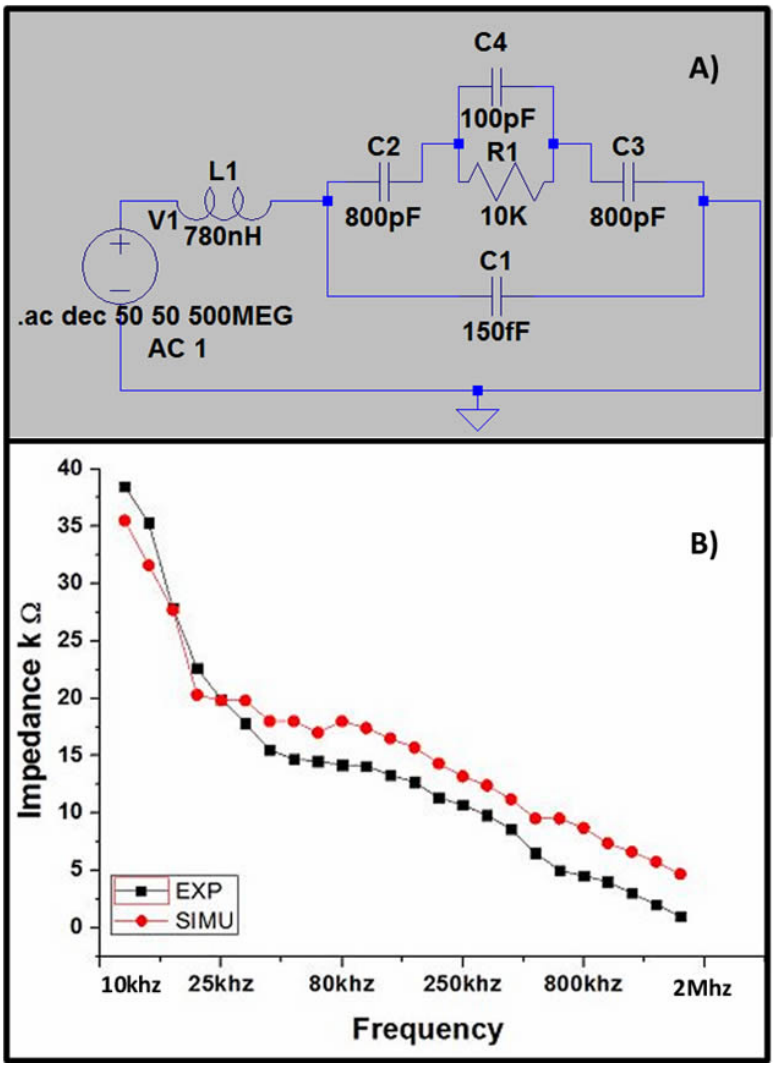

Figure 5.20: Circuit design for antibody sera in the simulation (a) and fitting results (b).

5.3.3 Conclusion

Based on the simulation results for the solutions in the channel, optimum working frequency was determined for impedimetric measurement. In order to do that, conductivity of the solutions that is used in the channel were searched. Based on the conductivity results, the resistance of the solutions were calculated as explained in the Equations 5.18, 5.19 and 5.20.

$$S_{oil} = 10.10^{-4} S/m \tag{5.18}$$

$$S_{antibody} = 1 S/m \tag{5.19}$$

$$R = \frac{\rho.l}{A}, \rho = \frac{A.R}{l} \tag{5.20}$$

where S_{oil}, $S_{antibody}$ are the conductivities of the silicone oil and antibody serum respectively. As shown in Equation 5.20 as the conductivity increases, the resistance of the material should decrease. Based on the given values in the literature, conductivity of the antibody serum is a thousand times higher than silicone oil. So that, the resistance of the silicone oil should be 1000 folds of the resistance of antibody serum. By looking the impedance values of the silicone oil and the antibody serum in the experimental data, 1000 fold difference between these solutions was achieved at around 100 kHz. Therefore, the impedance measurement of the entire experiment was run at 100 kHz applied voltage. Hence, by checking the impedance of silicone oil at 100 kHz during an experiment, reliability of the measurement was controlled one more time.

In addition, before modelling the droplet in the channel, it is important to mention the effect of the electrical double layer that was formed. At low frequencies, impedance of the ionic solution in the sensing region is dominated by the electrical double layer. As the excitation frequency increases the solution resistance becomes more dominated as shown in Figure 5.21. Therefore, the simulation and experiments were done between 50 kHz to 2 MHz frequency domain.

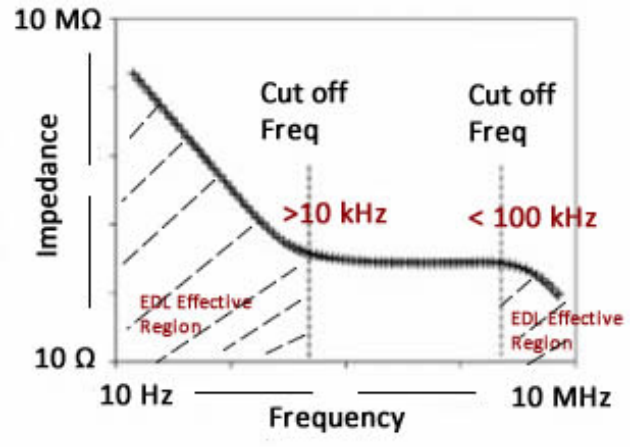

Figure 5.21: Frequency response of analytes impedance in the channel based on the EDL formation.

5.4 Modelling of Droplets in Microchannel

Single cell analysis in a microchannel that involves the lumped parameter model has been investigated very well. Sun et.al. [64] have shown that, an equivalent circuit of the single cell includes a capacitance of cell membrane, resistance and capacitance of cytoplasm of the cell as shown in Figure 5.1. Based on this model, a single droplet was simulated like a single cell in the channel as explained in the introduction part of this section. So that, in the equivalent circuit, a single droplet model was including membrane capacitance, resistance and capacitance of the solution inside the droplet as shown in Figures 5.2, 5.3, 5.4.

5.4.1 Modelling Antibody Serum Droplet in Channel

Equivalent circuit model of antigen solution droplet was designed in LTspice software as shown in Figure 5.22.

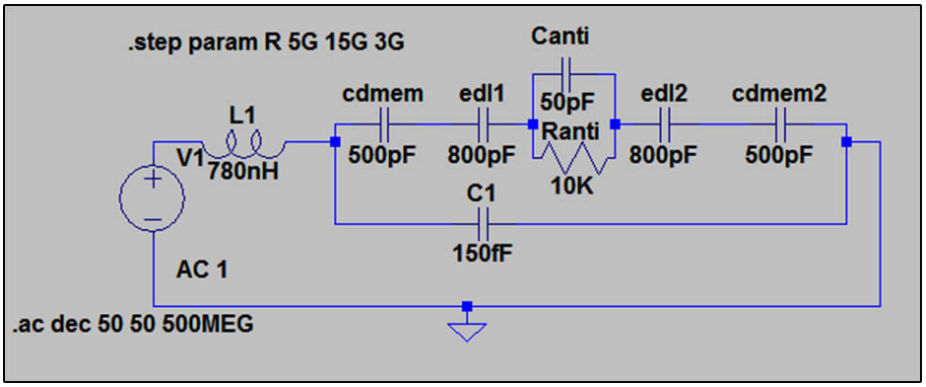

Figure 5.22: Circuit design for antibody sera droplet in the simulation.

The membrane capacitance was determined based on the capacitance of the electrical double layer. As the thickness of the dielectric material between parallel plate increases, the capacitance decreases. It was assumed that the thickness of the droplet membrane was much thicker than the electrical double layer that is formed on electrodes. Therefore, capacitance of the droplet membrane is less than capacitance of the electrical double layer that is derived in previous simulation in section 5.3.2. was used. Because of the material in contact with electrodes was antigen solution, the capacitance of the double electrical layer and R and C components were kept same as the capacitance in the previous simulation. In addition, while designing a circuit, the parasitic capacitance and inductance were included in circuit in order to achieve more realistic simulation that resembles the empirical environment. Experiment was done by generating only antigen droplets in the channel that were surrounded with silicone oil. Because of the experimental data were recorded at 50 kHz to 2 MHz applied frequencies, fitting of the simulation was done between this frequencies in the simulation. By sweeping the membrane capacitance, R and C in an order, the output impedance was fit with experimental data as shown in Figure 5.23. The droplet membrane capacitance was determined as 500 pF. Standard deviation was extracted based on the maximum and minimum impedance of two droplets.

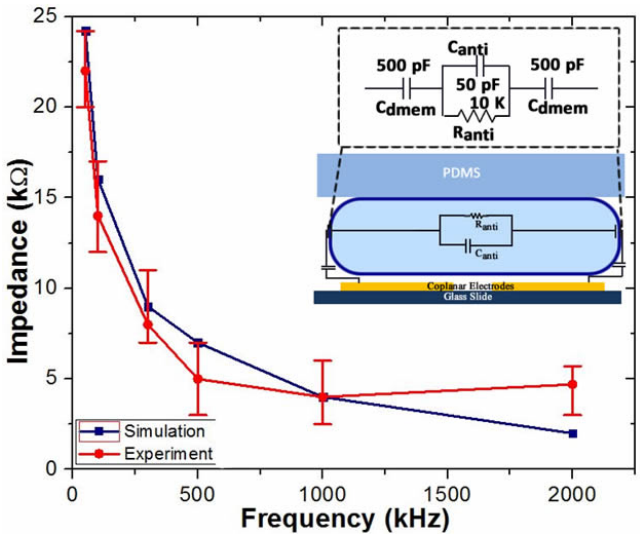

Figure 5.23: Impedance fitting of antibody serum droplet.

5.4.2 Modelling Whole Blood Droplet in Channel

In order to simulate whole blood droplet, the same single cell equivalent circuit model was applied. Only whole blood droplets were formed in the channel and impedance data were collected. Then simulation was designed. Since the whole blood droplet includes many individual cells inside, designing every single cell in droplet as R and C components and connecting them as a serial connections would be hard to simulate. Therefore, it was approximated the blood sample as a homogeneous solution like an antibody serum in droplet. So that, whole blood droplet included only R and C components in the circuit as shown in Figure 5.24. Because of the droplets were surrounded by silicone oil, the membrane capacitance of the whole blood droplet was kept same capacitance as in the antibody serum droplet simulation.

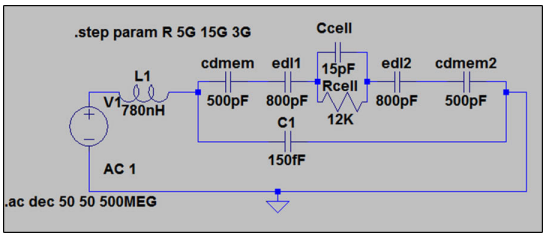

Figure 5.24: Circuit design for whole blood droplet in the simulation.

As shown in the Figure 5.24, since the whole blood is less conductive material than antibody serum, the whole blood resistance was determined as more resistive component than antibody serum resistance in circuit. In addition, from measurement that was executed for the single red blood cell on the channel, it was observed that, the capacitance decreases in the channel when the cell passed over electrodes. Therefore, the capacitance component was determined less than antibody serum droplet. By sweeping R and C component respectively, resistance and capacitance were determined as 12 kΩ and 50 pF, which fit the experimental data as shown in Figure 5.25.

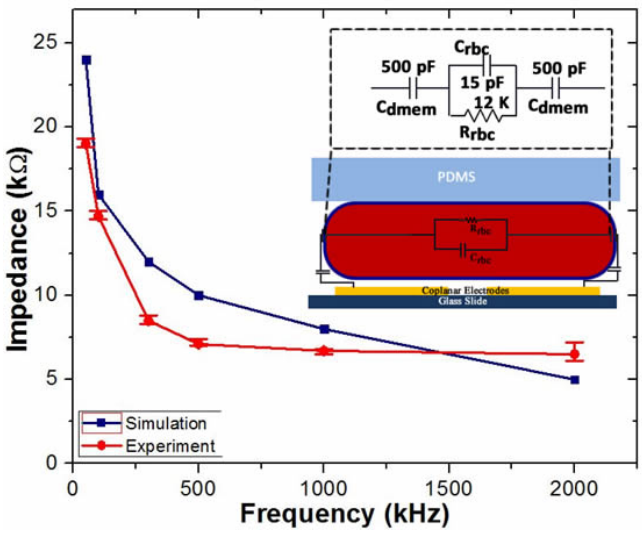

Figure 5.25: Impedance fitting of whole blood droplet.

5.4.3 Modelling Plasma in Droplet in Channel

After the agglutination reaction occurs, all RBC's release the plasma as explained in the section (formation). This antibody solution-PBS mixture was modelled as shown in Figure 5.26.

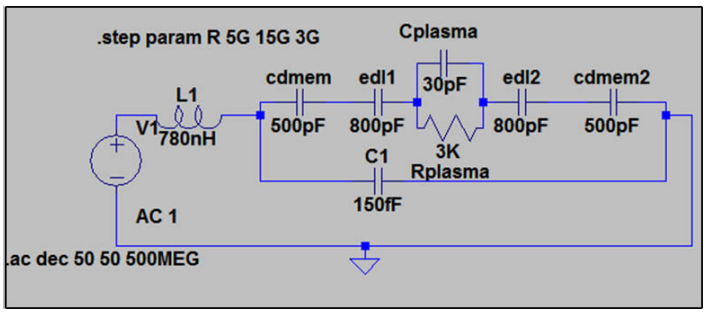

Figure 5.26: Circuit design for antibody sera and PBS mixture part in the simulation.

Based on the experimental results that were done for the agglutinated droplets at the frequencies between the 50 kHz to 2 MHz, it was observed that impedance of the antibody serum droplet was close to antibody solution-PBS mixture part in the droplet as shown in the Figure 4.9. So that the capacitance and resistance was kept close to the components in the antibody serum droplet simulation. Then, the R and C component was swept respectively; the best fitting results were achieved at 3 kΩ and 30 pF as shown in Figure 5.27.

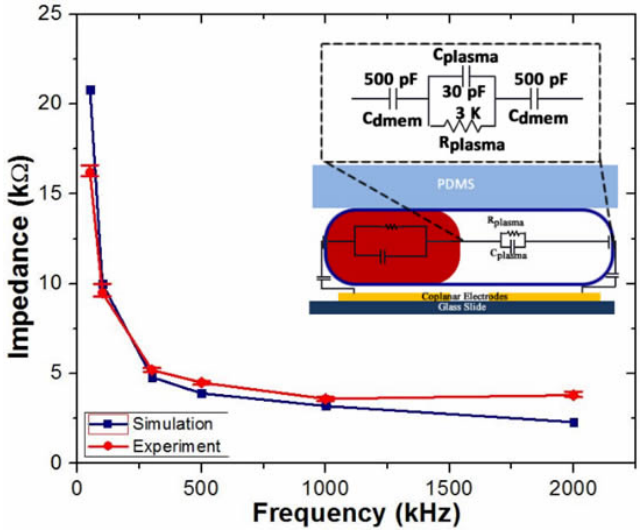

Figure 5.27: Impedance fitting of antibody sera and PBS mixture part of agglutinated blood droplet.

5.4.4 Modelling Agglutinated RBCs Droplet in Channel

In agglutination reaction, when RBC's binds to antibody serum, accumulation of every single cell occurs and clusters of the RBC's formed as explained in section 4.2.2. As explained in section 4.3, as the clusters entered in the detection region, increment in the impedance was observed. In order to understand this analytical phenomenon behind the change in the signal, it is important to estimate the values of the component in the equivalent circuit that comes from the cluster of cells. So that, it can be said that the detection system which is sensitive enough to measure that order of the resistance and capacitance in droplet, can detect the other type of agglutination reactions in droplet. Since the impedance reached its maximum level when the clusters entered the detection region, in order to estimate the R and C components, the peak in the impedance signal was investigated. Therefore, it was assumed that the resistance of the cluster should be higher than whole blood droplet resistance. Hence, the circuit was designed as shown in Figure 5.28.

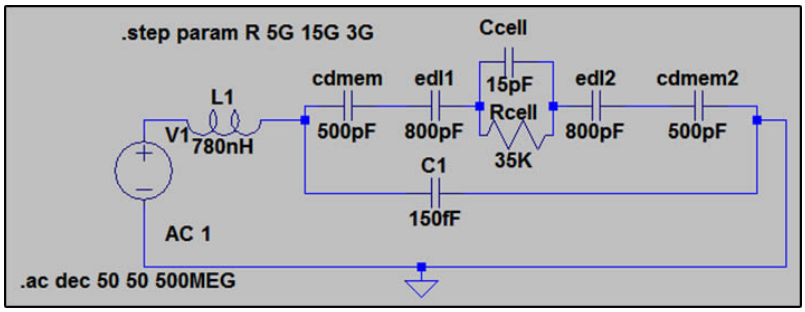

Figure 5.28: Circuit design for cluster part of agglutinated droplet in the simulation.

Because of the resistance of the clusters are dominant in the signal, by sweeping the R component in the circuit, output impedance was tried fitting with the experimental data for the frequencies between 50 kHz to 2 MHz. As shown in Figure 5.29, best result was achieved at 35 kΩ cluster resistance.

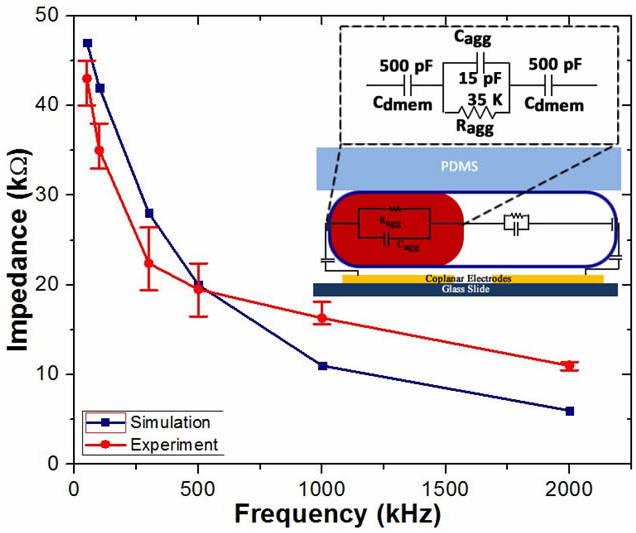

Figure 5.29: Impedance fitting of cluster part of agglutinated blood droplet.

5.5 Conclusion

In conclusion, each state of droplets in the reaction was modelled. In addition, the stray capacitance and inductance were extracted and were modelled in the simulation and optimum working frequency was determined as 100 kHz. Model of non-agglutinated droplet was not executed due to the similarity to whole blood droplet impedance result in the experimental study.

Chapter 6

Conclusions

6.1 Conclusion

In this study a microfluidic device to measure agglutination reaction in a droplet impedimetrically was developed. In order to form droplets several microfluidic chip designs and modification methods were developed. Without using any costly chemicals to modify the PDMS surface, hydrophobic treatment of the PDMS surface was achieved with a simple method. By using this treatment, droplet formation was accomplished using T-junction channel design. With the adjustment of the pressure, droplets formation and merging in the channel synchronously were completed in an automated way. Contents of merged droplets were mixed without using any external stimulator in the channel. Then impedance of droplets was measure to detect the agglutination reaction by using an LCR Meter. Moreover, effect of bias voltage that is applied on coplanar electrodes was demonstrated. In addition, effect of different concentrations of blood samples on the impedance signal was evaluated. Increase in applied voltage caused to increase shielding of ions which resulted adhesion of cells on electrodes. The concentration changes of blood sample did not show significant difference on impedance signals. Moreover, an equivalent circuit simulation of the microfluidic device was done. Based on the experimental results, components of circuits were achieved. Hence, an

impedimetric detection of any kind of agglutination reaction in droplets can be modelled by taking the components of this model as references.

6.2 Future Work

In order to realize a lab on a chip system, bulk components that are required to run an experiment in the microfluidic device is needed to replace with hand-held systems. For example, instead of using an LCR Meter for the measurement, a hand-held electronic device can be designed to measure impedance which is also enough to excite high frequencies.

As mentioned in chapter 5 stray capacitance and inductance have effect on the measurement system. In this study the effects of these capacitance and inductance were not cancelled. It is believed that, by designing a hand-held circuit which cancels the stray capacitance and inductance may improves the sensitivity of the system.

Since blood is the valuable source to diagnostic; other applications for blood related diseases that is assayed by agglutination reaction can be modelled and measured. In addition, not only agglutination based reaction can be detected but also variety of applications such as cell growth in droplet, protein crystallization in droplet can be applied to this system.

6.3 Contributions

This project was presented in one national and one international conference.

[1] M.Marcali, C.Elbuken, Impedimetric detection of agglutination reaction inside microfluidic droplets, Microfluidics, Physics and Chemistry of Microscale Technology for Advancing and Translating Discovery, Mount Snow, VT, USA, 31 May-5 June 2015 (poster)

[2] M. Marcali, C. Elbuken, Automated detection of blood type inside microfluidic droplets, 2nd International Congress on Biosensors ,Izmir, Turkey, 10-12 June 2015 (oral presentation)

[3] M.Marcali, C.Elbuken Impedimetric detection and lumped-element modelling of hemagglutination assay in microdroplets , Lab on a Chip (in preparation)

Bibliography

[1] M. Golay, "Vapor phase chromatography and telegrapher's equation," *Analytical Chemistry*, vol. 29, no. 6, pp. 928–932, 1957.

[2] S. C. Terry, J. H. Jerman, and J. B. Angell, "A gas chromatographic air analyzer fabricated on a silicon wafer," *Electron Devices, IEEE Transactions on*, vol. 26, no. 12, pp. 1880–1886, 1979.

[3] R. A. Mathies and X. C. Huang, "Capillary array electrophoresis: an approach to high-speed, high-throughput dna sequencing," *Nature*, vol. 359, no. 6391, pp. 167–169, 1992.

[4] H. A. Stone, A. D. Stroock, and A. Ajdari, "Engineering flows in small devices: microfluidics toward a lab-on-a-chip," *Annu. Rev. Fluid Mech.*, vol. 36, pp. 381–411, 2004.

[5] L. Shui, J. C. Eijkel, and A. van den Berg, "Multiphase flow in microfluidic systems–control and applications of droplets and interfaces," *Advances in Colloid and Interface Science*, vol. 133, no. 1, pp. 35–49, 2007.

[6] C. N. Baroud, F. Gallaire, and R. Dangla, "Dynamics of microfluidic droplets," *Lab on a Chip*, vol. 10, no. 16, pp. 2032–2045, 2010.

[7] H. A. Stone, "Dynamics of drop deformation and breakup in viscous fluids," *Annual Review of Fluid Mechanics*, vol. 26, no. 1, pp. 65–102, 1994.

[8] P. Guillot, A. Colin, A. S. Utada, and A. Ajdari, "Stability of a jet in confined pressure-driven biphasic flows at low reynolds numbers," *Physical review letters*, vol. 99, no. 10, p. 104502, 2007.

[9] R. Derda, A. Laromaine, A. Mammoto, S. K. Tang, T. Mammoto, D. E. Ingber, and G. M. Whitesides, "Paper-supported 3d cell culture for tissue-based bioassays," *Proceedings of the National Academy of Sciences*, vol. 106, no. 44, pp. 18457–18462, 2009.

[10] X. Li, D. R. Ballerini, and W. Shen, "A perspective on paper-based microfluidics: current status and future trends," *Biomicrofluidics*, vol. 6, no. 1, p. 011301, 2012.

[11] M. Zimmermann, H. Schmid, P. Hunziker, and E. Delamarche, "Capillary pumps for autonomous capillary systems," *Lab on a Chip*, vol. 7, no. 1, pp. 119–125, 2007.

[12] H.-H. Shen, S.-K. Fan, C.-J. Kim, and D.-J. Yao, "Ewod microfluidic systems for biomedical applications," *Microfluidics and Nanofluidics*, vol. 16, no. 5, pp. 965–987, 2014.

[13] R. Seemann, M. Brinkmann, T. Pfohl, and S. Herminghaus, "Droplet based microfluidics," *Reports on progress in physics*, vol. 75, no. 1, p. 016601, 2012.

[14] J. Xu, S. Li, J. Tan, Y. Wang, and G. Luo, "Preparation of highly monodisperse droplet in a t-junction microfluidic device," *AIChE journal*, vol. 52, no. 9, pp. 3005–3010, 2006.

[15] C. Priest, S. Herminghaus, and R. Seemann, "Generation of monodisperse gel emulsions in a microfluidic device," *Applied physics letters*, vol. 88, no. 2, p. 024106, 2006.

[16] S. L. Anna, N. Bontoux, and H. A. Stone, "Formation of dispersions using flow focusing in microchannels," *Applied physics letters*, vol. 82, no. 3, pp. 364–366, 2003.

[17] L. Yobas, S. Martens, W.-L. Ong, and N. Ranganathan, "High-performance flow-focusing geometry for spontaneous generation of monodispersed droplets," *Lab on a Chip*, vol. 6, no. 8, pp. 1073–1079, 2006.

[18] R. Ahmed and T. Jones, "Dispensing picoliter droplets on substrates using dielectrophoresis," *Journal of electrostatics*, vol. 64, no. 7, pp. 543–549, 2006.

[19] T. Jones, "Liquid dielectrophoresis on the microscale," *Journal of Electrostatics*, vol. 51, pp. 290–299, 2001.

[20] K. Wang, T. Jones, and A. Raisanen, "Dynamic control of dep actuation and droplet dispensing," *Journal of Micromechanics and Microengineering*, vol. 17, no. 1, p. 76, 2007.

[21] I. Moon and J. Kim, "Using ewod (electrowetting-on-dielectric) actuation in a micro conveyor system," *Sensors and Actuators A: physical*, vol. 130, pp. 537–544, 2006.

[22] J.-M. Roux, Y. Fouillet, and J.-L. Achard, "3d droplet displacement in microfluidic systems by electrostatic actuation," *Sensors and Actuators A: Physical*, vol. 134, no. 2, pp. 486–493, 2007.

[23] J. Lee, H. Moon, J. Fowler, T. Schoellhammer, and C.-J. Kim, "Electrowetting and electrowetting-on-dielectric for microscale liquid handling," *Sensors and Actuators A: Physical*, vol. 95, no. 2, pp. 259–268, 2002.

[24] Y.-C. Tan, J. S. Fisher, A. I. Lee, V. Cristini, and A. P. Lee, "Design of microfluidic channel geometries for the control of droplet volume, chemical concentration, and sorting," *Lab on a Chip*, vol. 4, no. 4, pp. 292–298, 2004.

[25] D. N. Adamson, D. Mustafi, J. X. Zhang, B. Zheng, and R. F. Ismagilov, "Production of arrays of chemically distinct nanolitre plugs via repeated splitting in microfluidic devices," *Lab on a Chip*, vol. 6, no. 9, pp. 1178–1186, 2006.

[26] L. Ménétrier-Deremble and P. Tabeling, "Droplet breakup in microfluidic junctions of arbitrary angles," *Physical Review E*, vol. 74, no. 3, p. 035303, 2006.

[27] T. H. Ting, Y. F. Yap, N.-T. Nguyen, T. N. Wong, J. C. K. Chai, and L. Yobas, "Thermally mediated breakup of drops in microchannels," *Applied Physics Letters*, vol. 89, no. 23, p. 234101, 2006.

[28] Y. Hong and F. Wang, "Flow rate effect on droplet control in a co-flowing microfluidic device," *Microfluidics and Nanofluidics*, vol. 3, no. 3, pp. 341–346, 2007.

[29] T. Wilhelm *et al.*, "Surface-induced droplet fusion in microfluidic devices," *Lab on a Chip*, vol. 7, no. 8, pp. 984–986, 2007.

[30] W.-H. Tan and S. Takeuchi, "Timing controllable electrofusion device for aqueous droplet-based microreactors," *Lab on a Chip*, vol. 6, no. 6, pp. 757–763, 2006.

[31] D. R. Link, E. Grasland-Mongrain, A. Duri, F. Sarrazin, Z. Cheng, G. Cristobal, M. Marquez, and D. A. Weitz, "Electric control of droplets in microfluidic devices," *Angewandte Chemie International Edition*, vol. 45, no. 16, pp. 2556–2560, 2006.

[32] K. Ahn, C. Kerbage, T. P. Hunt, R. Westervelt, D. R. Link, and D. Weitz, "Dielectrophoretic manipulation of drops for high-speed microfluidic sorting devices," *Applied Physics Letters*, vol. 88, no. 2, pp. 24104–24104, 2006.

[33] A. A. Deshmukh, D. Liepmann, and A. P. Pisano, "Characterization of a micro-mixing, pumping, and valving system," in *Proc. Transducers 01, 11th Int. Conf. on Solid-State Sensors and Actuators (Munich, Germany)*, pp. 779–82, 2001.

[34] A. A. Deshmukh, D. Liepmann, and A. P. Pisano, "Continuous micromixer with pulsatile micropumps," in *Technical Digest of the IEEE Solid State Sensor and Actuator Workshop (Hilton Head Island, SC)*, vol. 736, 2000.

[35] H. H. Bau, J. Zhong, and M. Yi, "A minute magneto hydro dynamic (mhd) mixer," *Sensors and Actuators B: Chemical*, vol. 79, no. 2, pp. 207–215, 2001.

[36] J. West, B. Karamata, B. Lillis, J. P. Gleeson, J. Alderman, J. K. Collins, W. Lane, A. Mathewson, and H. Berney, "Application of magnetohydrodynamic actuation to continuous flow chemistry," *Lab on a Chip*, vol. 2, no. 4, pp. 224–230, 2002.

[37] D.-W. Oh, J. S. Jin, J. H. Choi, H.-Y. Kim, and J. S. Lee, "A microfluidic chaotic mixer using ferrofluid," *Journal of Micromechanics and Microengineering*, vol. 17, no. 10, p. 2077, 2007.

[38] B. KrishnaáJuluri, T. JunáHuang, *et al.*, "A millisecond micromixer via single-bubble-based acoustic streaming," *Lab on a Chip*, vol. 9, no. 18, pp. 2738–2741, 2009.

[39] A. E. Kamholz, B. H. Weigl, B. A. Finlayson, and P. Yager, "Quantitative analysis of molecular interaction in a microfluidic channel: the t-sensor," *Analytical Chemistry*, vol. 71, no. 23, pp. 5340–5347, 1999.

[40] A. A. S. Bhagat and I. Papautsky, "Enhancing particle dispersion in a passive planar micromixer using rectangular obstacles," *Journal of Micromechanics and Microengineering*, vol. 18, no. 8, p. 085005, 2008.

[41] M. R. Bringer, C. J. Gerdts, H. Song, J. D. Tice, and R. F. Ismagilov, "Microfluidic systems for chemical kinetics that rely on chaotic mixing in droplets," *Philosophical Transactions of the Royal Society of London A: Mathematical, Physical and Engineering Sciences*, vol. 362, no. 1818, pp. 1087–1104, 2004.

[42] T. Hatakeyama, D. L. Chen, and R. F. Ismagilov, "Microgram-scale testing of reaction conditions in solution using nanoliter plugs in microfluidics with detection by maldi-ms," *Journal of the American Chemical Society*, vol. 128, no. 8, pp. 2518–2519, 2006.

[43] B. T. Lau, C. A. Baitz, X. P. Dong, and C. L. Hansen, "A complete microfluidic screening platform for rational protein crystallization," *Journal of the American Chemical Society*, vol. 129, no. 3, pp. 454–455, 2007.

[44] P. J. Hung, P. J. Lee, P. Sabounchi, N. Aghdam, R. Lin, and L. P. Lee, "A novel high aspect ratio microfluidic design to provide a stable and uniform microenvironment for cell growth in a high throughput mammalian cell culture array," *Lab on a Chip*, vol. 5, no. 1, pp. 44–48, 2005.

[45] H. N. Joensson, M. L. Samuels, E. R. Brouzes, M. Medkova, M. Uhlén, D. R. Link, and H. Andersson-Svahn, "Detection and analysis of low-abundance cell-surface biomarkers using enzymatic amplification in microfluidic droplets," *Angewandte Chemie*, vol. 121, no. 14, pp. 2556–2559, 2009.

[46] F. Xu, P. Datta, H. Wang, S. Gurung, M. Hashimoto, S. Wei, J. Goettert, R. L. McCarley, and S. A. Soper, "Polymer microfluidic chips with integrated waveguides for reading microarrays," *Analytical chemistry*, vol. 79, no. 23, pp. 9007–9013, 2007.

[47] P. Liu, T. S. Seo, N. Beyor, K.-J. Shin, J. R. Scherer, and R. A. Mathies, "Integrated portable polymerase chain reaction-capillary electrophoresis microsystem for rapid forensic short tandem repeat typing," *Analytical chemistry*, vol. 79, no. 5, pp. 1881–1889, 2007.

[48] P. S. Dittrich and A. Manz, "Lab-on-a-chip: microfluidics in drug discovery," *Nature Reviews Drug Discovery*, vol. 5, no. 3, pp. 210–218, 2006.

[49] T. Masadome, K. Yada, and S.-i. Wakida, "Microfluidic polymer chip integrated with an isfet detector for cationic surfactant assay in dental rinses," *Analytical sciences*, vol. 22, no. 8, pp. 1065–1069, 2006.

[50] P. Truman, P. Uhlmann, and M. Stamm, "Monitoring liquid transport and chemical composition in lab on a chip systems using ion sensitive fet devices," *Lab on a Chip*, vol. 6, no. 9, pp. 1220–1228, 2006.

[51] D. J. Shirale, M. A. Bangar, W. Chen, N. V. Myung, and A. Mulchandani, "Effect of aspect ratio (length: diameter) on a single polypyrrole nanowire fet device," *The Journal of Physical Chemistry C*, vol. 114, no. 31, pp. 13375–13380, 2010.

[52] D.-S. Kim, J.-E. Park, J.-K. Shin, P. K. Kim, G. Lim, and S. Shoji, "An extended gate fet-based biosensor integrated with a si microfluidic channel for detection of protein complexes," *Sensors and Actuators B: Chemical*, vol. 117, no. 2, pp. 488–494, 2006.

[53] C. Elbuken, T. Glawdel, D. Chan, and C. L. Ren, "Detection of microdroplet size and speed using capacitive sensors," *Sensors and Actuators A: Physical*, vol. 171, no. 2, pp. 55–62, 2011.

[54] P. K. Isgor, M. Marcali, M. Keser, and C. Elbuken, "Microfluidic droplet content detection using integrated capacitive sensors," *Sensors and Actuators B: Chemical*, vol. 210, pp. 669–675, 2015.

[55] T. Sun, N. G. Green, S. Gawad, and H. Morgan, "Analytical electric field and sensitivity analysis for two microfluidic impedance cytometer designs," *Iet Nanobiotechnology*, vol. 1, no. 5, pp. 69–79, 2007.

[56] J. Chen, C. Xue, Y. Zhao, D. Chen, M.-H. Wu, and J. Wang, "Microfluidic impedance flow cytometry enabling high-throughput single-cell electrical property characterization," *International journal of molecular sciences*, vol. 16, no. 5, pp. 9804–9830, 2015.

[57] S. Gawad, L. Schild, and P. Renaud, "Micromachined impedance spectroscopy flow cytometer for cell analysis and particle sizing," *Lab on a Chip*, vol. 1, no. 1, pp. 76–82, 2001.

[58] Y. Wang, Z. Ye, and Y. Ying, "New trends in impedimetric biosensors for the detection of foodborne pathogenic bacteria," *Sensors*, vol. 12, no. 3, pp. 3449–3471, 2012.

[59] L.-S. Jang and M.-H. Wang, "Microfluidic device for cell capture and impedance measurement," *Biomedical microdevices*, vol. 9, no. 5, pp. 737–743, 2007.

[60] H.-L. Gou, X.-B. Zhang, N. Bao, J.-J. Xu, X.-H. Xia, and H.-Y. Chen, "Label-free electrical discrimination of cells at normal, apoptotic and necrotic status with a microfluidic device," *Journal of Chromatography A*, vol. 1218, no. 33, pp. 5725–5729, 2011.

[61] D. Holmes and H. Morgan, "Single cell impedance cytometry for identification and counting of cd4 t-cells in human blood using impedance labels," *Analytical chemistry*, vol. 82, no. 4, pp. 1455–1461, 2010.

[62] J. Hong, D. S. Yoon, S. K. Kim, T. S. Kim, S. Kim, E. Y. Pak, and K. No, "Ac frequency characteristics of coplanar impedance sensors as design parameters," *Lab on a Chip*, vol. 5, no. 3, pp. 270–279, 2005.

[63] D. Holmes, D. Pettigrew, C. H. Reccius, J. D. Gwyer, C. van Berkel, J. Holloway, D. E. Davies, and H. Morgan, "Leukocyte analysis and differentiation using high speed microfluidic single cell impedance cytometry," *Lab on a Chip*, vol. 9, no. 20, pp. 2881–2889, 2009.

[64] T. Sun, C. Bernabini, and H. Morgan, "Single-colloidal particle impedance spectroscopy: complete equivalent circuit analysis of polyelectrolyte microcapsules," *Langmuir*, vol. 26, no. 6, pp. 3821–3828, 2009.

[65] H. Morgan, T. Sun, D. Holmes, S. Gawad, and N. G. Green, "Single cell dielectric spectroscopy," *Journal of Physics D: Applied Physics*, vol. 40, no. 1, p. 61, 2007.

[66] E. W. Kemna, L. I. Segerink, F. Wolbers, I. Vermes, and A. van den Berg, "Label-free, high-throughput, electrical detection of cells in droplets," *Analyst*, vol. 138, no. 16, pp. 4585–4592, 2013.

[67] M. Al-Tamimi, W. Shen, R. Zeineddine, H. Tran, and G. Garnier, "Validation of paper-based assay for rapid blood typing," *Analytical chemistry*, vol. 84, no. 3, pp. 1661–1668, 2012.

[68] S. Makulska, S. Jakiela, and P. Garstecki, "A micro-rheological method for determination of blood type," *Lab on a Chip*, vol. 13, no. 14, pp. 2796–2801, 2013.

[69] D. R. Ballerini, X. Li, and W. Shen, "An inexpensive thread-based system for simple and rapid blood grouping," *Analytical and bioanalytical chemistry*, vol. 399, no. 5, pp. 1869–1875, 2011.

[70] D. S. Kim, S. H. Lee, C. H. Ahn, J. Y. Lee, and T. H. Kwon, "Disposable integrated microfluidic biochip for blood typing by plastic microinjection moulding," *Lab on a Chip*, vol. 6, no. 6, pp. 794–802, 2006.

[71] M. K. Ramasubramanian and S. P. Alexander, "An integrated fiberoptic–microfluidic device for agglutination detection and blood typing," *Biomedical microdevices*, vol. 11, no. 1, pp. 217–229, 2009.

[72] T. R. Kline, M. K. Runyon, M. Pothiawala, and R. F. Ismagilov, "Abo, d blood typing and subtyping using plug-based microfluidics," *Analytical chemistry*, vol. 80, no. 16, pp. 6190–6197, 2008.

[73] M. S. Khan, G. Thouas, W. Shen, G. Whyte, and G. Garnier, "Paper diagnostic for instantaneous blood typing," *Analytical chemistry*, vol. 82, no. 10, pp. 4158–4164, 2010.

[74] D. C. Duffy, J. C. McDonald, O. J. Schueller, and G. M. Whitesides, "Rapid prototyping of microfluidic systems in poly (dimethylsiloxane)," *Analytical chemistry*, vol. 70, no. 23, pp. 4974–4984, 1998.

[75] J. R. Anderson, D. T. Chiu, H. Wu, O. Schueller, and G. M. Whitesides, "Fabrication of microfluidic systems in poly (dimethylsiloxane)," *Electrophoresis*, vol. 21, no. 1, pp. 27–40, 2000.

[76] Y. Shin, S. Han, J. S. Jeon, K. Yamamoto, I. K. Zervantonakis, R. Sudo, R. D. Kamm, and S. Chung, "Microfluidic assay for simultaneous culture of multiple cell types on surfaces or within hydrogels," *Nature protocols*, vol. 7, no. 7, pp. 1247–1259, 2012.

[77] F. Fassbender, G. Schmitt, M. Schöning, H. Lüth, G. Buss, and J.-W. Schultze, "Optimization of passivation layers for corrosion protection of silicon-based microelectrode arrays," *Sensors and Actuators B: Chemical*, vol. 68, no. 1, pp. 128–133, 2000.

[78] T. Aytug, J. T. Simpson, A. R. Lupini, R. M. Trejo, G. E. Jellison, I. N. Ivanov, S. J. Pennycook, D. A. Hillesheim, K. O. Winter, D. K. Christen, *et al.*, "Optically transparent, mechanically durable, nanostructured superhydrophobic surfaces enabled by spinodally phase-separated glass thin films," *Nanotechnology*, vol. 24, no. 31, p. 315602, 2013.

[79] Z. He, M. Ma, X. Lan, F. Chen, K. Wang, H. Deng, Q. Zhang, and Q. Fu, "Fabrication of a transparent superamphiphobic coating with improved stability," *Soft Matter*, vol. 7, no. 14, pp. 6435–6443, 2011.

[80] E. T. de Givenchy, S. Amigoni, C. Martin, G. Andrada, L. Caillier, S. Géribaldi, and F. Guittard, "Fabrication of superhydrophobic pdms surfaces by combining acidic treatment and perfluorinated monolayers," *Langmuir*, vol. 25, no. 11, pp. 6448–6453, 2009.

[81] D.-H. Lee and N.-G. Cho, "Assessment of surface profile data acquired by a stylus profilometer," *Measurement Science and Technology*, vol. 23, no. 10, p. 105601, 2012.

[82] M. Hein, M. Moskopp, and R. Seemann, "Flow field induced particle accumulation inside droplets in rectangular channels," *Lab on a Chip*, 2015.

[83] D.-T. Phan and N.-T. Nguyen, "Self-triggering regime for synchronized formation of two droplets," *Applied Physics Letters*, vol. 104, no. 8, p. 084104, 2014.

[84] H. Morgan and N. G. Green, *AC electrokinetics: colloids and nanoparticles*. No. 2, Research Studies Press, 2003.

[85] L. L. Zhang and X. Zhao, "Carbon-based materials as supercapacitor electrodes," *Chemical Society Reviews*, vol. 38, no. 9, pp. 2520–2531, 2009.